國 立 交 通 大 學

電 子 物 理 研 究 所

碩 士 論 文

自旋霍爾效應設置下在微結構附近所產生的殘餘電阻

偶極和自旋偶極的共振現象

RESONANT GENERATION OF
RESIDUAL RESISTIVITY DIPOLE AND SPIN DIPOLE
AROUND MICROSTRUCTURES
IN A SPIN-HALL CONFIGURATION

研 究 生：陳冠伊

指導教授：朱仲夏教授

中華民國九十六年七月

自旋霍爾效應設置下在微結構附近所產生的殘餘電阻偶極

和電子自旋偶極的共振現象

RESONANT GENERATION OF
RESIDUAL RESISTIVITY DIPOLE AND SPIN DIPOLE
AROUND MICROSTRUCTURES
IN A SPIN-HALL CONFIGURATION

研 究 生：陳冠伊   Student：Kuan-Yi Chen

指導教授：朱仲夏教授   Advisor：Prof. Chon Saar Chu

國 立 交 通 大 學

電 子 物 理 研 究 所

碩 士 論 文

A Thesis
Submitted to Department of Electrophysics
College of Science
National Chiao Tung University
in Partial Fulfillment of the Requirements
for the Degree of
Master
in
Electrophysics

July 2007
Hsinchu, Taiwan, Republic of China

中華民國九十六年七月

自旋霍爾效應設置下在微結構附近產生的殘餘電阻偶極和電子自旋偶極的共振現象

研究生：陳冠伊　　　　　　　　　　指導教授：朱仲夏教授

國立交通大學

電子物理研究所

摘要

　　此論文的焦點放在一個有外加電場的微結構附近，自旋軌道交互作用對電荷和電子自旋的堆積的影響。透過一個環形的微結構所可能造成的量子共振效應，我們進一步探討放大自旋軌道交互作用的可能性。

　　最重要的發現是，以往一直被忽略的，由電位梯度產生的自旋軌道耦合可以使一個微結構附近造成可觀的電子自旋堆積。藉由把在一個外電場中非平衡電自分佈裡所有電子波的空間機率加總，我們可以在量子彈道範圍內的微結構附近得到一個狀似偶極的電子自旋分佈，也就是自旋偶極。伴隨著量子散射的共振，此交互作用可以提供我們一個調控自旋偶極的方法。特別的是，隨著系統費米能的改變，自旋偶極會表現出方向的反轉和強度的放大。

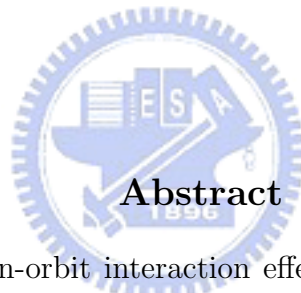　　藉由引入一個與自旋相關的非平衡電子分佈，材料背景雜質所產生的外秉自旋軌道耦合效應已經包含在我們的考慮裡面。此效應在共振時對自旋偶極的修正並沒有值得注意的貢獻。

RESONANT GENERATION OF
RESIDUAL RESISTIVITY DIPOLE AND SPIN DIPOLE
AROUND MICROSTRUCTURES
IN A SPIN-HALL CONFIGURATION

Student: Kuan-Yi Chen   Advisor: Prof. Chon-Saar Chu

Department of Electrophysics

National Chiao Tung University

Abstract

This thesis focuses on spin-orbit interaction effect on charge and spin accumulation around a microstructure in an external electric field. Furthermore, a ring type microstructure is introduced to explore possible amplification of the spin-orbit interaction effect from quantum resonances allowed by such microstructures.

A major finding in this thesis is that the mostly overlooked spin-orbit interaction arising from in-plane potential gradient can contribute to significant spin accumulation around a microstructure. By considering quantum-mechanical scattering of individual electrons in a nonequilibrium distribution acted upon by an external electric field, we obtain a spin dipole, or spin accumulation of a dipole-like spatial variation, around a microstructure within the ballistic range. The subsequent quantum scattering resonance provides and additional knob for the manipulation of spin dipole. Specifically, the spin dipole manifests both sign reversal and large amplification when the Fermi energy crosses a resonance.

We have included the extrinsic spin-orbit interaction effects from background spin-orbit scatterers by invoking a spin dependent nonequilibrium electron distribution. The correction of the spin dipole is found to be insignificant in the resonant region.

致 謝

感謝這兩年多來朱老師的教導，尤其是幫忙把研究結果發表在期刊上，以及對此論文最後階段的意見及修改，讓我獲益良多。也感謝唐志雄學長、鄔其君學長給了我很多寶貴的意見，還有實驗室夥伴們陪我度過研究生的生涯，學長靖航、奧斯卡、宇廷、阿民，學姊淑維、淑娟，感謝你們給我許多經驗上的幫助。尤其感謝學長老王、興哥、還有學弟志宣在最後的日子裡的鼓勵和相依為命，還有禹鈞的陪伴和打氣。最感謝的是爸媽的栽培、支持和體諒，還有妹妹的關心。感謝所有關心我的人。

Contents

List of Figures

Chapter 1

Introduction

The main stream of present day technology is built upon charge-based electronics where charge rather than spin of electrons is endeared as the carrier of information. The spin of an electron, however, is essentially neglected in the technology arena.

This trend of neglecting spin in the application sector may have set a different course in the past decades when prototypes of new, spin-based electronics, or spintronics, were proposed and realized.

Earlier spin-based devices made use of the physics of giant magnetoresistance (GMR) in a system consisting of magnetic materials [1]. More recent research takes on the greater challenge of achieving spintronics in all semiconductor configurations: without magnetic materials and applying magnetic fields.

To achieve an all electric control on spin transport and spin accumulation in semi-conductors, we should invoke the spin-orbit interaction (SOI). According to the physical origin of the SOI, the SOI can be divided into intrinsic and extrinsic types. The intrinsic type, such as Rashba [2], or Dresselhaus [3] SOI are associated with the lacking of structural inversion symmetry, or spatial inversion symmetry, respectively. On the other hand, the extrinsic SOI is due to the presence of SOI scatterers, or Mott scattering by nonmagnetic impurities in the system [4, 5].

Recently, building on these SOI mechanisms, a physical phenomenon called spin-Hall

effect (SHE) has attracted intensive attentions. This is a phenomenon where a dc charge current can give rise to transverse spin current, in the lateral direction, and spin accumulation at lateral edges of a strip-like sample [6–8]. This development has promoted great hope in meeting the challenge of all-electric generation of spin transport and accumulation.

Experiment contribution of intrinsic SHE has been established in p-doped 2D semiconductor quantum wells [9], and of extrinsic SHE has been observed in n-doped 3D semiconductor thin film strips of GaAs [10].

That the electron spin can precess when it moves in an electric or magnetic field, complicates our lifes because any component of spin is not a conserved quantity. Hence connecting the spin current to the spin accumulation is an issue that demands great caution. As such, a proper definition was a great issue and remains to be entirely settled [11–13].

Since experimentally it is as yet a tough issue concerning the direct measurement of the spin current, the spin accumulation is the only alternative for the detection of SHE. However, the spin accumulation on the lateral edges of a sample should not be the only signature of SHE. Similar to Landauer's picture of residual resistivity dipole (RRD) around , where a dipole-like charge accumulation is generated by a dc charge current around a local scatterer, a nonequilibrium spin dipole might be expected to form in a spin-Hall configuration. That a spin dipole accumulated around a non-SOI scatterer in a Rashba-type two dimensional electron gas (2DEG) has indeed be found recently [14]. On the other hand, even though there are many recent works on spin-dependent quantum scattering around microstructures [15–19], the SOI due to in-plane potential gradient has essentially been neglected. In this thesis, we will show that this in-plane potential gradient SOI can contribute to significant spin accumulation when quantum resonance is invoked.
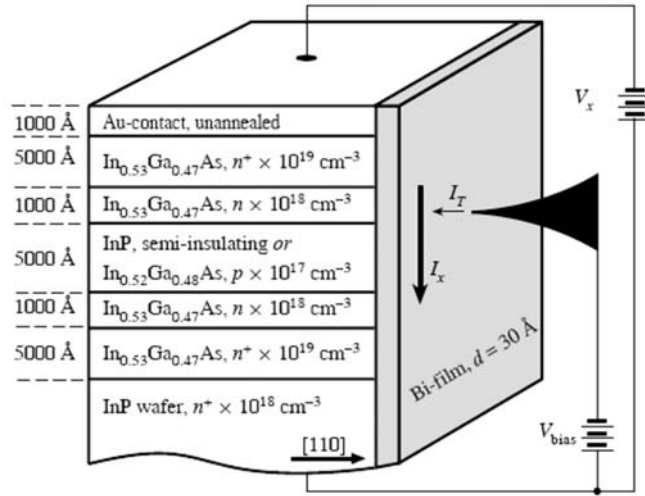
Figure 1.1: An illustration of sample geometry for cross sectional STP experiments. [Superlattices and Microstructures **23**, 699 (1998)].
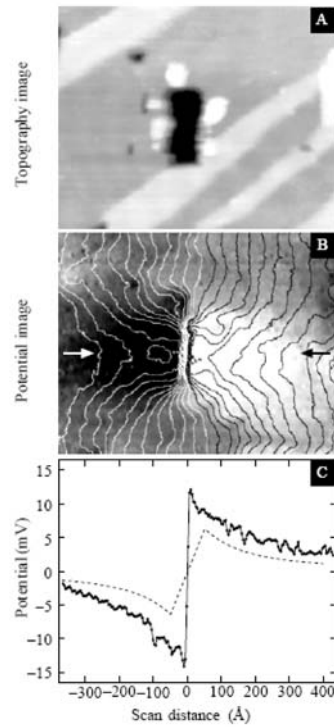
Figure 1.2: A. STM-topogragh, B. STP potential image and C. Cross sectional cut of B. [Superlattices and Microstructures **23**, 699 (1998)]

1.1 Introduction to Landauer's residual resistivity dipole

The charge accumulation around a local scatterer that we will discuss in this section is referred to as the residual resistivity dipole (RRD), first predicted by R. Landauer in

1957 [20]. According to Landauer, local scatterers are expected to give rise to spatial variations in the electric field. This forms a microscopic point of view for the set-up of the macroscopic potential drop from these individual electric dipole fields. In other words, the Landauer RRD is the microscopic origin of the macroscopic resistance. Theoretical formalism for the calculation of the RRD is built upon the asymptotic scattering wave function around a target scatterer [21, 22]. Experiment confirmation of the Landauer RRD has to wait until 1996, when the electric potential around a defect on a bismuth surface was picked up by a scanning tunneling potentiometry (STP) [23].

1.2 Spin-orbit coupling in solid-state systems

Electron spin, the only internal degree of freedom of electrons, follows naturally from the Dirac equation when Dirac tried to put wave function in a covariant form, when space and time appear on equal footing. A nonrelativistic limit of the Dirac equation gives rise to the spin-orbit interaction term, a term that has found great success in atomic energy spectra. The form of this spin-orbit interaction, in vacuum, is [24]

$$H_{\mathrm{SO}} = -\frac{e\hbar}{4m_0^2 c^2}\,\boldsymbol{\sigma}\cdot(\mathbf{E}\times\mathbf{p}) = \frac{\hbar}{4m_0^2 c^2}\,\boldsymbol{\sigma}\cdot(\boldsymbol{\nabla}V\times\mathbf{p})\,, \tag{1.1}$$

where m_0 is the free electron mass, $\hbar$ the Planck constant and c the velocity of light. The physical interpretation of H_{SO} is given below. An electron moving in an electric potential region sees, in its frame of reference, an effective magnetic field which couples with the electron spin through the magnetic moment of the electron spin. Through this effective magnetic field, which certainly depends on the orbital motion of the electron, the SOI is established. This physics holds in semiconductor too, when $V(\mathbf{r})$ becomes the periodic potential of the host lattice and also the impurities.

Electronic state calculation in semiconductor is best described by the $\mathbf{k}\cdot\mathbf{p}$ model, when the states in the vicinity of the band edges is of our interest. Furthermore, within the envelope function approximation (EFA), the energy band can be characterized by effective

masses. The SOI in semiconductors requires, first of all, an effective electric field in the material. Such effective electric field can find contribution from the build-in crystal field when the crystal has bulk inversion asymmetric (BIA) the so-called Dresselhaus SOI, or structural inversion asymmetry (SIA), the so-called Rashba SOI. The BIA is found in zinc-blende structure and the SIA in asymmetric quantum wells (QWs) or heterostructures.

Within the effective mass approximation, the effect of all the fast-varying atomic potential has been incorporated into the effective mass. Slower varying $V(\mathbf{r})$, with variation length scale much greater than the lattice spacing, is found to contribute to SOI with a much greater SO coupling constant λ. For a central potential $V(\mathbf{r}) = V(r)$ in vacuum, the SO coupling is

$$\frac{\hbar}{4m_0^2 c^2} \boldsymbol{\sigma} \cdot (\boldsymbol{\nabla} V \times \mathbf{p}) = \frac{\hbar}{4m_0^2 c^2} \frac{1}{r} \frac{dV}{dr} \boldsymbol{\sigma} \cdot (\mathbf{r} \times \mathbf{p}) = \frac{\hbar^2}{4m_0^2 c^2} \frac{1}{r} \frac{dV}{dr} \frac{\mathbf{L}}{\hbar} \cdot \boldsymbol{\sigma} = -\frac{\lambda_{\text{vac}}}{\hbar} \frac{1}{r} \frac{dV}{dr} \mathbf{L} \cdot \boldsymbol{\sigma}$$

where $\mathbf{L}$ is the orbital angular momentum, $\boldsymbol{\sigma}$ is the vector Pauli matrices and $\lambda_{\text{vac}} = -\hbar^2/(4m_0^2 c^2) \approx -3.72 \times 10^{-6} \, \text{Å}^2$.

But in a semiconductor, also for a central potential $V(\mathbf{r}) = V(r)$, the SO coupling is

$$H_{\text{SO}} = -\frac{\lambda}{\hbar} \frac{1}{r} \frac{dV}{dr} \mathbf{L} \cdot \boldsymbol{\sigma},$$

where

$$\lambda \approx \frac{P^2}{3} \left[\frac{1}{E_g^2} - \frac{1}{(E_g + \Delta_0)^2} \right].$$

For a 2DEG, the SOI becomes

$$H_{\text{SO}} = -\frac{\lambda}{\hbar} \frac{1}{\rho} \frac{dV(\rho)}{d\rho} L_z \sigma_z.$$

Here P is the momentum matrix element between s- and p-orbitals, E_g is the energy band gap, and Δ_0 represents the SOI energy split to the spin split-off hole band [8, 25]. Of

particular interest is that $\lambda = 120 \,\text{Å}^2$ in InAs, which is seven order of magnitude greater than λ_{vac} [25, 26].

Very roughly speaking, this large enhancement of SO coupling constant can be understood in the following. With $\lambda_{\text{vac}} \propto \frac{1}{m_0^2 c^2} = \frac{1}{m_0} \frac{1}{m_0 c^2}$, we can see that

$$\frac{\lambda}{\lambda_{\text{vac}}} \sim \frac{m_0}{m^*} \frac{m_0 c^2}{E_g}.$$

For InAs, $m_0/m^* \sim \frac{1}{0.023}$; $\frac{m_0 c^2}{E_g} \sim \frac{0.5\,\text{MeV}}{0.418\,\text{eV}}$; leading to

$$\frac{\lambda}{\lambda_{\text{vac}}} \sim 52 \times 10^6.$$

Comparing to $\frac{120\,\text{Å}^2}{3.73 \times 10^{-6}\,\text{Å}^2} = 32 \times 10^6$, we see that the above hand waving argument has captured the essential physical origin of the great enhancement.

1.3 Motivation

It is this great enhancement in the SO coupling constant that causes us to take the in-plane potential SOI very seriously and to study its effect. As a result, we propose a
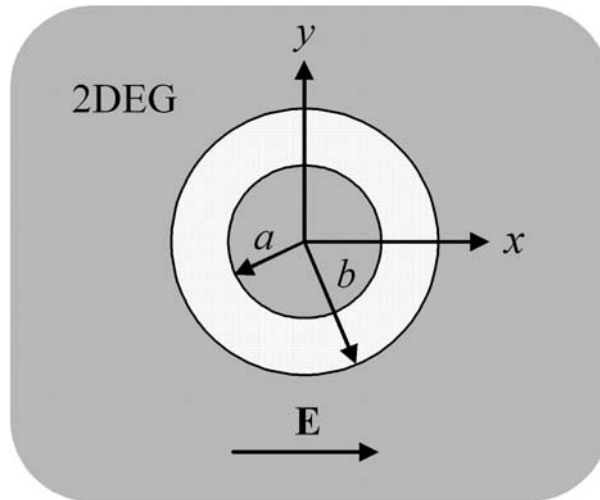
Figure 1.3: System configuration: A ring-shaped potential embedded in a two dimensional electron gas (2DEG). An electric field $\mathbf{E}$ sets up a current in the 2DEG.
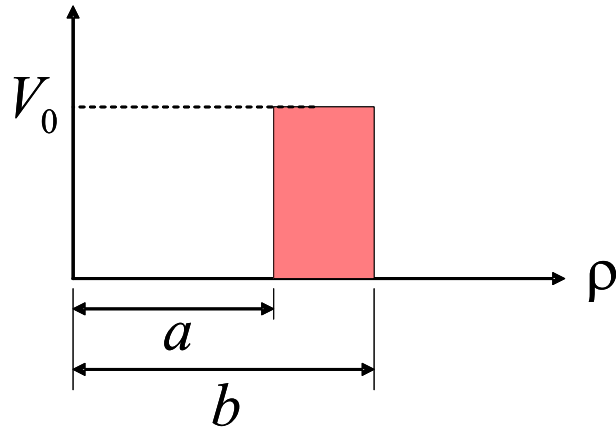
Figure 1.4: Radial profile of the central ring-shaped repulsive potential.

ring-shaped potential pattern.

To concentrate on the effect of the in-plane potential gradient SOI from the microstructure, we will not include other intrinsic and extrinsic SOI. Neglecting Rashba-type SOI is justified in a symmetric quantum well. In our results, particulary near the quantum resonances, to remain intact even when Dresselhaus SOI would be included. Extrinsic SOI effect we will discuss in this thesis is found to be a small correction to our conclusion.

1.4   A guiding tour to this thesis

In Chapter 2, we will review the physics and formalism of a charge RRD around a local scatterer. Concepts such as nonequilibrium distribution of incident electrons, obtained from the Boltzmann kinetic equation, scattering wave functions of these electrons, and Thomas-Fermi screening of these pile-up of charges to the electric potential field of the electric dipole. As a preview to the resonant behavior, we will also consider the resonant behavior of the RRD around a ring-shaped microstructure. No in-plane potential gradient SOI is included in this preview session.

In Chapter 3, we reconsider the ring-shaped microstructure, but with in-plane po-

tential gradient SOI included. The 2D quantum-mechanical scattering becomes spin-dependent and asymmetric. The resonant behavior in the charge RRD and the spin accumulation is presented.

In Chapter 4, the effect of the extrinsic SOI to the resonant spin accumulation around the ring-shaped microstructure is presented. Correction is shown to be small.

In Chapter 5, we consider a smooth potential profile of a ring-shaped microstructure. The resonant behavior is shown to remain intact.

Finally in chapter 6, we present our conclusion and possible future work.

Chapter 2

Landauer's residual resistivity dipole around a ring-shaped microstructure

In this chapter, we will present the physics of Landauer's residual resistivity dipole (RRD) and formalism leading to such an entity. The distribution of the charge pile up of the RRD around a local scatterer is obtained by summing up the density distribution of electrons scattering from a target scatterer. The distribution of the electrons is set up by an external field. The coulomb interaction between electrons causes screening to occur and results in an induced potential variation around a scatterer. In the lowest order in $1/(k\rho)$ where k is the Fermi wave number and and ρ the distance from the scatterer, the induced potential takes on a dipole field from which we can define a RRD strength. We present the energy dependence of the RRD which, as expected, exhibits resonant behavior in the case of a ring-shaped microstructure.

2.1 Quantum-mechanical scattering in two dimensions

For a 2D central potential, the cylindrical symmetry governs that the scattering wave function be most conveniently expressed in polar coordinates. The scattering wave function from an incident plane wave contains a scattered wave component representing cylindrical

outgoing wave co-centered with the central potential.

Without the central potential, the free particle Schrödinger equation is given by

$$(\nabla^2 + k^2)\psi = 0,$$

with the particle energy $\varepsilon = \hbar^2 k^2 / 2m^*$. Expressed in polar coordinates, the equation is

$$\frac{1}{\rho} \frac{\partial}{\partial \rho} \rho \frac{\partial \psi}{\partial \rho} + \frac{1}{\rho^2} \frac{\partial^2 \psi}{\partial \phi^2} + k^2 \psi = 0 \,. \tag{2.1}$$

Applying the factored form $\psi(\boldsymbol{\rho}) = R(\rho)\,\Phi(\phi)$, it can be decoupled separately into the radial and azimuthal coordinates,

$$\frac{d^2 R}{d\rho^2} + \frac{1}{\rho} \frac{dR}{d\rho} + \left(k^2 - \frac{l^2}{\rho^2} \right) R = 0 \,;$$
$$\frac{d^2 \Phi}{d\phi^2} = -l^2 \Phi \,,$$

where the radial equation is the Bessel equation. Therefore the free electron wave function in two dimensions can be written in the form

$$\psi(\rho, \phi) = J_l(k\rho)\, e^{il\phi},$$

where $J_l(x)$ is the Bessel function of the first kind with $l = 0, \pm 1, \pm 2, \ldots$ the quantum number of the azimuthal motion, along the coordinate ϕ which is the angle between $\boldsymbol{\rho}$ and $\hat{\mathbf{x}}$.

2.1.1 Method of partial waves

To perform the quantum scattering calculation from a cylindrical central potential, we first expand the incident plane wave, along $\hat{\mathbf{x}}$, in terms of the cylindrical waves, the

Jacobi-Anger expansion [27], given by

$$e^{ikx} = e^{ik\rho\cos\phi} = \sum_{l=-\infty}^{+\infty} i^l J_l(k\rho) e^{il\phi}. \tag{2.2}$$

Since $J_l(k\rho)$ is a standing wave along the radial direction, it is convenient, for our purpose, to express it in terms of two radial propagating waves, the Hankel functions,

$$J_l(k\rho) = \frac{1}{2} \left[H_l^{(1)}(k\rho) + H_l^{(2)}(k\rho) \right],$$

where $H_l^{(1)}(x)$ and $H_l^{(2)}(x)$ are defined as

$$H_l^{(1)}(x) = J_l(x) + iY_l(x);$$
$$H_l^{(2)}(x) = J_l(x) - iY_l(x).$$

The radial propagating nature of these Hankel functions is most transparent in their asymptotic form, i.e. the region where $k\rho \gg 1$,

$$\lim_{k\rho\to\infty} H_l^{(1)}(k\rho) = \sqrt{\frac{2}{\pi k\rho}} e^{i(k\rho - l\pi/2 - \pi/4)};$$
$$\lim_{k\rho\to\infty} H_l^{(2)}(k\rho) = \sqrt{\frac{2}{\pi k\rho}} e^{-i(k\rho - l\pi/2 - \pi/4)}. \tag{2.3}$$

It is clear that $H_l^{(1)}$, $H_l^{(2)}$ can be viewed as circular waves propagating radial outwards from, inwards towards the scattering center, respectively. The cylindrical symmetry of the scattering potential causes waves to be coupled only within the same l. This is essentially the conservation of orbital angular momentum, which is true for a central potential but without SOI. The total wave function, including the incident and the scattered waves, is written in the form

$$\Psi(\boldsymbol{\rho}) = \sum_{l=-\infty}^{+\infty} i^l R_l(\rho) e^{il\phi}, \tag{2.4}$$

where R_l is yet to be determined. Substituting Eq. (2.4) into the Schrödinger equation
Eq. (2.1), the radial equation becomes

$$\frac{1}{\rho}\frac{d}{d\rho}\rho\frac{dR_l(\rho)}{d\rho} + \left[k^2 - \frac{l^2}{\rho^2} - \frac{2m^*}{\hbar^2}V(\rho)\right]R_l(\rho) = 0. \tag{2.5}$$

Boundary conditions will be established in the next section for the solving of $R_l(\rho)$.

2.1.2   Phase shift and the unitarity relation

For a scattering center, whatever goes in should be eventually go out. Hence physically, the
only thing that can be changed is the phase of the outgoing cylindrical waves. Therefore
phase shift in the asymptotic outgoing cylindrical wave, where $V(\rho) = 0$, should carry
information about $V(\rho)$. Therefore, the asymptotic form of $R_l(\rho)$ should be of the form

$$\lim_{k\rho\to\infty} R_l(\rho) \propto \sqrt{\frac{2}{\pi k\rho}}\cos\left(k\rho - \frac{l\pi}{2} - \frac{\pi}{4} + \delta_l\right),$$

or more transparently,

$$\lim_{k\rho\to\infty} R_l(\rho) = \frac{1}{\sqrt{2\pi k\rho}}\left[e^{2i\delta_l}e^{i(k\rho-l\pi/2-\pi/4)} + e^{-i(k\rho-l\pi/2-\pi/4)}\right]. \tag{2.6}$$

where δ_l is the phase shift of the outgoing wave. Clearly $\delta_l = 0$ reduces $R_l(\rho)$ to $J_l(k\rho)$ as
expected. Note that δ_l is the sole quantity to be determined since the amplitude of the
two cylindrical wave components in Eq. (2.6) should be the same, for unitary requirement.
On the same token, δ_l must be real.

We need to find a boundary condition for the determination of δ_l. For an arbitrary
radial potential profile, we need to integrate the radial equation for $R_l(\rho)$ and matches it
with the expected form, Eq. (2.6), outside the potential. The radial wave function outside
the range of the potential can be expressed in the form

$$R_l^{\text{out}}(\rho) = e^{i\delta_l}\left[\cos\delta_l J_l(k\rho) - \sin\delta_l Y_l(k\rho)\right], \tag{2.7}$$

where the superscript 'out' stands for 'outside'. Eq. (2.7) coincides with Eq. (2.6) in
its asymptotic region. The boundary condition for the radial differential equation, via
integrating Eq. (2.5), is that, the logarithmic derivative of R_l,

$$\mathcal{L}\left[R_l(\rho)\right] \equiv \rho \frac{d \ln R_l(\rho)}{d\rho}, \tag{2.8}$$

must be continuous at any ρ. Since the phase shift δ_l is defined in the potential-vanishing
region, we have

$$\frac{k\rho_b \left[\cos\delta_l J_l'(k\rho_b) - \sin\delta_l Y_l'(k\rho_b)\right]}{\cos\delta_l J_l(k\rho_b) - \sin\delta_l Y_l(k\rho_b)} = \left.\frac{\rho}{R_l}\frac{dR_l}{d\rho}\right|_{\rho=\rho_b^-},$$

where ρ_b is the 'outer edge' of the scattering potential, beyond which the potential is
vanishing, and $J_l'(x) \equiv dJ_l(x)/dx$. After some rearrangement, the phase shift is cast into
the form

$$\tan\delta_l = \frac{k\rho_b J_l'(k\rho_b) - \beta_l J_l(k\rho_b)}{k\rho_b Y_l'(k\rho_b) - \beta_l Y_l(k\rho_b)}, \tag{2.9}$$

where

$$\beta_l \equiv \left.\frac{\rho}{R_l}\frac{dR_l}{d\rho}\right|_{\rho=\rho_b^-}$$

is the logarithmic derivative of the radial functions evaluated at ρ smaller but infinitesi-
mally close to ρ_b. Thus far the discussion is general, without being limited to any radial
potential profile inside ρ_b. Taking a unity amplitude for the plane wave, the total wave
function outside the range of the scattering potential is given by

$$\Psi_k^{\text{out}}(\boldsymbol{\rho}) = \sum_{l=-\infty}^{+\infty} i^l e^{i\delta_l}\left[\cos\delta_l J_l(k\rho) - \sin\delta_l Y_l(k\rho)\right] e^{il\phi}. \tag{2.10}$$

The incident wave is along $\hat{\mathbf{x}}$, and the incident energy is ε, giving a free particle wave
number $k = \sqrt{2m^*\varepsilon}/\hbar$.

2.1.3 Asymptotic expansion of scattering wave and the differential cross section

The phase shift is related to the differential cross section. Separating out the plane wave, in the total wave function in Eq. (2.10), we have

$$\Psi_{\mathbf{k}}(\boldsymbol{\rho}) = e^{i\mathbf{k}\cdot\boldsymbol{\rho}} + \frac{1}{2} \sum_{l=-\infty}^{+\infty} i^l \left(e^{2i\delta_l} - 1 \right) H_l^{(1)}(k\rho) \, e^{il(\phi_\rho - \phi_k)}, \tag{2.11}$$

where incident wave direction $\mathbf{k} = (k, \phi_k)$, rather than being restricted to $\hat{k} = \hat{x}$. In the asymptotic region, the above equation is in the form

$$\Psi_{\mathbf{k}}(\boldsymbol{\rho}) \approx e^{i\mathbf{k}\boldsymbol{\rho}} + \frac{e^{ik\rho}}{\sqrt{\rho}} f(\phi),$$

with $\phi \equiv \phi_\rho - \phi_k$, and

$$f_k(\phi) = \sqrt{\frac{2i}{\pi k}} \sum_{l=-\infty}^{+\infty} e^{i\delta_l} \sin\delta_l \, e^{il\phi}, \tag{2.12}$$

is the two dimensional scattering amplitude [28]. The scattering differential cross sections is givne by $D(\phi) \equiv |f(\phi)|^2$.

2.2 Nonequilibrium distribution of electrons: Theory of the Boltzmann kinetic equation

In this section we will give a brief review on the Boltzmann equation which we will use to obtain the nonequilibrium electron distribution when an electric field is applied. In a semiclassical regime, the state of a N particle system can be given by the set of coordinates (p_i, q_i), where $i = 1, 2, 3, \cdots, dN$. This constitutes a state point in the phase space. The Boltzmann equation aims to calculate the single? particle distribution $f(\mathbf{k}, \mathbf{r})$ by tracing

its time evolution in the phase space, given by

$$\frac{\partial f}{\partial t} + \dot{\mathbf{k}} \cdot \frac{\partial f}{\partial \mathbf{k}} + \dot{\mathbf{r}} \cdot \frac{\partial f}{\partial \mathbf{r}} = \left. \frac{\partial f}{\partial t} \right|_{\text{coll}},$$
(2.13)

The left-hand side originates form the tracing of an infinitesimal phase space volume,
taking its volume changes in due course of its motion in the phase space, and requires
that the number of states enclosed remain the same. The right hand-side is the jump into
or out of the infinitesimal phase space volume due to collision with background impurities
and is given by

$$\left. \frac{\partial f(\mathbf{k})}{\partial t} \right|_{\text{coll}} = -\sum_{\mathbf{k}'} \left\{ W_{\mathbf{k},\mathbf{k}'} f(\mathbf{k}) \left[1 - f(\mathbf{k}') \right] - W_{\mathbf{k}',\mathbf{k}} f(\mathbf{k}') \left[1 - f(\mathbf{k}) \right] \right\},$$
(2.14)

where $W_{\mathbf{k},\mathbf{k}'}$ is the transition rate at which electrons are scattered from a state $\mathbf{k}$ to
another state $\mathbf{k}'$, and its dimension is inverse of time. For the case when the scattering
by the background impurities preserve, then we have $W_{\mathbf{k},\mathbf{k}'} = W_{\mathbf{k}',\mathbf{k}}$, and Eq. (2.14) can
be simplified to

$$\left. \frac{\partial f(\mathbf{k})}{\partial t} \right|_{\text{coll}} = -\sum_{\mathbf{k}'} W_{\mathbf{k},\mathbf{k}'} \left[f(\mathbf{k}) - f(\mathbf{k}') \right].$$
(2.15)

2.2.1 Relaxation time approximation

If $W_{\mathbf{k},\mathbf{k}'}$ is assumed to be momentum independent, then we have

$$\left. \frac{\partial f(\mathbf{k})}{\partial t} \right|_{\text{coll}} = -\frac{g(\mathbf{k})}{\tau},$$
(2.16)

where $g(\mathbf{k}) \equiv f(\mathbf{k}) - f_0(\mathbf{k})$ is the nonequilibrium part of the distribution and τ the
relaxation time. Eq. (2.16) describes the tendency of the nonequilibrium distribution
$f(\mathbf{k})$ to evolve back to its equilibrium $f_0(\mathbf{k})$ in a time scale τ.

2.2.2   The linear response to the uniform electric field

In a spatially homogeneous and time-independent system, according to Eq. (2.13) and
Eq. (2.16), the Boltzmann equation reads, to the lowest order in the electric field $\mathbf{E}$, or
for weak $\mathbf{E}$,

$$-e\mathbf{E} \cdot \frac{1}{\hbar}\frac{\partial f_0}{\partial \mathbf{k}} = -\frac{g}{\tau},$$

where $e > 0$. The equilibrium distribution f_0 takes on the Fermi-Dirac distribution,

$$f_0(\mathbf{k}) = \frac{1}{e^{(\varepsilon_\mathbf{k}-\mu)/k_\mathrm{B}T} + 1}, \tag{2.17}$$

where $\varepsilon_\mathbf{k} = \frac{\hbar^2 k^2}{2m^*}$ is the electron energy, μ the chemical potential of the system, k_B the
Boltzmann constant, and T the temperature. Therefore, the nonequilibrium distribution
is,

$$g(\mathbf{k}) = \frac{e\tau\hbar}{m^*}\frac{\partial f_0}{\partial \varepsilon} \mathbf{E} \cdot \mathbf{k}, \tag{2.18}$$

which describes a edge-broadened, shifted Fermi sphere under the external applied electric
filed $\mathbf{E}$.

2.3   Landauer's residual resistivity dipole

2.3.1   Charge accumulation due to nonequilibrium incident distribution

The total nonequilibrium distribution in a uniform applied electric is

$$f(\mathbf{k}) = f_0(\mathbf{k}) + g(\mathbf{k}),$$
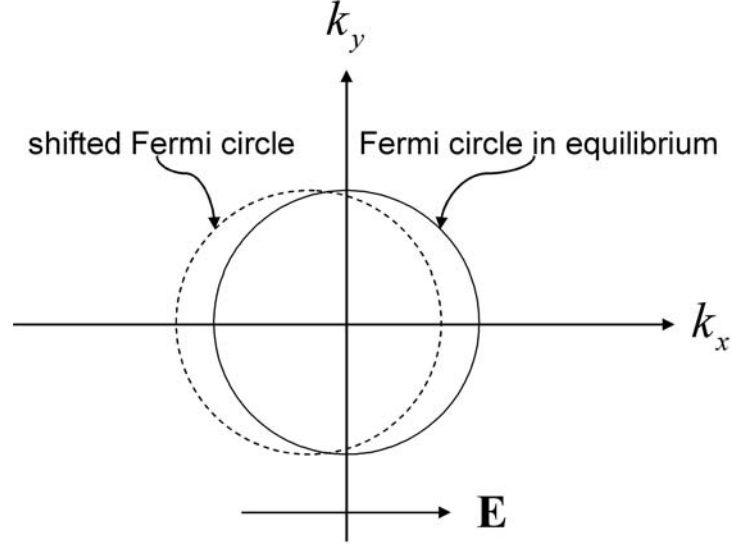
Figure 2.1: Qualitative sketch of $g(\mathbf{k})$ in the presence of a driving field $\mathbf{E}$. The shifted Fermi circle is towards negative x-axis because negatively charged electrons are driven opposite to the direction of $\mathbf{E}$.

where $f_0(\mathbf{k})$ is the equilibrium distribution. At very low temperature, f_0 can be approximated by a Heaviside step function,

$$f_0(k) = \theta(\mu - \varepsilon_{\mathbf{k}}), \tag{2.19}$$

and thus the nonequilibrium solution to the Boltzmann equation, according to Eq. (2.18), is

$$g(\mathbf{k}) = -\frac{e\tau\hbar}{m^*}\delta(\varepsilon_{\mathbf{k}} - \mu)\mathbf{E} \cdot \mathbf{k}, \tag{2.20}$$

where $\mathbf{E} = E_0\hat{\mathbf{x}}$ is the applied electric field.

Taking into account the incident direction $\hat{\mathbf{k}}$ and the direction of the position $\hat{\boldsymbol{\rho}}$ at which the scattering wave function is referred, we have

$$\Psi_{\mathbf{k}}(\boldsymbol{\rho}) = \sum_{l=-\infty}^{+\infty} i^l R_l(\rho)e^{il(\phi_\rho - \phi_k)}, \tag{2.21}$$

17

where $R_l(\rho)$ is assumed to be determined from the radial Schrödinger equation Eq. (2.5).
The total charge density distribution can therefore be evaluated by summing over the
scattering wave functions of all these electrons

$$n(\boldsymbol{\rho}) = 2 \times \frac{1}{4\pi^2} \int d\mathbf{k}\, f(\mathbf{k}) \left| \Psi_{\mathbf{k}}(\boldsymbol{\rho}) \right|^2 = n_{\text{eq}}(\boldsymbol{\rho}) + \delta n(\boldsymbol{\rho}), \qquad (2.22)$$

where

$$n_{\text{eq}}(\boldsymbol{\rho}) = \frac{1}{2\pi^2} \int d\mathbf{k}\, f_0(k) \left| \Psi_{\mathbf{k}}(\boldsymbol{\rho}) \right|^2$$

is the contribution due to equilibrium distribution, and

$$\delta n(\boldsymbol{\rho}) = \frac{1}{2\pi^2} \int d\mathbf{k}\, g(\mathbf{k}) \left| \Psi_{\mathbf{k}}(\boldsymbol{\rho}) \right|^2$$

is due to the nonequilibrium part of the distribution, which is also linear in $\mathbf{E}$. The
multiplying factor 2 in Eq. (2.22) is due to spin degeneracy. Integrating over $\mathbf{k}$ gives us a
dipole-like distribution with the dipole aligned parallel to $\mathbf{E}$,

$$\delta n(\boldsymbol{\rho}) = -\frac{2e\tau E_0 k_\mu}{\pi\hbar} \cos\phi_\rho \operatorname{Im} \sum_{l=0}^{\infty} R_l(\rho) R_{l+1}^*(\rho), \qquad (2.23)$$

where $k_\mu = \sqrt{2m^*\mu}/\hbar$. The detailed derivation of Eq. (2.23) is presented in Appendix A.

2.3.2 Screening effect and potential induced by charge accumulation

The pile up of charges in the previous section invite screening by the electrons in the
system which then results in a local drop in the electric potential.

Although the local pile up of charges is expressed completely by Eq. (2.22), the only
contribution to the potential 'drop' between electrodes is from the dipole-like distribution
$\delta n(\boldsymbol{\rho})$. This is because the n_{eq}, being cylindrical symmetry, does not contribute to the

potential drop. Only the $\delta n(\mathbf{q})$ term contributes to the potential drop. This potential
drop is identified to be a dipole-like form, leading Landauer to the RRD picture. In the
following, we use the well-known method of Thomas-Fermi (T-F) screening [29] to obtain
the potential induced by this local pile up of charges.

2.3.3 Thomas-Fermi screening in two dimensions

It is found to be more convenient to discuss the T-F screening in 2D system in the integral
form than in the differential form, given by the Laplace equation. Let $\sigma(\boldsymbol{\rho})$ be the total
charge distribution, including the external charge $\sigma^{\text{ext}}(\boldsymbol{\rho})$ and the screening charge $\sigma^{\text{ind}}(\boldsymbol{\rho})$.
The total potential $\phi(\boldsymbol{\rho})$ is given by

$$\phi(\boldsymbol{\rho}) = \frac{1}{4\pi\epsilon_0} \int \frac{\sigma(\boldsymbol{\rho}')}{|\boldsymbol{\rho} - \boldsymbol{\rho}'|} \, d\boldsymbol{\rho}' \tag{2.24}$$

By performing a Fourier transform on Eq. (2.24), and incorporating the convolution the-
orem, we obtain

$$\phi(\mathbf{q}) = \frac{1}{2\epsilon_0} \frac{1}{q} \sigma(\mathbf{q}) \, , \tag{2.25}$$

where $\phi(\mathbf{q})$, $\sigma(\mathbf{q})$ stand for the Fourier transforms of $\phi(\boldsymbol{\rho})$, $\sigma(\boldsymbol{\rho})$, respectively, at wave
vector $\mathbf{q}$. The equilibrium electron number density is given by

$$n_0 = 2 \times \frac{1}{4\pi^2} \int d\mathbf{k} f_0(k) = \frac{1}{2\pi^2} \int d\mathbf{k} \frac{1}{e^{(\varepsilon-\mu)/k_B T} + 1},$$

and the factor 2 is due to the spin degeneracy. This density is neutralized by a corre-
sponding positively charged background. In the presence of $\phi(\boldsymbol{\rho})$, the electron density
becomes

$$n(\boldsymbol{\rho}) = 2 \times \frac{1}{(2\pi)^2} \int d\mathbf{k} \frac{1}{e^{(\varepsilon-e\phi(\boldsymbol{\rho})-\mu)/k_B T} + 1}.$$

From the assumption of the neutrality, the positive charge number density is n_0, and the

induced charge density is $\sigma(\boldsymbol{\rho}) = -en(\boldsymbol{\rho})$, is written as

$$\sigma^{\text{ind}}(\boldsymbol{\rho}) = -en(\boldsymbol{\rho}) + en_0 = -e\left[n_0(\mu + e\phi(\boldsymbol{\rho})) - n_0(\mu)\right].$$

Assume that $\phi(\boldsymbol{\rho})$ is weak enough and can be regarded as a perturbation, then

$$\sigma^{\text{ind}}(\boldsymbol{\rho}) \approx -e^2\frac{\partial n_0}{\partial \mu}\phi(\boldsymbol{\rho}) = e^2\frac{\partial n_0}{\partial \varepsilon}\phi(\boldsymbol{\rho}). \tag{2.26}$$

The total potential can be written as

$$\phi(\boldsymbol{\rho}) = \phi^{\text{ext}}(\boldsymbol{\rho}) + \phi^{\text{ind}}(\boldsymbol{\rho}) \tag{2.27}$$

which contains both the external and induced parts of potential. From Eq. (2.25), the

Fourier transform of Eq. (2.27) in $\mathbf{q}$ space is

$$\phi(\mathbf{q}) = \frac{1}{2\varepsilon_0 q}\left[\sigma^{\text{ext}}(\mathbf{q}) + \sigma^{\text{ind}}(\mathbf{q})\right]. \tag{2.28}$$

By substituting Eq. (2.26) for σ^{ind} in Eq. (2.28), one can relate the external charge or

number density to the total electric potential

$$\phi(\mathbf{q}) = \frac{1/2\varepsilon_0 q}{1 + k_0/q}\sigma^{\text{ext}}(\mathbf{q}) = \frac{-e}{2\varepsilon_0(q + k_0)}n^{\text{ext}}(\mathbf{q}), \tag{2.29}$$

with $k_0 \equiv \frac{e^2}{2\varepsilon_0}\frac{\partial n_0}{\partial \mu}$ the reciprocal of screening length. In the spatial asymptotic regime of

the external charge location, the screening is dominated by $\mathbf{q} = 0$ behavior. While $\mathbf{q} = 0$,

we obtain

$$\phi(\boldsymbol{\rho}) = -\left(e\frac{\partial n_0}{\partial \mu}\right)^{-1}n^{\text{ext}}(\rho). \tag{2.30}$$

In 2D system, the density of states is

$$\frac{\partial n_0}{\partial \mu} = \frac{m^*}{\pi \hbar^2} \,.$$

Therefore, the final induced potential by the charge accumulation is given by

$$\phi(\boldsymbol{\rho}) = -\frac{\pi \hbar^2}{em^*} \, n^{\text{ext}}(\boldsymbol{\rho}) \,. \tag{2.31}$$

2.3.4 Definition of the strength of the residual resistivity dipole

From Eq. (2.23) and Eq. (2.30), the RRD potential is given by

$$\delta\phi(\boldsymbol{\rho}) = \frac{2E_0 \hbar k_\mu \tau}{m^*} \cos \phi_\rho \, \text{Im} \sum_{l=0}^{\infty} R_l(\rho) R_{l+1}^*(\rho). \tag{2.32}$$

Therefore, we can identify the RRD from Eq. (2.32). From Eq. (2.6) we can see that Bessel
function is proportional to $\rho^{-1/2}$ in the asymptotic region, and therefore the potential in
Eq. (2.32) is proportional to ρ^{-1}. Hence Eq. (2.32) indicates a 2D electric dipole potential.
After averaging away the Friedel oscillation and in the asymptotic region,

$$\delta\phi(\boldsymbol{\rho}) \sim p_{\text{c}} \, \frac{\cos \phi_\rho}{\tilde{\rho}} \,, \tag{2.33}$$

where p_{c} corresponds to the RRD strength written as

$$p_{\text{c}} = -\frac{E_0 \hbar \tau}{2\pi m^*} \, k_\mu \sigma_{\text{tr}} \,. \tag{2.34}$$

Here $\tilde{\rho} = k^* \rho$ is a dimensionless ρ, k_μ is the wave number corresponding to μ, and

$$\sigma_{\text{tr}} = \frac{4}{k_\mu} \sum_{l=0}^{\infty} \sin^2 (\delta_l - \delta_{l+1}), \tag{2.35}$$

is exactly the transport cross section of the scattering potential, being defined as

$$\sigma_{\text{tr}} \equiv \int_{-\pi}^{\pi} d\phi \, (1 - \cos \phi) \, D(\phi). \tag{2.36}$$

Eq. (2.36) describes the extent in which the electron population is deflected by the potential and plays the role of reflectance in 1d system. The forward scattering is strong, or reflection is small, when σ_{tr} is small. Meanwhile, the larger σ_{tr} is, the more the particles are scattered into every directions.

2.4 Resonance generation of RRD around a ring-shaped structure

Units

In the following expressions, all the physical quantities are dimensionless in units according to a typical carrier concentration n_e. The wave number is in units of $k^* = \sqrt{2\pi n_e}$, where $n_e = 7.4 \times 10^{11} \, \text{cm}^{-2}$ is the typical carrier concentration; The system chemical potential is in units of $E^* = \hbar^2 k^{*2}/2m^*$, and length is in $1/k^*$.

Ring-shaped step potential

We consider a ring-shaped square potential barrier, described by step functions,

$$V(\rho) = V_0[\theta(\rho - a) - \theta(\rho - b)], \tag{2.37}$$

where a, b and V_0 are inner, outer radii and the potential energy height, respectively. No in-plane potential gradient SOI is included here. With this simple model of a ring-shaped potential Eq. (2.37), the radial wave function can be exactly solved, for $\varepsilon > V_0$,

$$R_l(\rho) = \begin{cases} C_l J_l(k\rho), & \rho \leq a \\ A_l \left[J_l(\kappa\rho) - B_l Y_l(\kappa\rho) \right], & a < \rho \leq b \\ e^{i\delta_l} \left[\cos\delta_l J_l(k\rho) - \sin\delta_l Y_l(k\rho) \right], & \rho > b \end{cases} \tag{2.38}$$

with $\kappa = \sqrt{2m^*|\varepsilon - V_0|}/\hbar$. For $\varepsilon < V_0$, the Bessel functions $J_l(\kappa\rho)$, $Y_l(\kappa\rho)$ in the region $a < \rho \leq b$ ought to be substituted by the modified Bessel functions, $I_l(\kappa\rho)$, $K_l(\kappa\rho)$, respectively. The undetermined coefficient B_l and δ_l can be obtained via matching the boundary condition of the radial derivatives $\rho \left(d \ln R_l/d\rho \right)$ at the inner and outer edges of the scattering potential. At $\rho = a$,

$$B_l = \frac{\kappa a J_l'(\kappa a) - \gamma_l J_l(\kappa a)}{\kappa a Y_l'(\kappa a) - \gamma_l Y_l(\kappa a)},$$

where $\gamma_l \equiv ka J_l'(ka)/J(ka)$; at $\rho = b$, we obtain

$$\delta_l = \tan^{-1} \left[\frac{kb J_l'(kb) - \beta_l J_l(kb)}{kb Y_l'(kb) - \beta_l Y_l(kb)} \right], \tag{2.39}$$

where $\beta_l \equiv \kappa b \left[J_l'(\kappa b) - B_l Y_l'(\kappa b) \right] / \left[J_l(\kappa b) - B_l Y_l(\kappa b) \right]$.

One can obtain the amplitudes of partial waves A_l and C_l by simply matching the function values R_l at each boundary. At $\rho = b$,

$$A_l = \frac{e^{i\delta_l} \left[\cos\delta_l J_l(kb) - \sin\delta_l Y_l(kb) \right]}{J_l(\kappa b) - B_l Y_l(\kappa b)};$$

at $\rho = a$,

$$C_l = \frac{A_l \left[J_l(\kappa a) - B_l Y_l(\kappa a) \right]}{J_l(ka)};$$

The radial function $R_l(\rho)$ is completely solved.

In the following we review conventional resonance phenomena involving atomic scattering, and then discuss the resonant behavior of the strength of RRD.

We now discuss properties of phase shift through the expression Eq. (2.39). First of all, δ is well defined within an interval of π. The partial wave analysis can also be of help to explain resonance phenomena of the total scattering cross section. From the optical theorem, or directly integrating the differential cross section $D(\phi)$ with respect to ϕ, the total cross section is given by

$$\sigma_{\text{tot}} = \frac{1}{k} \sum_{l=-\infty}^{+\infty} \sin^2 \delta_l. \tag{2.40}$$

For a ring-shaped potential barrier, the dependence of σ_{tot} on the Fermi energy exhibits resonant peak structures. At a certain resonance energy, there shows an enhancement peak of σ_{tot}. It can be shown that the resonant peak is due solely to on phase shift term in Eq. (2.40). The resonance occurs only when the phase shift of the dominant partial wave crosses $n\pi/2$ (n is odd integer) with positive $d\delta_l/d\varepsilon$ [30].

Furthermore, the resonant energy is found to correspond to the bound state energy set up within a cylindrical disc of radius a, the inner radius. Fig. 2.2 shows, in the upper diagram, energy levels of a infinite circular disc well with radius a. The energy levels are labeled by (n, l) where n is the radial quantum number and l the azimuthal quantum number. Levels of the same l are indicated by the same color. The lower diagram of Eq. (2.2) shows the μ dependence of the phase shift δ_l. The resonant structures in δ_l are connected by arrows, and resonances of the same l have the same color. It can be seen that, even the energy levels in the upper diagram do not align exactly with the resonant energies in the lower diagram, they do correspond well in the color and all shows red shift
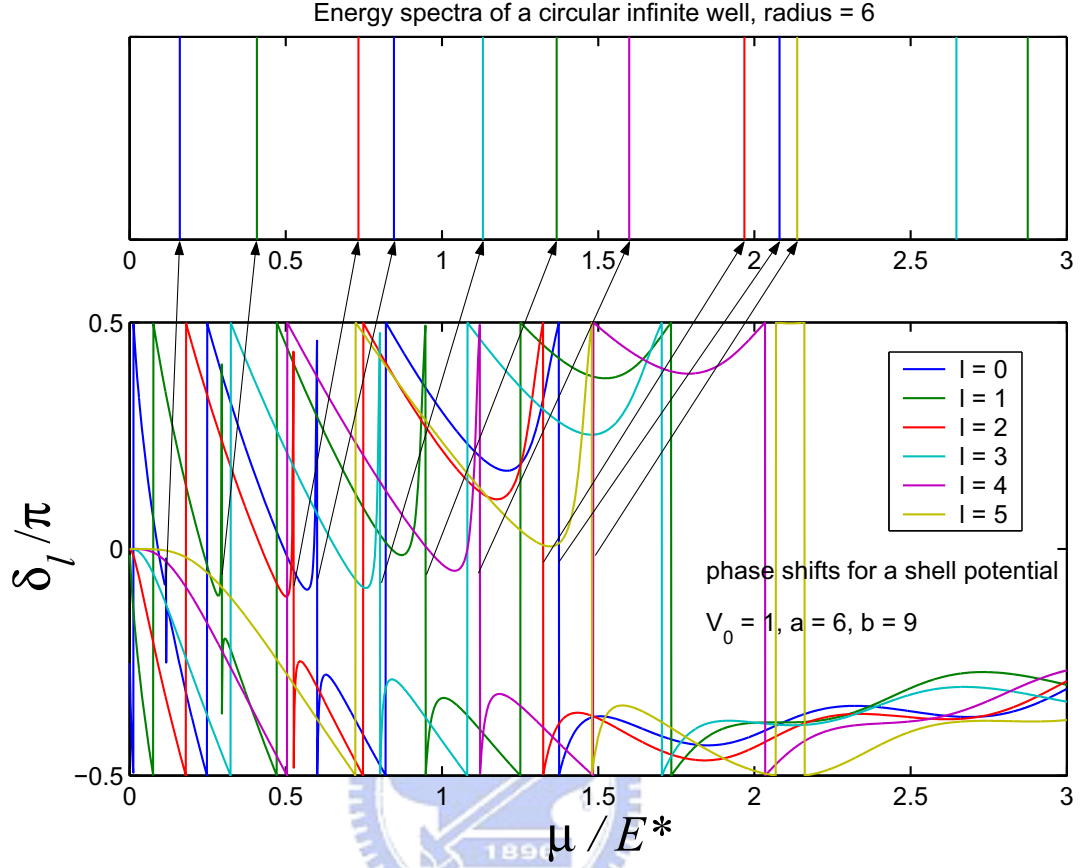
Figure 2.2: Energy spectra of an infinite circular well and phase shifts versus the chemical potential for a ring-shaped step potential barrier with parameters: $V_0 = 1$ the potential height, $a = 6$ the inner radius, and $b = 9$ the outer radius.

in the resonant energies. Thus we have established the physical origin of the resonances, and we can label them with a set of resonance numbers (n, l), associated with the quantum numbers in a disk-shaped infinite well. The physical origin of the resonances looks like to be that when the resonance occurs, the incident wavelength of certain electron partial waves match some characteristic resonant lengths that fits the geometry of the ring.

As for the RRD, Eq. (2.3) shows that the RRD strength exhibits dip structures at resonant energies. For the purpose of clarifying the physical picture, we choose a ring-shaped structure of a smaller radius with parameters: inner, outer radii $a = 6$, $b = 9$, respectively. The potential height $V_0 = 1$. All of parameters are in the chosen units mentioned previously. In the Fig. 2.3, we plot the quantity $k\sigma_{\mathrm{tr}}$ versus the chemical potential of the
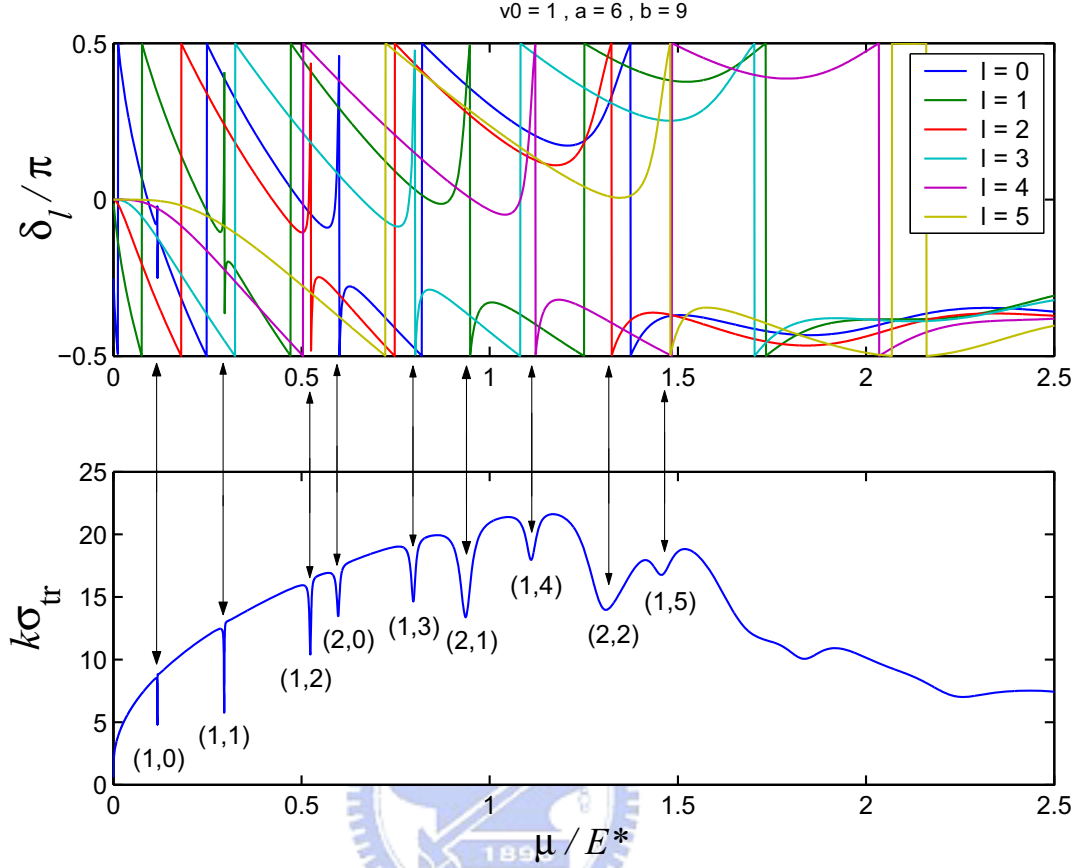
Figure 2.3: $k\sigma_{\rm tr}$ versus the chemical potential with parameters of a ring-shaped step
potential barrier: the potential height $V_0 = 1$, the inner radius $a = 6$, and the outer
radius $b = 9$.

system because the dimensionless quantity $k\sigma_{\rm tr}$ can represent the charge dipole strength.
The dip structures at resonances imply that when resonance occurs, the pile up of charges
is smaller. This can be explained by the transport differential cross section $\sigma_{\rm tr}$ and the
reminiscent of the resonance behavior in one dimensional scattering on a double barrier
structure. When $\sigma_{\rm tr}$ is small, according to the definition of it Eq. (2.36), the forward
scattering is strong, that is, the particles encounters little impediment so that few parti-
cles are deflected into any other directions but the forward one. The small impediment
also implies a small pile up of charges, small potential drop, and most importantly, low
resistance around the ring-shaped structure.

In Fig. 2.3, the overall trend of $\sqrt{\mu}$ in the RRD strength near the low μ regime, i.e.

$\mu \leq V_0$, is because the nonequilibrium part of distribution $g(\mathbf{k})$ is linear in k, and thus
the strength is a square root in energy, except at resonance structures.

2.5 Brief summary

Thus far in this chapter, we reviewed the theoretical formalism for Landuaer's RRD and
analyzed its resonance around a repulsive, ring-shaped step potential within the ballistic
range. The resonance dips structures in the $k\sigma_{\text{tr}}$ characterizing RRD strength which
has an analog of 1D resonant tunneling through a double barrier. The position of the
resonant dips below for electron energy lower than the potential barrier height is found
to correspond with the quantized energy levels, labeled by quantum numbers (n, l), for a
circular disk of radius a.

Chapter 3

Residual resistivity dipole and spin dipole in the presence of spin-orbit interaction arising from in-plain potential gradient of a microstructure

The main focus in this chapter is to explore the significance of the spin-orbit interaction arising from the in-plane potential gradient. Towards this end, we consider a ring-shaped potential profile as an explicit example. The SOI effect from the in-plane potential gradient to the Landauer RRD and the spin accumulation in driving electric field will be studied.

We first present the spin dependent quantum scattering calculation and then make use of the symmetry properties in the phase shifts to arrive at an analytical forms of the charge RRD and the spin dipole that shows explicitly the dipole features as well as their orientations.

3.1 Spin dependent asymmetric scattering in the presence of SOI

The Hamiltonian of the system, together with a spin-orbit potential arising from the in-plane gradient of the scattering potential in 2D, is written as

$$H = \frac{p^2}{2m^*} + V(\rho) + \frac{\lambda}{\hbar}\frac{1}{\rho}\frac{dV(\rho)}{d\rho}\sigma_z L_z\,, \tag{3.1}$$

where $V(\boldsymbol{\rho}) = V(\rho)$ is the cylindrical symmetric potential from the ring-shaped microstructure. The third term of H causes spin dependent scattering because of the presence of the Pauli matrix σ_z but it does not cause spin flipping if we choose our basis spin states in the $\hat{\mathbf{z}}$ direction.

Taking on a step-like profile, the ring-shaped potential $V(\rho) = V_0\left[\theta(\rho - a) - \theta(\rho - b)\right]$ gives rise to the SOI term

$$H_{\text{SO}} = \frac{\lambda}{\hbar}\frac{1}{\rho}\left[\delta(\rho - a) - \delta(\rho - b)\right]\sigma_z L_z. \tag{3.2}$$

The total wave function for an electron incident along arbitrary direction $\hat{\mathbf{k}}$ and in spin state χ_σ is written as $\Psi_{\mathbf{k}\sigma}(\boldsymbol{\rho}) = \psi_{\mathbf{k}}^\sigma(\boldsymbol{\rho})\chi_\sigma$, where

$$\psi_{\mathbf{k}}^\sigma(\boldsymbol{\rho}) = \sum_{l=-\infty}^{+\infty} i^l R_l^\sigma(\rho)e^{il(\phi_\rho - \phi_k)}\,. \tag{3.3}$$

Here $\sigma_z\chi_\sigma = \sigma\chi_\sigma$. Substituting Eq. (3.3) into the Schrödinger equation, the radial differential equation reads

$$\frac{1}{\rho}\frac{d}{d\rho}\rho\frac{dR_l^\sigma(\rho)}{d\rho} + \left\{k^2 - \frac{l^2}{\rho^2} - \frac{2m^*}{\hbar^2}\left[V(\rho) + l\sigma H_{\text{SO}}(\rho)\right]\right\}R_l^\sigma(\rho) = 0. \tag{3.4}$$

The radial function $R_l^\sigma(\rho)$ as well as its coefficients in the three radial regions are all spin

dependent, that is, depend on the index σ, and are given by

$$
R_l^\sigma(\rho) =
\begin{cases}
C_l^\sigma J_l(k\rho), & \rho \le a \,, \\[2mm]
A_l^\sigma \left[J_l(\kappa\rho) - B_l^\sigma Y_l(\kappa\rho) \right], & a < \rho \le b \,, \\[2mm]
e^{i\delta_l^\sigma} \left[\cos\delta_l^\sigma J_l(k\rho) - \sin\delta_l^\sigma Y_l(k\rho) \right], & \rho > b \,.
\end{cases}
\tag{3.5}
$$

For incident energy ε, we have $\varepsilon = \frac{\hbar^2 k^2}{2m^*}$, and in the barrier region, we have $\varepsilon = V_0 + \frac{\hbar^2 k^2}{2m^*}$.

Since H_{SO} is nonzero only at the inner and the outer radii, namely, $\rho = a, b$, respectively, the boundary condition that bring forth the spin degeneracy is given by

$$
\begin{aligned}
\frac{\rho}{R_l^\sigma} \frac{dR_l^\sigma}{d\rho} \bigg|_{\rho=a^+} &= \frac{\rho}{R_l^\sigma} \frac{dR_l^\sigma}{d\rho} \bigg|_{\rho=a^-} + \frac{2m^* V_0 \lambda l \sigma}{\hbar^2}; \\
\frac{\rho}{R_l^\sigma} \frac{dR_l^\sigma}{d\rho} \bigg|_{\rho=b^+} &= \frac{\rho}{R_l^\sigma} \frac{dR_l^\sigma}{d\rho} \bigg|_{\rho=b^-} - \frac{2m^* V_0 \lambda l \sigma}{\hbar^2}.
\end{aligned}
\tag{3.6}
$$

The coefficient B_l^σ is given by,

$$
B_l^\sigma = \frac{\kappa a J_l'(\kappa a) - \gamma_l^\sigma J_l(\kappa a)}{\kappa a Y_l'(\kappa a) - \gamma_l^\sigma Y_l(\kappa a)},
$$

where

$$
\gamma_l^\sigma = \frac{k a J_l'(ka)}{J_l(ka)} + \frac{2m^* V_0 \lambda l \sigma}{\hbar^2} \,.
$$

The phase shift is obtained to be

$$
\delta_l^\sigma = \tan^{-1} \left[\frac{kb J_l'(kb) - \beta_l^\sigma J_l(kb)}{kb Y_l'(kb) - \beta_l^\sigma Y_l(kb)} \right],
$$

where

$$
\beta_l^\sigma = \frac{\kappa b \left[J_l'(\kappa b) - B_l^\sigma Y_l'(\kappa b) \right]}{J_l(\kappa b) - B_l^\sigma Y_l(\kappa b)} - \frac{2m^* V_0 \lambda l \sigma}{\hbar^2} \,.
$$

Finally, by imposing the condition that wave function is continuous, we obtain the coef-

ficients A_l^σ and C_l^σ, given by

$$A_l^\sigma = \frac{e^{i\delta_l^\sigma}\left[\cos\delta_l^\sigma J_l(kb) - \sin\delta_l^\sigma Y_l(kb)\right]}{J_l(\kappa b) - B_l^\sigma Y_l(\kappa b)};$$

and

$$C_l^\sigma = \frac{A_l^\sigma\left[J_l(\kappa a) - B_l^\sigma Y_l(\kappa a)\right]}{J_l(ka)}.$$

We note in passing that in the low energy situation, when $\varepsilon < V_0$, Bessel functions $J_l(\kappa\rho)$, $Y_l(\kappa\rho)$ are replaced by modified Bessel functions $I_l(\kappa\rho)$, $K_l(\kappa\rho)$, respectively.

The effect of H_{SO} is to lift the spin degeneracy such that the differential cross section becomes $D_\sigma(\phi) = |f_\sigma(\phi)|^2$, where the spin-dependent scattering amplitude is given by

$$f_\sigma(\phi) \equiv \sqrt{\frac{2i}{\pi k}} \sum_{l=-\infty}^{+\infty} e^{i\delta_l^\sigma}\sin\delta_l^\sigma e^{il\phi}. \tag{3.7}$$

3.1.1 Two useful relations

Two important symmetry properties int he phase shift and the radial wave function are to be presented in this section. The first symmetry can be seen from Eq. (3.6), when the spin dependent term, the second term on the right-hand side, involves a product $l\sigma$ of the orbital and the spin quantum number. Thus we must have the symmetry

$$\delta_{-l}^\sigma = \delta_l^{-\sigma}, \ \ \text{or} \ \ \delta_{-l}^{-\sigma} = \delta_l^\sigma. \tag{3.8}$$

Another symmetry relation is a direct consequence of the δ_l^σ symmetry. The radial wave function is related to δ_l^σ via Bessel functions. For instance, outside the range of the potential $V(\rho)$, the radial function is given by

$$R_l^\sigma(\rho) = e^{i\delta_l^\sigma}\left[\cos\delta_l^\sigma J_l(k\rho) - \sin\delta_l^\sigma Y_l(k\rho)\right].$$

The Bessel functions has a symmetry relation for l

$$Z_{-l}(x) = (-1)^l Z_l(x),$$

where $Z_l(x)$ stands for any one of the two kinds of Bessel functions. Thus imposing both

the symmetry properties in the phase shift and the Bessel function to $R_l^\sigma(\rho)$, we have

$$R_{-l}^\sigma(\rho) = (-1)^l R_l^{-\sigma}(\rho), \text{ or } R_{-l}^{-\sigma}(\rho) = (-1)^l R_l^\sigma(\rho). \tag{3.9}$$

This two symmetry relations Eq. (3.8) and Eq. (3.9) are useful for putting our expression, in the next section, for the RRD and spin dipole into elegant and physically most transparent forms.

3.2 Residual resistivity dipole in the presence of local structure SOI

Following similar procedure for obtaining the charge accumulation in Eq. (2.18), except here the spin degeneracy is lifted, we write down the total charge accumulation $n(\boldsymbol{\rho})$ as follows

$$\begin{aligned}
n(\boldsymbol{\rho}) &= \frac{1}{4\pi^2} \int d\mathbf{k}\, f(\mathbf{k}) \sum_\sigma \Psi_{\mathbf{k}\sigma}^\dagger(\boldsymbol{\rho}) \Psi_{\mathbf{k}\sigma}(\boldsymbol{\rho}) \\
&= n_{\text{eq}}(\boldsymbol{\rho}) + \delta n(\boldsymbol{\rho}),
\end{aligned}$$

where

$$\delta n(\boldsymbol{\rho}) = -\frac{e\tau E_0 k_\mu}{\pi\hbar} \cos\phi_\rho \, \text{Im} \sum_\sigma \sum_{l=0}^\infty R_l^\sigma(\rho) R_{l+1}^{\sigma*}(\rho). \tag{3.10}$$

To obtain Eq. (3.10), we have to impose the symmetry relation given by Eq. (3.8) and

Eq. (3.9). With the T-F screening incorporated, the total potential becomes

$$\delta\phi(\boldsymbol{\rho}) = \frac{E_0 \hbar k_\mu \tau}{m^*} \cos\phi_\rho \, \mathrm{Im} \sum_\sigma \sum_{l=0}^\infty R_l^\sigma(\rho) R_{l+1}^{\sigma*}(\rho), \tag{3.11}$$

which is a dipole field form. The strength p_c of the charge dipole, again, is obtained from

the asymptotic region,

$$p_c = -\frac{E_0 \hbar \tau}{2\pi m^*} k_\mu \sigma_{\mathrm{tr}}, \tag{3.12}$$

where σ_{tr} is the transport cross section with removed spin degeneracy

$$\begin{aligned}
\sigma_{\mathrm{tr}} &\equiv \frac{1}{2} \int_{-\pi}^\pi d\phi \, (1 - \cos\phi) \sum_\sigma D_\sigma(\phi) \\
&= \frac{2}{k_\mu} \sum_\sigma \sum_{l=0}^\infty \sin^2\left(\delta_l^\sigma - \delta_{l+1}^\sigma\right).
\end{aligned}$$

3.3 Spin dipole due to spin-independent nonequilib-
rium incident distribution

In addition to Landauer's RRD, the presence of asymmetric Mott scattering [4], caused

by the SOI in the ring-shaped potential, should give rise to interesting spin accumulation.

The results of resonant scattering for the incident plane wave are in Appendix E. Following

similar procedure for the RRD calculation, the spin density, in units of $\hbar/2$, is given by

$$\begin{aligned}
S_z(\boldsymbol{\rho}) &= \frac{1}{4\pi^2} \int d\mathbf{k} \, f(\mathbf{k}) \sum_\sigma \sigma \, \Psi_{\mathbf{k}\sigma}^\dagger(\boldsymbol{\rho}) \Psi_{\mathbf{k}\sigma}(\boldsymbol{\rho}) \\
&= S_z^{\mathrm{eq}}(\boldsymbol{\rho}) + \delta S_z(\boldsymbol{\rho}),
\end{aligned}$$

where

$$S_z^{\text{eq}}(\boldsymbol{\rho}) = \frac{1}{4\pi^2} \int d\mathbf{k} f_0(k) \sum_\sigma \sigma \, |\psi_\mathbf{k}^\sigma(\boldsymbol{\rho})|^2 \,.$$

That the equilibrium spin accumulation must be zero, $S_z^{\text{eq}} = 0$, identically can be shown by direct calculation. Simply that the equilibrium spin distribution is isotropic for each spin causes exact cancellation between opposite spin. The total spin accumulation is then determined solely by the nonequilibrium part

$$S_z(\boldsymbol{\rho}) = \delta S_z(\boldsymbol{\rho}) = \frac{1}{4\pi^2} \int d\mathbf{k} \, g(\mathbf{k}) \sum_\sigma \sigma \, |\Psi_{\mathbf{k}\sigma}(\boldsymbol{\rho})|^2 \,.$$

Again, making use of the symmetry properties in Eq. (3.8) and Eq. (3.9), we get

$$S_z(\boldsymbol{\rho}) = n_E \sin\phi_\rho \, \text{Re} \sum_\sigma \sigma \sum_{l=0}^\infty R_l^\sigma(\rho) R_{l+1}^{\sigma*}(\rho), \tag{3.13}$$

by the use of relation Eq. (3.9). The factor $n_E = \frac{eE_0 \tau k_\mu}{\pi\hbar}$ has the dimension of density, linear in E_0, and with an energy dependence via k_μ. The momentum relaxation time τ is assumed to be a constant, independent of energy. The angular dependence, $\sin\phi$, of the spin density $S_z(\boldsymbol{\rho})$ indicates a dipole-like distribution, aligned perpendicular to the driving field $\mathbf{E}$. This expression of spin accumulation holds within a radial distance shorter than the mean free path.

The screening of spin is assumed to be negligible because of the spin-spin interaction between electrons. As in the charge dipole case, we can define a spin dipole strength from the asymptotic form of the spin accumulation,

$$S_z(\boldsymbol{\rho}) \sim p_\text{s} \frac{\sin\phi_\rho}{\tilde{\rho}}, \tag{3.14}$$

where $\tilde{\rho} \equiv k^* \rho$ is the dimensionless radial coordinate, and p_s is the spin dipole strength.

The expression for p_s is

$$p_\text{s} = -\frac{\tilde{n}_E}{2\pi} k_\mu \sigma_\perp, \tag{3.15}$$

where

$$\sigma_\perp \equiv \frac{1}{2} \int_{-\pi}^{+\pi} d\phi \sin \phi \sum_\sigma \sigma D_\sigma(\phi) \tag{3.16}$$

is essentially the transverse moment of the net spin differential cross section, which we may call the **transverse transport cross section**. In terms of phase shifts,

$$\sigma_\perp = \frac{1}{k_\mu} \sum_\sigma \sigma \sum_{l=0}^{\infty} \sin[2(\delta_l^\sigma - \delta_{l+1}^\sigma)]. \tag{3.17}$$

The constant factor $\tilde{n}_E = \frac{m^* e E_0 l_0^*}{\pi \hbar^2}$, where $l_0^* = \hbar k^* \tau / m^*$, is the product of the 2d density of state $\frac{m^*}{\pi \hbar^2}$ and the work done by the electric field within the range of mean free path $e E_0 l_0^*$. The minus sign appearing in Eq. (3.15) indicates that the direction of electron motion is opposite to **E**. As the electric field is driving in positive x-direction, the electron is driven in the negative x-direction and therefore the orientation of the spin dipole is opposite to that of $k\sigma_\perp$.

3.3.1 Second-order correction to the spin dipole strength at resonance

The radial dependence of S_z for typical physical parameters is shown in Fig. 3.1. The exact numerical result is given by the solid curve, the asymptotic form, Eq. (3.14), is given by the dashed curve, whereas the dot-dashed curve denotes results that goes beyond the usual asymptotic from, and has included a correction term. It is clearly shown that the
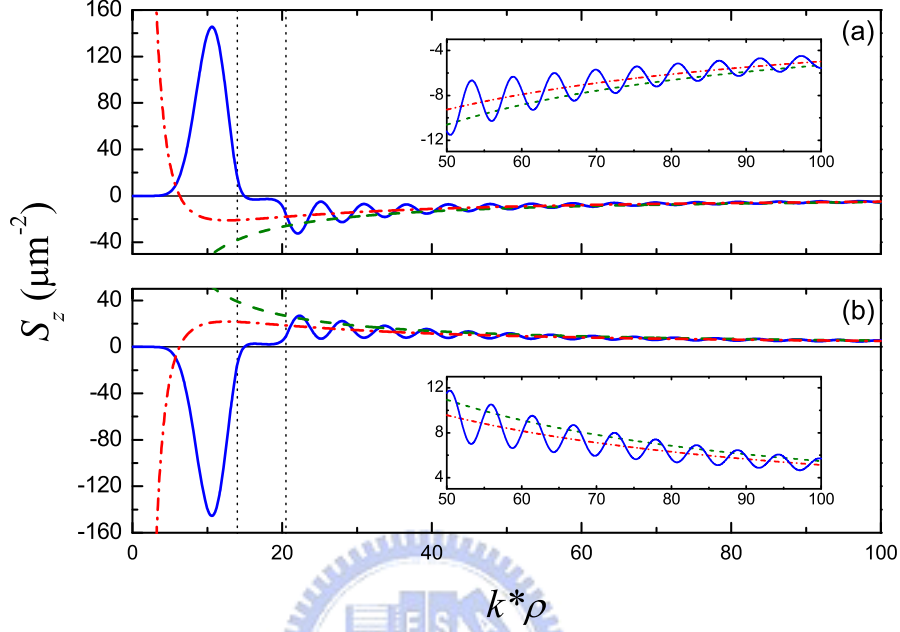
Figure 3.1: Radial variation of $S_z(\boldsymbol{\rho})$ along $\phi_\rho = \pi/2$ at the two resonant energies (a) $\mu = 0.3312$, and (b) $\mu = 0.3328$ in the resonance pair labeled (1,5). The green dashed curve is $p_s/k^*\rho$; the red dot-dashed curve includes the 2nd-order correction $\wp_s$. The geometry of the ring: the potential height $V_0 = 0.75$, the inner radius $a = 14$, and the outer radius $b = 20.5$.

corrected curve fits better. Thus

$$S_z \sim \frac{\sin \phi_\rho}{\tilde{\rho}} \left[p_s + \frac{\wp_s}{\tilde{\rho}} \right], \tag{3.18}$$

where

$$\wp_s = \frac{\tilde{n}_E}{4\pi} \, k^* \sigma'_\perp, \tag{3.19}$$

with

$$\sigma'_\perp = \frac{1}{k} \sum_\sigma \sigma \sum_{l=0}^\infty (2l+1) \cos \left[2(\delta_l^\sigma - \delta_{l+1}^\sigma) \right]. \tag{3.20}$$

It is still reasonable to use p_s for the representation of the spin dipole strength.

3.4   Resonance of charge and spin dipole in the presence of the SOI from the microstructure

In this section we discuss in detail the resonant features in the presence of SOI. First of all, the SOI lifts the spin degeneracy at the resonance. That is, to every resonance in the absence of SOI, we will have two resonances when SOI is introduced. This is shown in Fig. 3.2, when the phase shifts are plotted against electron energy μ. In the upper part of Fig. 3.2, the resonances denoted by the profile where the phase shift jumps from $\pi/2$ to $-\pi/2$, are for zero SOI (λ=0). In the lower part of Fig. 3.2, when $\lambda \neq 0$, the number of curves are doubled, representing the spin-split, and subsequently the number of resonant energies are doubled.

From the insight we obtained in Chapter 2, each resonance associated with quantum numbers (n, l) occurs because the incident wavelength of the l'th and the $-l$'th partial waves match certain characteristic resonant length (labeled by n) fitting the geometry of the ring. In the absence of the SOI, there is spin degeneracy in the resonant lengths of the l and the $-l$ partial waves with the same radial mode n. When the SOI is introduced, the spin degeneracy is lifted and hence the resonant energy in the phase shift is doubled. We can see from Fig. 3.2 that the energies at which the phase shifts jump from $\pi/2$ to $-\pi/2$ are different for the l'th and the $-l$'th partial waves.

3.4.1   Resonant asymmetric skew scattering

Asymmetric scattering near a resonant energy shows interesting characteristics. As the asymptotes of the scattered wave is related to the differential scattering cross section, it becomes spin dependent here, and the resonant energies are spin-split. If we want to define a quantity representing the extent of lateral deflection in the scattering wave, the
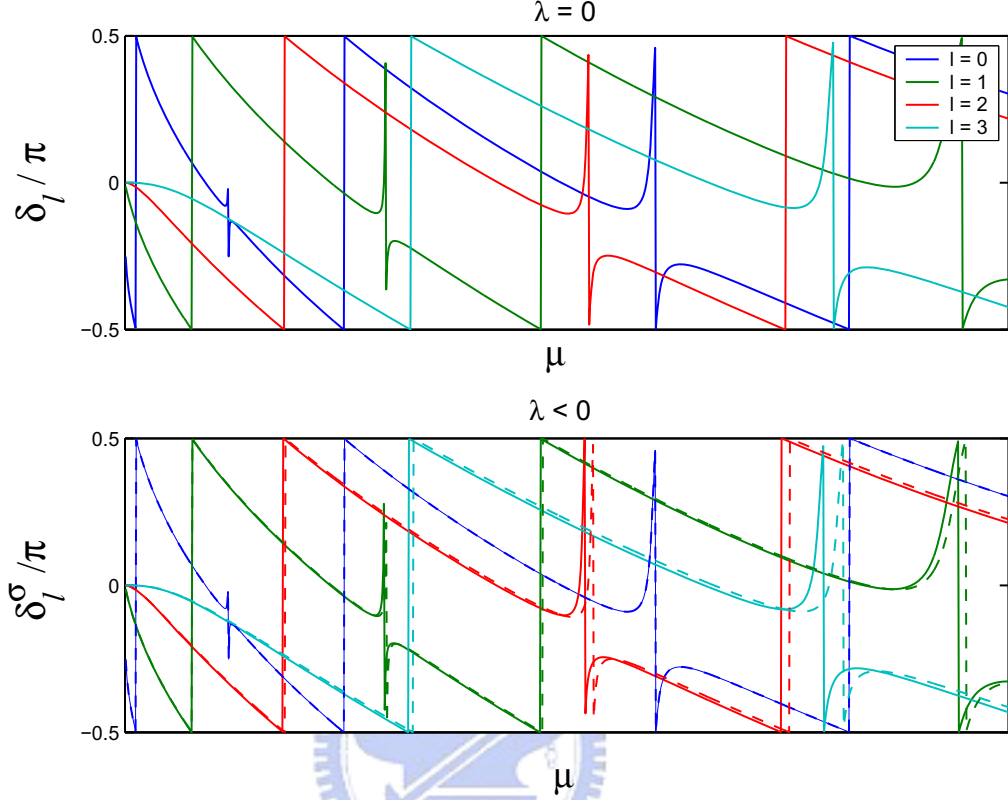
Figure 3.2: Qualitative sketch of the phase shift in the presence SOI: for the up-spin
partial waves, the solid curves in the lower plot is for positive l, and the dashed curves
are for negative l; or equivalently, for partial waves with positive l, the solid curves are
for up-spin waves, and the dashed curves are for down-spin waves.

following moment is a good choice

$$\sigma_\perp^\eta \equiv \int_{-\pi}^{\pi} d\phi \sin \phi D_\eta(\phi) \tag{3.21}$$

where $\eta = \pm$ stands for the spin state, along $\hat{\mathbf{z}}$, of the incident electron. Expressed in
terms of phase shifts, we have

$$\sigma_\perp^\eta = \frac{1}{k} \sum_{l=0}^{\infty} \left\{ \sin[2(\delta_l^\eta - \delta_{l+1}^\eta)] - \sin[2(\delta_{-l}^\eta - \delta_{-(l+1)}^\eta)] \right\}. \tag{3.22}$$

If this integral is positive, the incoming electron will be scattered to its left, or positive y-direction, assuming $\hat{\mathbf{x}}$ is the incident direction. One can see from Eq. (3.22), that

$$\sigma_\perp^+ = -\sigma_\perp^- , \tag{3.23}$$

which implies that incident electrons with opposite spin-polarization along $\hat{\mathbf{z}}$ are deflected in opposite directions laterally. If there were no SOI, the spin degeneracy would be recovered, and $\sigma_\perp^\eta = 0$ for both spin states, as it should be. The expression for $\sigma_\perp^\eta$, according to Eq. (3.22), contains the difference of two terms, each is a summation over l, but with $l \geq 0$ and $l \leq 0$, separately. If we have an amplification of $k\sigma_\perp^\eta$ at the energy $E_{n,+l}^\eta$, we should have similar amplification, but of the opposite sign, at the energy $E_{n,-l}^\eta$, according to Eq. (3.22). We plot individually the two terms that constitutes $k\sigma_\perp^+$, as shown in Fig. 3.3. We see from Fig. 3.3 that the positive-l curve, denoted by the red curve, has peak structures; the negative-l curve, as denoted by the blue curve, has peak structures as well but is shifted in energy relative to the red curve. The black curve denotes $k\sigma_\perp^+$, which is the difference of the blue and the red curves.

3.4.2 Resonant RRD in the presence of the SOI

The resonant dip structures of charge dipole strength are spin-split, as shown in Fig. 3.4. The resonant energy ε_{nl}^0 is split into $\varepsilon_{n,\pm l}^\sigma$ so that a dip structure in the RRD strength, or $k\sigma_{\mathrm{tr}}$, becomes double dips. This is clearly seen in the (1,2), (1,3) and (1,4) structures in the upper curve of Fig. 3.4. The split in energy $\left|\varepsilon_{n,+l}^\sigma - \varepsilon_{n,-l}^\sigma\right|$ is larger for larger l. This is reasonable because the spin dependent term in Eq. (3.6) in creases with l. For the sake of simplifying the notation, we denote each spin-split resonant pair by (n,l), the resonant number for the mother resonant dip in $k\sigma_{\mathrm{tr}}$.
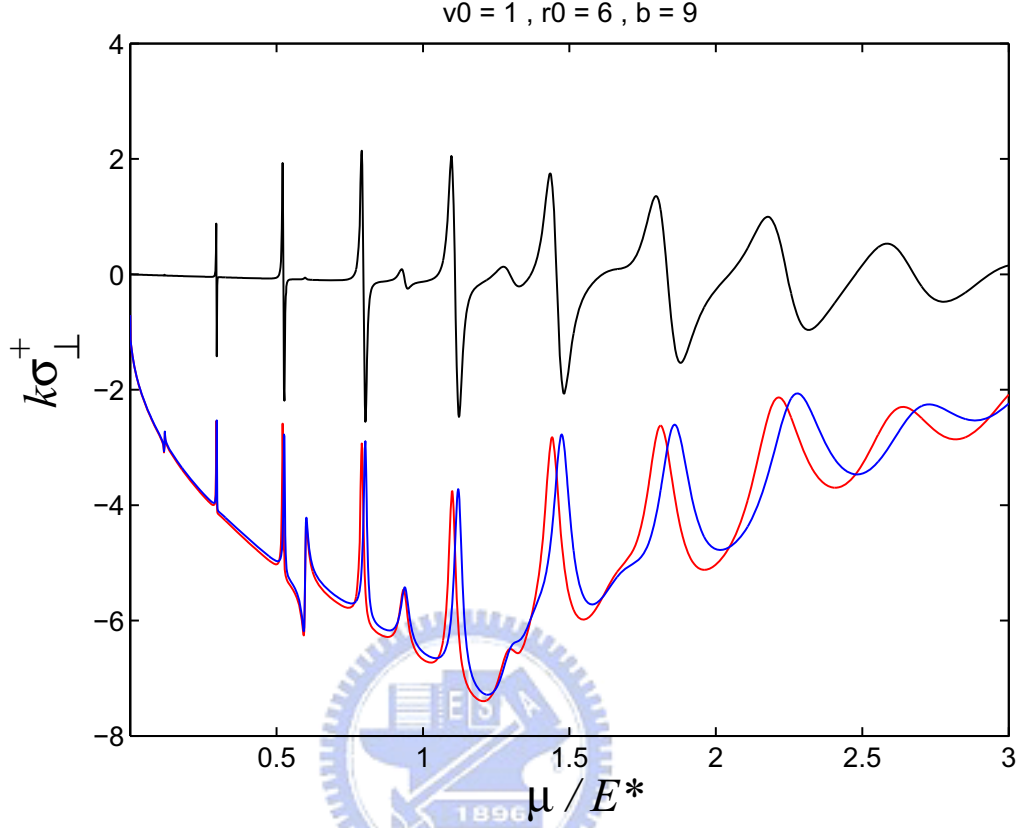
Figure 3.3: $\sigma_\perp^+$ versus system energy: the red curve denotes the summation over positive l, $\sum_{l=0}^{\infty} \sin[2(\delta_l^+ - \delta_{l+1}^+)]$; the blue curve stands for the summation over negative l, $\sum_{l=0}^{\infty} \sin[2(\delta_{-l}^+ - \delta_{-(l+1)}^+)]$; the total $\sigma_\perp^+$ is denoted by the black curve.

3.4.3   Resonance of spin dipole

In this section, we present the resonant characteristics of the spin dipole. The spin dipole strength is shown to manifest large enhancement and sign reversal at resonance.

From the lower curve of Fig. 3.4, the resonant features in the spin dipole strength, or $k\sigma_\perp$, is shown to carry a peak-dip structure. To show that this resonant feature is indeed remarkable, we plot, for comparison, the spin dipole strength due to a potential disc with the same outer radius a, but having the inner radius $b = 0$. Denoted by the red line in the $k\sigma_\perp$ curve in Fig. 3.4, this line matches very well with the ring-shaped potential result in the non-resonant and low energy regions. From this we also see that quantum resonance has lead to very large enhancement in the spin dipole strength. Furthermore,
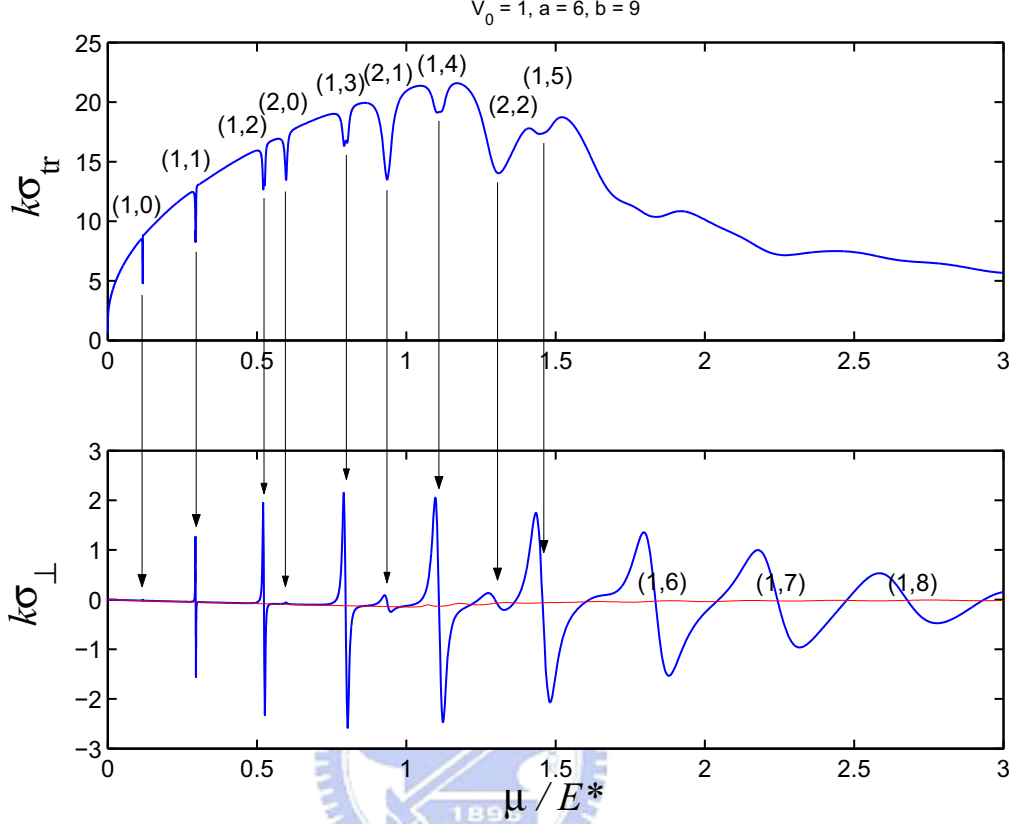
Figure 3.4: $k\sigma_{\mathrm{tr}}$ (the upper plot) and $k\sigma_\perp$ (the lower plot) versus the chemical potential μ with parameters of a ring-shaped step potential barrier: the potential height $V_0 = 1$, the inner radius $a = 6$, and the outer radius $b = 9$. The red line in the lower plot is $k\sigma_\perp$ for a disk-shaped potential barrier with its radius equal to 9.

Fig. 3.4 contains two series of resonant peak-dip pairs. Labeled by (n,l), the first series is the $n = 1$ series, and starts from $l = 1$ at energy $\mu = 0.295$ (energy unit $E^* = 77.1\,\mathrm{meV}$). The second series is the $n = 2$ series, and starts from $l = 1$ at energy $\mu = 0.94$. There is no peak-dip resonant structures in $k\sigma_\perp$ for $l = 0$ because again, the spin dependent term in Eq. (3.6), vanishes for $l = 0$.

From definitions Eq. (3.16), Eq. (3.21) and the relation Eq. (3.23), we have

$$\sigma_\perp = \frac{1}{2}\left(\sigma_\perp^+ - \sigma_\perp^-\right) = \frac{1}{2}\left(\sigma_\perp^+ - \left(-\sigma_\perp^+\right)\right) = \sigma_\perp^+.$$

From $\sigma_\perp = \sigma_\perp^+$, and that the physical meaning of $\sigma_\perp^+$ is the lateral moment of the spin dependent differential scattering cross section, we have a better physical understanding
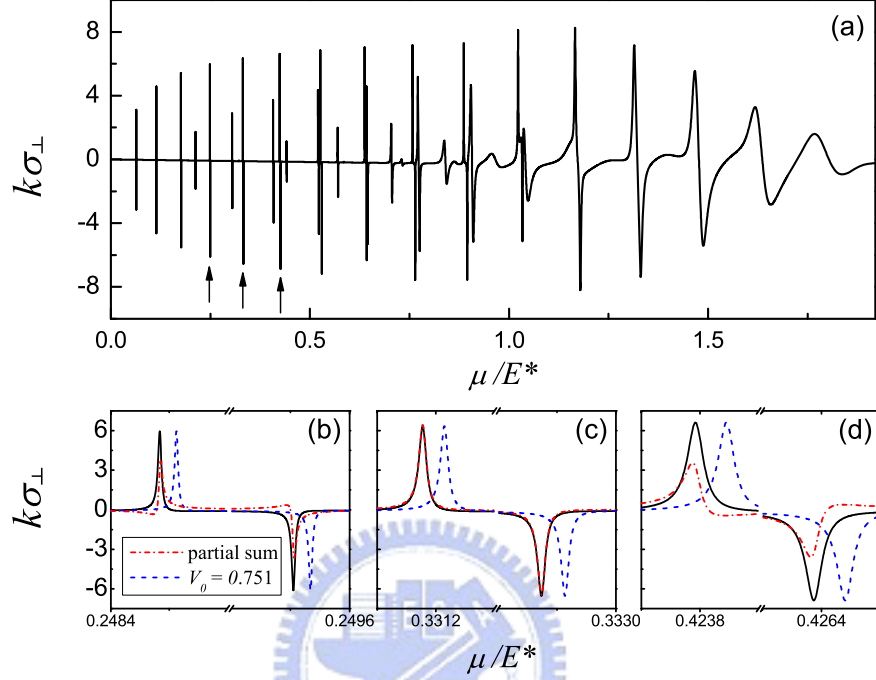
Figure 3.5: (a) $k\sigma_\perp$ versus the Fermi energy in units of $E* = 77.1\,\text{meV}$. Parameters of a ring-shaped step potential barrier: the potential height $V_0 = 0.75$, the inner radius $a = 14$, and the outer radius $b = 20.5$. (b)-(d) Blowups of the resonance pair labeled in the same series $n = 1$ and $l = 4, 5, 6$, respectively. The dot-dashed (red) curves are the partial summations of $k\sigma_\perp$ including only terms involving δ_5^σ. The dashed (blue) curves are $k\sigma_\perp$ for $V_0 = 0.751$. The smallest abscissa in (b)-(d) is 0.0001.

of the spin dipole, which strength is $k\sigma_\perp$.

In our numerical examples, physical parameters are chosen according to practical experimental situation and for the material InAs. Parameters units typical for InAs are: electron density $n_e^* = 7.4 \times 10^{11}\,\text{cm}^{-2}$; energy unit $E* = n_e^*\pi\hbar^2/m^* = 77.1\,\text{meV}$; $m^* = 0.023\,m_e$; $k^* = 2.16 \times 10^8\,\text{m}^{-1}$; length unit $L = 1/k^* = 46.3\,\text{Å}$. In these units, the ring-shaped potential has radii $a = 14$ and $b = 20.5$, and potential barrier height $V_0 = 0.75$; mean free path $l_0^* = 238$. The magnitude of electric field is $E_0 = 0.1\,\text{kV/cm}$. The spin dipole strength is fully characterized by $k\sigma_\perp$ except for a factor $-\tilde{n}_E/(2\pi) = -1.7 \times 10^{10}\,\text{cm}^{-2}$ which is in units of density.

In Fig. 3.5, the enhancement of spin dipole strength is large. Away from resonance, $|k\sigma_\perp| \approx 10^{-1}$, while at resonance its maximum magnitude can be reach up to 3.5. The factor of enhancement reaches to 70. The peak-dip series labeled by n is clearly shown here. Having the largest resonant enhancement, the $n = 1$ series starts from $\mu = 0.064$, with $l = 1$, and up to $l = 16$. The $n = 2$ series starts from $\mu = 0.213$ and $n = 3$ from $\mu = 0.44$. There are two other series, with smaller resonant enhancement, the $n = 2$ and $n = 3$ series, which starts at $\mu = 0.213$ and $\mu = 0.44$, respectively.

That the resonance features in $k\sigma_\perp$ are contributed by the energy dependence of phase shifts $\delta_l^\pm$ associated with one l only can be seen in Fig. 3.5 (b)-(d), which are blowups of Fig. 3.5 (a) at resonance pairs $(n = 1, l = 4, 5, 6)$. The solid curves are the full expression evaluation of Eq. (3.17); the dot-dashed (red) curves are partial summations including terms that only involves $l = 5$ in Eq. (3.17); and the dashed (blue) curves are full expression evaluation of Eq. (3.17) but for $V_0 = 0.751$. The dot-dashed (red) curve of partial summation matches very well with the (1,5) peak-dip structure while producing qualitative features for the peak-dip structures (1,4) and (1,6). The former confirms that each peak-dip resonant structure is contributed from terms in Eq. (3.17) associated with one l value only. The partial, or qualitative matches, in Fig. 3.5 (b) and (d) are due to the fact that the summation involving only $l = 5$ have included partial contribution from $l = 4$ and $l = 6$.

We comment on a general feature in a n-series of the peak-dip resonant structures. Peak-dip pairs in an series trace out an envelope which strength is increasing in low l and decreasing in high l. This demonstrates the competition between the trend of stronger SOI for larger l, and the weakening of the resonance due to the wider resonance width at energies higher than the potential height.

In Fig. 3.1, we present the radial variation of the spin density distribution $S_z(\boldsymbol{\rho})$, as is given in Eq. (3.13). Energies at (a) 0.3312, and (b) 0.3328, are the peak and dip energies, respectively, of the $(1, 5)$ resonance in Fig. 3.5 (a). The dashed curves are the asymptotes, given by the first term in Eq. (3.18), and the dashed-dot curves are the adjusted ones,

including the second term. Apart from the Friedel oscillations, the dash-dotted curves
traces the spin distribution outside the ring remarkably. Fig. 3.1 (a) and (b) reveal that
the sign of the spin density can be reversed by a small change in energy $\Delta\mu = 0.0016\,E^*$,
or 0.12 meV. The spin density at $\tilde{\rho} = 50$, or $\rho = 0.23\,\mu$m, is (a) $-9.276\,\mu$m^{-2}, and (b)
$9.568\,\mu$m^{-2}, or in terms of percentage of the electron density $n = 2.45 \times 10^{11}\,$cm^{-2}, the
spin density is (a) -3.79%, and (b) 0.39% of n, respectively. If we take the thickness of the
QW to be 100 Å, the 3D spin density becomes (a) $-928\,\mu$m^{-3}, and (b) $957\,\mu$m^{-3}, which is
certainly large enough for observation [31]. The spin density at $\tilde{\rho} = 100$, or $\rho = 0.46\,\mu$m
is half of the above results. Finally in Fig. 3.6, we present the full 2D dependence of the
spin dipole $S_z(\boldsymbol{\rho})$ for the case of $\mu = 0.3312$.

The proposed ring-shaped potential barrier pattern is expected to be within reach of
the present experimental capability. Such pattern can be fabricated by recently developed
focused ion/molecular beam epitaxy technique for the pattering of the δ-doped layer [32].
The assumed step-like profile in the ring-shaped potential might look oversimplified, but
it provide us a clear physical picture for the spin dipole formation. We have considered
smooth profile situations. The resonant feature remain intact. This will be discussed in
Chapter 5.

3.5   Brief summary

The effect of the in-plane potential gradient SOI has a relatively small effect on the
Landauer RRD. The resonance gives rise to double dip structures in the RRD strength.

However for the spin accumulation, the effect of in-plane potential gradient SOI has a
large impact on it. There is no spin accumulation without the presence of SOI. With the
SOI, quantum resonance leads to large spin dipole strength enhancement and also sign
changes. The spin dipole orients perpendicularly to the applied electric field.
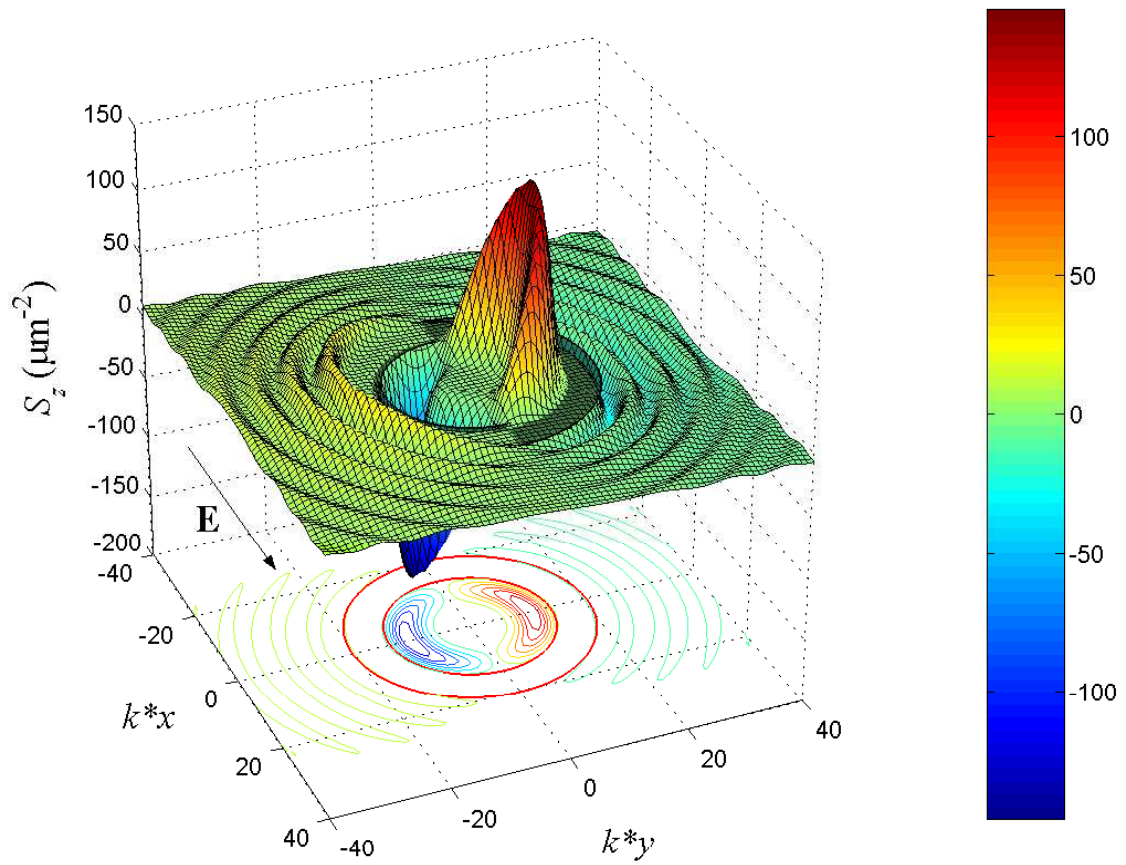
Figure 3.6: Spatial distribution $S_z(\boldsymbol{\rho})$ at the a resonant energy $\varepsilon = 0.3312$ with the geometry of the ring: the potential height $V_0 = 0.75$, the inner radius $a = 14$, and the outer radius $b = 20.5$. The electric field $\mathbf{E}$ is applied along positive x-direction.

Chapter 4

Spin dipole correction due to effect of extrinsic spin-orbit interaction

In this chapter we explore the correction to the spin dipole picture obtained in the previous chapter, if there are background spin-orbit scatterers (extrinsic SOI effect) in the system.

To obtain the electron distribution in the presence of these background scatterers, our procedure follows closely to that detailed in a paper by H.-A. Engel *et al.* [8] except that our derivation is 2D whereas the reference [8] is for 3D and they had mentioned 2D results in their footnote. Using this spin dependent nonequilibrium electron distribution, we obtain the spin dipole correction.

4.1 Differential cross section in terms of spin density operator

4.1.1 Density operator formalism

The density operator formalism is used for dealing with the ensemble of a quantum system via operators and wave functions characterizing the physical states.

The density operator is defined as

$$\hat{\rho} = \sum_i w_i |\alpha^{(i)}\rangle\langle\alpha^{(i)}|,$$

where $|\alpha^{(i)}\rangle$ could be any quantum state and the expectation values of the states $|\alpha^{(i)}\rangle$ is further weighted by the corresponding populations w_i. The ensemble average of a specific observable represented by an operator $\hat{A}$ is obtained by taking the trace of the matrix product of density operator $\hat{A}$ and density operator $\hat{\rho}$

$$\langle\hat{A}\rangle = \mathrm{tr}(\hat{\rho}\hat{A}),$$

given that the density operator should satisfy the normalization condition,

$$\begin{aligned}
\mathrm{tr}(\hat{\rho}) &= \sum_i \sum_a w_i \langle a|\alpha^{(i)}\rangle\langle\alpha^{(i)}|a\rangle \\
&= \sum_i w_i \langle\alpha^{(i)}|\alpha^{(i)}\rangle \\
&= 1,
\end{aligned}$$

otherwise the ensemble average of $\hat{A}$ should be modified to be

$$\langle\hat{A}\rangle = \frac{\mathrm{tr}(\hat{\rho}\hat{A})}{\mathrm{tr}(\hat{\rho})}.$$

Since the trace is independent of representations, $\mathrm{tr}(\hat{\rho}\hat{A})$ can be evaluated using any convenient basis. Observables can be expressed in terms of density operators as well, as will be shown in the following.

4.1.2 Spin dependent scattering cross section in terms of spin density operator

Any 2×2 matrix can be written as a linear combination of the identity and Pauli matrices. A state describing an incident flux of particles can be expressed in terms of a density

operator,

$$\hat{\rho} = a_0 \mathbf{1} + \mathbf{a} \cdot \boldsymbol{\sigma}.$$

The physical meaning of the constants a_0 is associated with the intensity of incident beam,
by using the relation $\text{tr}(\sigma_i \sigma_j) = \delta_{ij}$, we have

$$I = \text{tr}(\hat{\rho}) = 2a_0,$$

and $\mathbf{a} = (a_1, a_2, a_3)$ are simply related to the polarization of the beam, given by

$$\mathbf{P}_0 = \frac{\text{tr}(\hat{\rho}\boldsymbol{\sigma})}{\text{tr}(\hat{\rho})} = \frac{2\mathbf{a}}{I}.$$

Normalized to I, the particle beam with a polarization $\mathbf{P}_0$ can be expressed as

$$\hat{\rho} = \frac{I}{2}\left(1 + \mathbf{P}_0 \cdot \boldsymbol{\sigma}\right).$$

The scattering matrix in a 2d system is written as

$$\hat{S} = \begin{pmatrix} f_+(\phi) & 0 \\ 0 & f_-(\phi) \end{pmatrix},$$

where $f_\sigma(\phi)$ is the spin dependent scattering amplitude, and $\phi \equiv \phi_{\mathbf{k}'} - \phi_{\mathbf{k}}$. In the special
case of 2d spin dependent scattering, since the scattering under SOI does not mix the
spin components of the incident beam aligned out-of plane, therefore off-diagonal terms
are vanishing.

The density matrix of the particle beam under the scattering is therefore obtained by
operating the scattering matrix from the both side of the incident scattering matrix

$$\hat{\rho}' = \hat{S}\hat{\rho}\hat{S}^\dagger.$$

Letting the intensity I to be unity, we can write

$$
\begin{aligned}
\hat{\rho}' &= \frac{1}{2}\hat{S}\left(1 + \mathbf{P}_0 \cdot \boldsymbol{\sigma}\right)\hat{S}^\dagger \\
&= \frac{1}{2}\hat{S}\hat{S}^\dagger + \frac{1}{2}\hat{S}\mathbf{P}_0 \cdot \boldsymbol{\sigma}\hat{S}^\dagger,
\end{aligned}
$$

where

$$
\hat{S}\hat{S}^\dagger = \begin{pmatrix} |f_+(\phi)|^2 & 0 \\ 0 & |f_-(\phi)|^2 \end{pmatrix}.
$$

The differential cross section for the unpolarized incident beam $(\mathbf{P}_0 = 0)$ is given by

$$
I(\phi) \equiv \mathrm{tr}(\hat{\rho}') = \frac{1}{2}\hat{S}\hat{S}^\dagger = \frac{1}{2}\left[|f_+(\phi)|^2 + |f_-(\phi)|^2\right]. \tag{4.1}
$$

Since that the order of the density operators does not matter after taken the trace and that $\mathbf{P}_0$ is a constant, therefore we can obtain the second term in Eq. (4.1), describing the spin polarization distribution in $\mathbf{k}$ space after the beam being scattered is

$$
\mathbf{P}_u(\phi) \equiv \frac{\mathrm{tr}(\hat{\rho}'\boldsymbol{\sigma})}{\mathrm{tr}(\hat{\rho}')} = \frac{\mathrm{tr}(\hat{S}\hat{S}^\dagger\boldsymbol{\sigma})}{\mathrm{tr}(\hat{S}\hat{S}^\dagger)} = S(\phi)\,\hat{\mathbf{z}}, \tag{4.2}
$$

where

$$
S(\phi) \equiv \frac{|f_+(\phi)|^2 - |f_-(\phi)|^2}{|f_+(\phi)|^2 + |f_-(\phi)|^2}
$$

is the Sherman function [4]. Therefore the spin dependent differential cross section for arbitrary incident polarization $(\mathbf{P}_0 \neq 0)$ is given by

$$
\overleftrightarrow{D}(\phi) \equiv \mathrm{tr}(\hat{\rho}') = \frac{1}{2}\mathrm{tr}\left[\hat{S}\left(1 + \mathbf{P}_0 \cdot \boldsymbol{\sigma}\right)\hat{S}^\dagger\right].
$$

Using Eq. (4.1) and Eq. (4.2),

$$\overleftrightarrow{D}(\phi) = I(\phi)\left[1 + \mathbf{P}_0 \cdot \hat{\mathbf{z}} S(\phi)\right]. \tag{4.3}$$

From Eq. (4.3), for a spin unpolarized beam, the scattering cross section $I(\phi)$ is symmetric in angle with respect to $\phi = 0$, and the spin polarization in $\mathbf{k}$-space is aligned normal to the plane, i.e. along $\hat{\mathbf{z}}$, in our 2D case. For a initially polarized beams, Eq. (4.3) depicts a asymmetric differential cross section.

4.2 The spin dependent nonequilibrium distribution

The distribution function in phase space $(\boldsymbol{\rho}, \mathbf{k})$ should reveal the spin dependence in the presence of impurity-induced SOI in the system background. The total distribution function in $\mathbf{k}$ space can be described in terms of a two-by-two spin density operator

$$\hat{f}(\mathbf{k}) = [f_0(k) + g(\mathbf{k})]\,\mathbf{1} + \mathbf{h}(\mathbf{k}) \cdot \boldsymbol{\sigma}$$

where $g(\mathbf{k})$ and $\mathbf{h}(\mathbf{k})$ are assumed to possess the form

$$g(\mathbf{k}) = \mathbf{a}(k) \cdot \mathbf{k} \tag{4.4a}$$

$$\mathbf{h}(\mathbf{k}) = \mathbf{b}(k) \times \mathbf{k}, \tag{4.4b}$$

where $\mathbf{a}(k)$ and $\mathbf{b}(k)$ are central symmetric functions in $\mathbf{k}$ space, provided that the scattering is elastic and in an isotropic material. The form of $\mathbf{h}(\mathbf{k})$, motivated by the Mott scattering, describes a spin polarization aligned in an effective magnetic field with its direction relative to a normal line of a plane formed between the driving source $\mathbf{E}$ and a scattered direction $\mathbf{k}$. With solution of forms Eq. (4.4a) and Eq. (4.4b), $\hat{f}(\mathbf{k})$ is a solution to the full Boltzmann equation in the relaxation time approximation after evaluating the collision integral. The spatially homogeneous and time-independent Boltzmann equation

is given by

$$-\frac{e\mathbf{E}}{\hbar} \cdot \frac{\partial \hat{f}(\mathbf{k})}{\partial \mathbf{k}} = \frac{\partial \hat{f}(\mathbf{k})}{\partial t}\bigg|_{\text{coll}}$$

with $e > 0$. The right-hand side is the collision integral

$$\frac{\partial \hat{f}(\mathbf{k})}{\partial t}\bigg|_{\text{coll}} = -n_i \sum_{\mathbf{k}';k'=k} \frac{\hbar k}{m^*} \overset{\leftrightarrow}{D}(\mathbf{k},\mathbf{k}')[\hat{f}(\mathbf{k}) - \hat{f}(\mathbf{k}')] \tag{4.5}$$

where n_i is the impurity density. In 2d case, the scattering cross section $\hat{D}(\mathbf{k},\mathbf{k}')$ is spin dependent and mixes the spin components of the incoming flux except those along z-direction. The spin dependent scattering cross section expanded in SOI and in terms of spin density operator is written as

$$\overset{\leftrightarrow}{D}(\mathbf{k},\mathbf{k}') = I(\phi)\left[1 + \sigma_z S(\phi)\right],$$

where $I(\phi)$ is the differential cross section for spin-unpolarized incident particles, and $S(\phi)$ is the Sherman function, with ϕ the angle between $\mathbf{k}$ and $\mathbf{k}'$; σ_z is the Pauli matrix of z-component. The scattering cross section describes the transition rate at which electrons are scattered from $\mathbf{k}$ into $\mathbf{k}'$, while multiplied by a total incident flux on all the impurities, $n_i \hbar k/m^*$, which is the incoming velocity of a electron times n_i the number density of impurities.

Therefore, the collision integral can be simplified by neglecting the cross terms of spin dependent part of both $\hat{D}$ and $\hat{f}$ in the right hand side of Boltzmann equation

$$\begin{aligned}
&\sum_{\mathbf{k}';k'=k} \overset{\leftrightarrow}{D}(\mathbf{k},\mathbf{k}')[\hat{f}(\mathbf{k}) - \hat{f}(\mathbf{k}')] \\
&= \int d\phi_{\mathbf{k}'} \left\{ I(\phi)[\delta\hat{f}(\mathbf{k}) - \delta\hat{f}(\mathbf{k}')] + \sigma_z I(\phi)S(\phi)\left[g(\mathbf{k}) - g(\mathbf{k}')\right] \right\},
\end{aligned} \tag{4.6}$$

with $\delta\hat{f} \equiv g + \mathbf{h} \cdot \boldsymbol{\sigma}$, the nonequlibrium part of $\hat{f}$. The integrals in Eq. (4.6) are equal to

$$
\int d\phi_{\mathbf{k}'} I(\phi)[\delta\hat{f}(\mathbf{k}) - \delta\hat{f}(\mathbf{k}')] = [\mathbf{a}(k) \cdot \mathbf{k} + \sigma_z \hat{\mathbf{z}} \cdot (\mathbf{b}(k) \times \mathbf{k})] \left(\int_{-\pi}^{\pi} d\phi I(\phi) (1 - \cos\phi) \right);
$$

$$
\int d\phi_{\mathbf{k}'} \sigma_z I(\phi) S(\phi) [g(\mathbf{k}) - g(\mathbf{k}')] = \sigma_z \hat{\mathbf{z}} \cdot (\mathbf{a}(k) \times \mathbf{k}) \left(\int_{-\pi}^{\pi} d\phi I(\phi) S(\phi) \sin\phi \right);
$$

the detailed evaluation of the integrals is left in the appendix.

To the lowest order in the electric filed, $\delta\hat{f}$ is linear in $\mathbf{E}$ and the left hand side of the Boltzmann equation reads

$$
-\frac{e\mathbf{E}}{\hbar} \cdot \frac{\partial\hat{f}}{\partial\mathbf{k}} = -\frac{e\hbar}{m^*} \frac{\partial f_0}{\partial\varepsilon} \mathbf{E} \cdot \mathbf{k},
$$

provided that $\mathbf{E}$ is weak enough so that the product of δf and $\mathbf{E}$ can be neglect. Thus the left-hand side of the equation should not have any spin dependence.

Since the lack of spin dependence of the right-hand-side of Boltzmann equation, the second and the third term resulting from the collision integral (eq.1) must cancel each other. With the terms surviving after the collision integral is done, the rest of the Boltzmann equation reads

$$
-\frac{e\hbar}{m^*} \frac{\partial f_0}{\partial\varepsilon} \mathbf{E} \cdot \mathbf{k} = -\frac{\mathbf{a}(k) \cdot \mathbf{k}}{\tau},
$$

where $\tau^{-1} = \frac{n_i \hbar k}{m^*} \int_0^{2\pi} d\phi I(\phi) (1 - \cos\phi)$, and τ is the relaxation time. Therefore

$$
\mathbf{a}(k) = D_k \mathbf{E};
$$

where $D_k = \frac{e\hbar\tau}{m^*} \frac{\partial f_0}{\partial\varepsilon}$. The requirement of cancellation of the spin dependence in the right-hand-side leads to

$$
\mathbf{b}(k) = -\gamma_k \mathbf{a}(k) = -\gamma_k D_k \mathbf{E},
$$

where γ_k denotes the transport skewness

$$\gamma_k \equiv \frac{\int_0^\pi d\phi I(\phi) S(\phi) \sin\phi}{\int_0^\pi d\phi I(\phi)\left(1 - \cos\phi\right)},$$

which describes the effect of skew scattering and depends on the detailed structure of the
scattering potential and on the energy of the elastic scattering. Therefore the nonequilib-
rium part of the solution to the Boltzmann equation is,

$$g(\mathbf{k}) = D_k \mathbf{E} \cdot \mathbf{k};$$

$$\mathbf{h}(\mathbf{k}) = -\gamma_k D_k \mathbf{E} \times \mathbf{k}$$

$$= -\gamma_k D_k E_0 k \sin\phi_k \,\hat{\mathbf{z}}; \tag{4.7}$$

where $D_k = -\frac{e\tau\hbar}{m^*}\delta(\varepsilon_{\mathbf{k}} - \mu)$ at low temperature around $0\,\mathrm{K}$. The spin-independent part
$g(\mathbf{k})$ depicts a shifted Fermi circle with its shifted direction opposite to the perturbing
electric field $\mathbf{E}$ as in the normal impurity case; the spin dependent part $\mathbf{h}(\mathbf{k}) \cdot \boldsymbol{\sigma} = \sigma_z h_z(\mathbf{k})$
because $\mathbf{h}$ always points along the z-axis and it describes a spread of spin polarization
along z-axis in $\mathbf{k}$ space. According to Eq. (4.7), the explicit angular dependence of spin
polarization is $\sin\phi_k$, which indicates left- and right-deflected electrons possess opposite
signs of spin polarization: with negative γ_μ, the left-deflected electrons (states in negative
y-plane) possess spin polarization aligned in the negative z-direction while the right-
deflected electrons (states in negative y-plane) have its spin polarization along the positive
z-direction, and vice versa. A qualitative sketch of the nonequilibrium distribution of
electron is depicted in Fig. 4.1. Furthermore, this spin dependent distribution $\mathbf{h}(\mathbf{k}) \cdot \boldsymbol{\sigma}$ is
partially responsible for a bulk spin-Hall current set up transversely across the 2DEG [8],
flowing towards positive y-axis. Thus the total nonequilibrium distribution of electrons is

$$\hat{f}(\mathbf{k}) = f_0(k) + D_k \mathbf{k} \cdot \left[\mathbf{E} - \gamma_k\left(\boldsymbol{\sigma} \times \mathbf{E}\right)\right].$$
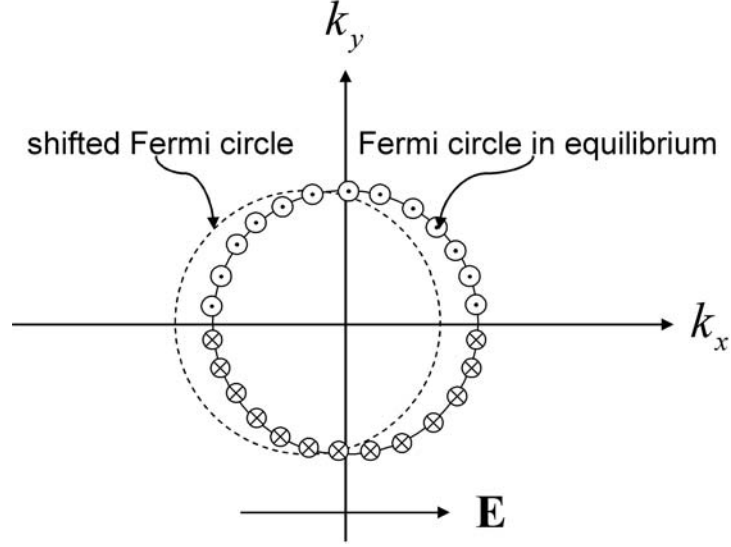
Figure 4.1: Qualitative sketch of **k**-dependent spin polarization due to the extrinsic SOI
for a negative SO coupling constant λ. Spin polarization of the upper semicircle (in the
positive y-plane) is up (aligned in positive z-direction); while spin polarization of the lower
semicircle (in the negative y-plane) is down (aligned in positive z-direction).

4.3 The correction to the spin dipole due to the term $\mathbf{h}(\mathbf{k}) \cdot \boldsymbol{\sigma}$

In the language of quantum-mechanical ensemble theory, the spin polarization distribution
is defined by an ensemble average of spin operator σ_z projected on the real space,

$$S_z^{\text{tot}}(\boldsymbol{\rho}) \equiv \langle \boldsymbol{\rho}| \operatorname{tr}(\sigma_z \hat{\rho})|\boldsymbol{\rho}\rangle \,, \tag{4.8}$$

where

$$\hat{\rho} = \sum_{\mathbf{k},\sigma} \hat{f}(\mathbf{k}) \, |\mathbf{k}, \sigma\rangle \, \chi_\sigma \chi_\sigma^\dagger \, \langle \mathbf{k}, \sigma|$$

is the density operator of the system represented in the basis of wavevector $\mathbf{k}$ and z-component of spin σ_z, and $|\boldsymbol{\rho}\rangle$ is the ket eigenstate of the position operator. Therefore,

$$S_z^{\mathrm{tot}}(\boldsymbol{\rho}) = \mathrm{tr}\left[\sigma_z \sum_{\mathbf{k},\sigma} \hat{f}(\mathbf{k}) \langle \boldsymbol{\rho}\,|\mathbf{k},\sigma\rangle \chi_\sigma \chi_\sigma^\dagger \langle \mathbf{k},\sigma\,|\boldsymbol{\rho}\rangle\right],$$

where $\langle \boldsymbol{\rho}\,|\mathbf{k},\sigma\rangle = \psi_{\mathbf{k}}^\sigma(\boldsymbol{\rho})$. As in the previous chapter, since the equilibrium part of distribution f_0 does not contribute to the spin accumulation, therefore,

$$S_z^{\mathrm{tot}} = \mathrm{tr}\left[\sigma_z \sum_{\mathbf{k},\sigma} (g + \mathbf{h}\cdot\boldsymbol{\sigma})\,|\psi_{\mathbf{k}}^\sigma(\boldsymbol{\rho})|^2\,\chi_\sigma \chi_\sigma^\dagger\right],$$

after taking the trace, we find there are two contributions to the spin accumulation. The first one is

$$
\begin{aligned}
S_z &= \mathrm{tr}\left\{\sigma_z \sum_{\mathbf{k},\sigma} g(\mathbf{k})\,|\psi_{\mathbf{k}}^\sigma(\boldsymbol{\rho})|^2\,\chi_\sigma \chi_\sigma^\dagger\right\} \\
&= \sum_{\sigma'} \chi_{\sigma'}^\dagger \left\{\sigma_z \sum_{\mathbf{k},\sigma} g(\mathbf{k})\,|\psi_{\mathbf{k}}^\sigma(\boldsymbol{\rho})|^2\,\chi_\sigma \chi_\sigma^\dagger\right\} \chi_{\sigma'} \\
&= \sum_{\mathbf{k},\sigma} g(\mathbf{k})\,|\psi_{\mathbf{k}}^\sigma(\boldsymbol{\rho})|^2 \sum_{\sigma'} \chi_{\sigma'}^\dagger \sigma_z \chi_\sigma \chi_\sigma^\dagger \chi_{\sigma'} \\
&= \sum_{\mathbf{k},\sigma} g(\mathbf{k})\,\sigma\,|\psi_{\mathbf{k}}^\sigma(\boldsymbol{\rho})|^2.
\end{aligned}
$$

This is the spin accumulation $S_z = \frac{1}{4\pi^2}\int d\mathbf{k}\,g(\mathbf{k})\sum_\sigma \sigma\,|\Psi_{\mathbf{k}\sigma}(\boldsymbol{\rho})|^2$ we consider in the previous chapter; the second contribution due to the extrinsic effect

$$
\begin{aligned}
S_z^{\mathrm{ex}} &= \mathrm{tr}\left\{\sigma_z \sum_{\mathbf{k},\sigma} \mathbf{h}(\mathbf{k})\cdot\boldsymbol{\sigma}\,|\psi_{\mathbf{k}}^\sigma(\boldsymbol{\rho})|^2\,\chi_\sigma \chi_\sigma^\dagger\right\} \\
&= \sum_{\sigma'} \chi_{\sigma'}^\dagger \left\{\sigma_z \sum_{\mathbf{k},\sigma} h_z(\mathbf{k})\sigma_z\,|\psi_{\mathbf{k}}^\sigma(\boldsymbol{\rho})|^2\,\chi_\sigma \chi_\sigma^\dagger\right\} \chi_{\sigma'} \\
&= \sum_{\mathbf{k},\sigma} h_z(\mathbf{k})\,|\psi_{\mathbf{k}}^\sigma(\boldsymbol{\rho})|^2 \sum_{\sigma'} \chi_{\sigma'}^\dagger \sigma_z{}^2 \chi_\sigma \chi_\sigma^\dagger \chi_{\sigma'} \\
&= \sum_{\mathbf{k},\sigma} h_z(\mathbf{k})\,|\psi_{\mathbf{k}}^\sigma(\boldsymbol{\rho})|^2,
\end{aligned}
$$

where $h_z(\mathbf{k}) = -\gamma_k D_k E_0 k \sin \phi_k$. Thus the spin accumulation due to the spin dependent
distribution is therefore, after converting the summation into a integral,

$$S_z^{\text{ex}}(\boldsymbol{\rho}) = \frac{1}{4\pi^2} \int d\mathbf{k} \, h_z(\mathbf{k}) \, |\psi_{\mathbf{k}}^\sigma(\boldsymbol{\rho})|^2 .$$

Finally we can obtain the spin dipole due the extrinsic SOI, given by

$$S_z^{\text{ex}} = -\gamma_\mu n_E \sin \phi_\rho \, \text{Im} \sum_\sigma \sum_{l=0}^\infty R_l^\sigma(\rho) R_{l+1}^{\sigma*}(\rho), \tag{4.9}$$

where γ_μ is short for γ_{k_μ} and $n_E = \frac{eE_0\tau k}{\pi \hbar}$. In this spin dipole correction, $\sin \phi_\rho$ indicates,
again, a dipole distribution perpendicular to the driving field $\mathbf{E}$, but its radial dependence
is the same as that of the charge dipole. This implies that the resonant structure of spin
dipole should be similar to the charge dipole. Obviously, the physical origin of different
contributions to the generation of spin dipole is different.
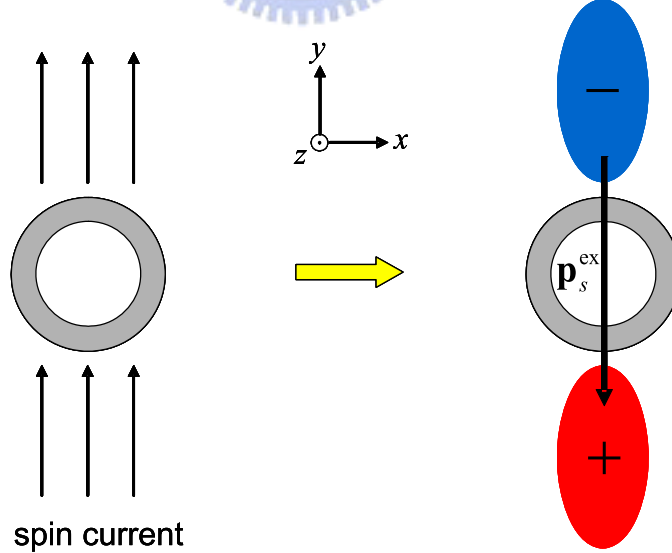

Figure 4.2: The relation between spin current direction and spin dipole $\mathbf{p}_s^{\text{ex}} = p_s^{\text{ex}} \hat{\mathbf{y}}$ for
negative SO coupling constant λ. $p_s^{\text{ex}} < 0$ is shown in this figure. The plus sign below the
ring stands for spin up accumulation , and vice versa.

The strength of spin dipole contribution Eq. (4.9) can be defined by

$$p_s^{\text{ex}} = \frac{\gamma_\mu \tilde{n}_E}{2\pi} \, k\sigma_{\text{tr}}, \tag{4.10}$$

where $\tilde{n}_E = \frac{m^* e E_0 l_0^*}{\pi \hbar^2}$. The sign of p_s^{ex} (or the orientation of the spin dipole) is determined by the sign of γ_μ because $k\sigma_{\text{tr}}$ and $\tilde{n}_E$ are always positive. Therefore, it seems that the orientation of this spin dipole can be related to a direct consequence of the transverse spin-Hall current set up due to extrinsic SOI. Since a spin current is the transport of electrons with spin polarization, there should be a direct pile up of spin against the structure of the ring. Unlike the case in the previous chapter that the spin accumulation is duo to direct asymmetric scattering by the ring structure, since this spin accumulation may be due to the direct pile up of spin along the direction of transported spin, its resonance characteristics should be similar to that of the RRD.

The above conjecture can be implied by the spin dependent part of nonequilibrium distribution of electrons $\mathbf{h}(\mathbf{k})$ and by the sign of p_s^{ex}. For more explicit demonstration, we can look at Eq. (4.7) and Eq. (4.10): when $\gamma_\mu < 0$, Fig. 4.1 indicates that the spin current is flowing towards positive y-direction, and the sign of spin dipole is always negative, i.e. $p_s^{\text{ex}} < 0$. The relation between the spin current and the orientation of the spin dipole is shown in Fig. 4.2. The spin dipole p_s^{ex} is always directed towards the negative y-axis.

Next, we present the total contribution to the spin dipole strength. Since p_s^{ex} is proportional to $k\sigma_{\text{tr}}$, its resonance behavior is similar to that of charge RRD, in contrary to the resonance behavior of p_s, both are depicted in Fig. 4.3, with a chosen $\gamma_\mu = -1/500$. At resonance, the dipole strength p_s is enhanced and is either positive or negative; the dipole strength p_s^{ex} is always negative and a local minimum of strength takes place. Therefore this concludes that away from resonance, dipole strength p_s and p_s^{ex} are comparable and thus almost eliminate each other due to their opposite signs; on the other hand, at resonance, p_s is dominant, as shown in Fig. 4.4 and Fig. 4.5.
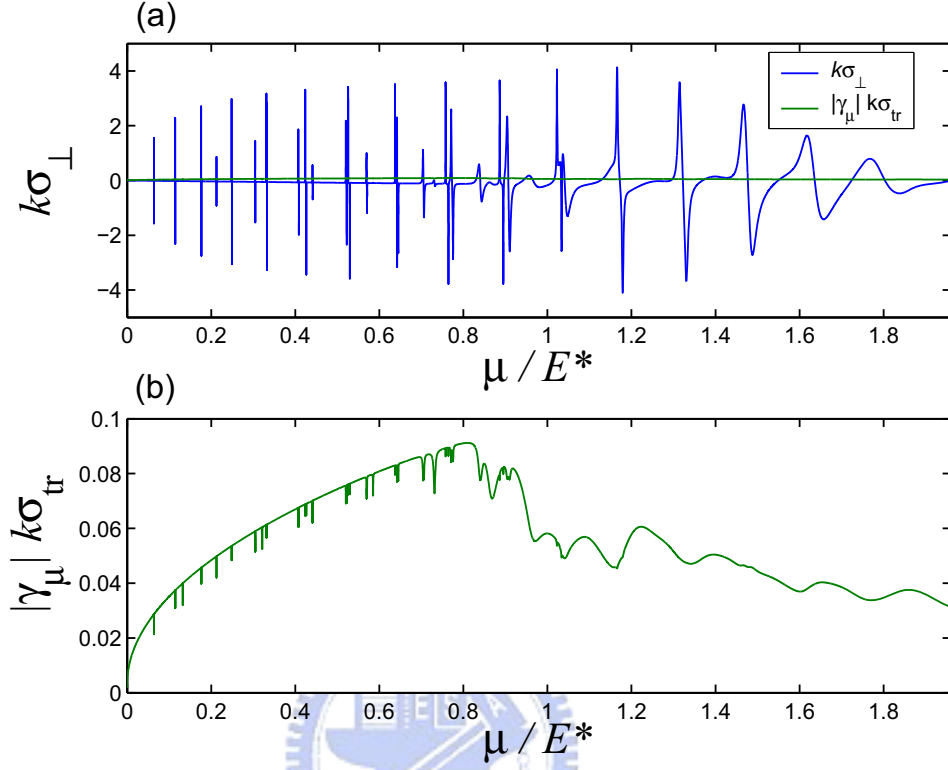
Figure 4.3: (a) $k\sigma_\perp$ versus energy with parameters the same as in Fig. 3.5-(a),and (b) a
blow-up of $|\gamma_\mu|k\sigma_{\rm tr}$ versus energy.

4.4 Brief summary

The correction to the spin dipole $S_z^{\rm ex}$ due to extrinsic SOI effect (SOI from background
impurities) is found to be negligible at resonances. Although this correction is significant
away from the resonances, the total spin dipole strength in this region is still insignificant
when comparing to that at resonances.
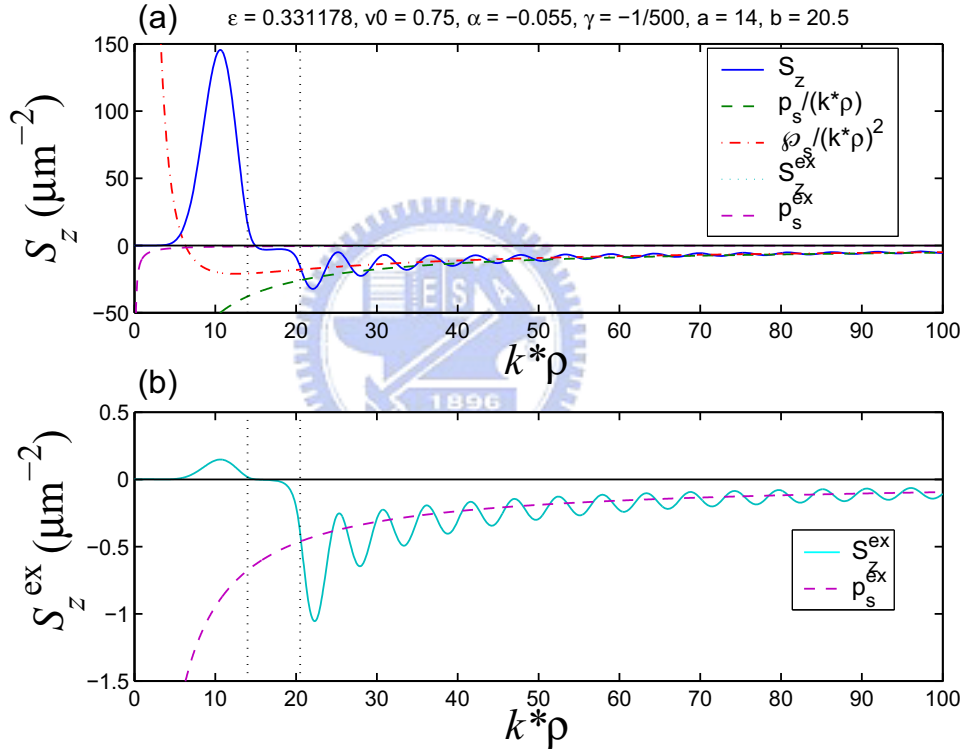
Figure 4.4: (a) Radial variation of $S_z(\boldsymbol{\rho})$, $S_z^{\mathrm{ex}}(\boldsymbol{\rho})$, and (b) Blowup of the radial radiation $S_z^{\mathrm{ex}}(\boldsymbol{\rho})$ along $\phi_\rho = \pi/2$ at the resonant energy $\mu = 0.331178$. At resonance, S_z^{ex} so tiny that it is negligible. Parameters are on top of the figure.
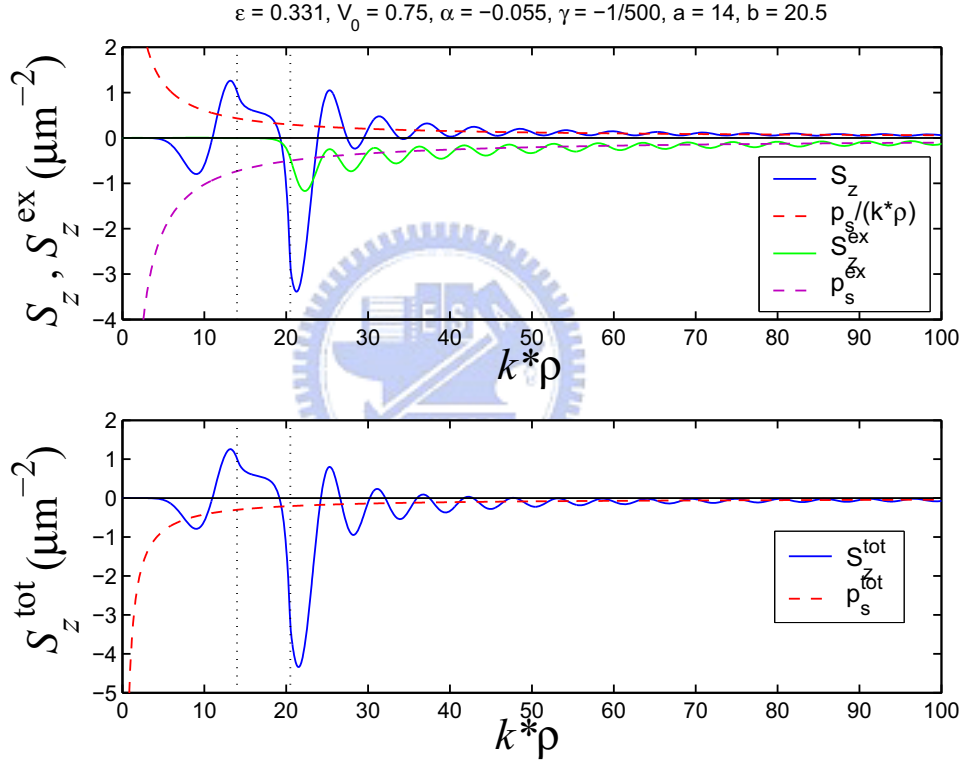
Figure 4.5: (a) Radial variation of $S_z(\boldsymbol{\rho})$, $S_z^{\text{ex}}(\boldsymbol{\rho})$, and (b) a blow-up of the radial radiation $S_z^{\text{ex}}(\boldsymbol{\rho})$ along $\phi_\rho = \pi/2$ at the energy away from $\mu = 0.331000$. Away from resonance, S_z^{ex} is comparable to S_z, so nearly no spin polarization in the region away from the ring structure. Other parameters are the same as Fig. 4.4.

Chapter 5

Numerical calculation for smooth potential variation

As is mentioned in previous Chapter 3, the results of a step-like radial profile of the potential of a ring-shaped microstructure may be valid merely within the regime that the Fermi wavelength is comparable with or larger than the thickness of the ring of the potential, therefore in this chapter, we will demonstrate the robustness of the results in Chapter 3 if the step-like radial profile of the ring structure is replaced by a smoother profile, via performing the variable phase approach.

5.1 Variable phase approach

In determining the scattering amplitude, only the radial function far outside the range of the scattering potential is relevant. It can be completely determined by the given phase shifts. All we need is the determination of phase shifts outside the range of the scattering potential. Therefore we will introduce the concept of the phase of the wave as a position-dependent function, that is, the variable phase approach [33, 34].

Another reason to introduce the variable phase approach is that when the detailed wave variation within the range of scattering potential cannot be exactly solved with an

arbitrary radial potential profile, coupled with the amplitude function, one can obtain the
particle wave function in the whole space via numerically integrating and radial differential
equation satisfied by a phase function $\delta_l^\sigma(\rho)$ from the origin to the exterior of the potential.

The phase shifts are defined from the asymptotic region of the radial functions, or the
potential-free region. That is to say, the scattering phase shifts in our previous analysis
is produced by the total scattering potential. Thus we can generalize this concept that
phase shifts can be produced by part of the scattering potential within the sphere of a
certain radius ρ. Therefore the phase shift is a position dependent function $\delta_l^\sigma(\rho)$, whose
value varies with non-vanishing potential and saturates to δ_l^σ in the asymptotic region,
that is,

$$\lim_{\rho \to \infty} \delta_l^\sigma(\rho) \equiv \delta_l^\sigma \tag{5.1}$$

The phase function $\delta_l^\sigma(\rho)$ and the amplitude function $A_l^\sigma(\rho)$ is introduced by the
relation to the definition of the radial function

$$R_l^\sigma(\rho) = A_l^\sigma(\rho) \left[\cos \delta_l^\sigma(\rho) J_l(k\rho) - \sin \delta_l^\sigma(\rho) Y_l(k\rho)\right]. \tag{5.2}$$

This radial function should satisfy the radial Schrödinger equation Eq. (3.4). To make the
two function governed by the independent differential equation, the derivative of Eq. (5.2)
possesses the form

$$\frac{dR_l^\sigma(\rho)}{d\rho} = A_l^\sigma(\rho) \left[\cos \delta_l^\sigma(\rho) \frac{dJ_l(k\rho)}{d\rho} - \sin \delta_l^\sigma(\rho) \frac{dY_l(k\rho)}{d\rho}\right]. \tag{5.3}$$

This form of radial derivative implies an extra restriction,

$$\begin{aligned}
&\frac{dA_l^\sigma(\rho)}{d\rho} \left[\cos \delta_l^\sigma(\rho) J_l(k\rho) - \sin \delta_l^\sigma(\rho) Y_l(k\rho)\right] \\
&\quad - A_l^\sigma(\rho) \frac{d\delta_l^\sigma(\rho)}{d\rho} \left[\sin \delta_l^\sigma(\rho) J_l(k\rho) - \cos \delta_l^\sigma(\rho) Y_l(k\rho)\right] = 0.
\end{aligned} \tag{5.4}$$

The second-order derivative of radial function is

$$\frac{d^2 R_l^\sigma(\rho)}{d\rho^2} = \frac{dA_l^\sigma(\rho)}{d\rho} \left[\cos \delta_l^\sigma(\rho) \frac{dJ_l(k\rho)}{d\rho} - \sin \delta_l^\sigma(\rho) \frac{dY_l(k\rho)}{d\rho} \right]$$
$$- A_l^\sigma(\rho) \frac{\delta_l^\sigma(\rho)}{d\rho} \left[\sin \delta_l^\sigma(\rho) \frac{dY_l(k\rho)}{d\rho} + \cos \delta_l^\sigma(\rho) \frac{dY_l(k\rho)}{d\rho} \right]$$
$$+ A_l^\sigma(\rho) \left[\cos \delta_l^\sigma(\rho) \frac{d^2 J_l(k\rho)}{d\rho^2} - \sin \delta_l^\sigma(\rho) \frac{d^2 Y_l(k\rho)}{d\rho^2} \right]. \tag{5.5}$$

Substitute Eq. (5.2), Eq. (5.3) and Eq. (5.5) into the Scrödinger equation Eq. (3.4), and making use of the Bessel equation Eq. (2.1), we obtain

$$\frac{dA_l^\sigma(\rho)}{d\rho} \left[\cos \delta_l^\sigma(\rho) \frac{dJ_l(k\rho)}{d\rho} - \sin \delta_l^\sigma(\rho) \frac{dY_l(k\rho)}{d\rho} \right]$$
$$- A_l^\sigma(\rho) \frac{d\delta_l^\sigma(\rho)}{d\rho} \left[\sin \delta_l^\sigma(\rho) \frac{dJ_l(k\rho)}{d\rho} + \cos \delta_l^\sigma(\rho) \frac{dY_l(k\rho)}{d\rho} \right] \tag{5.6}$$
$$- V(\rho) A_l^\sigma(\rho) \left[\cos \delta_l^\sigma(\rho) J_l(k\rho) - \sin \delta_l^\sigma(\rho) Y_l(k\rho) \right] = 0 \,.$$

Eq. (5.4) and Eq. (5.6) forms a set of differential equations sufficient for the unambiguous description of the phase function $\delta_l^\sigma(\rho)$ and the amplitude function $A_l^\sigma(\rho)$. By eliminating the derivative of $A_l^\sigma(\rho)$ using Eq. (5.4), one can obtain the differential equation for the phase function $\delta_l^\sigma(\rho)$ for the 2d system

$$\frac{d\delta_l^\sigma(\rho)}{d\rho} = -\frac{\pi}{2} \rho V(\rho) \left[\cos \delta_l^\sigma(\rho) J_l(k\rho) - \sin \delta_l^\sigma(\rho) Y_l(k\rho) \right]^2 \,, \tag{5.7}$$

with the boundary condition

$$\delta_l^\sigma(0) = 0.$$

The detailed derivation of this differential equation is in the appendix. From Eq. (5.7), $\delta_l^\sigma(\rho)$ is independent of the wave amplitude because of the unitarity relation of the phase shift, or the conservation of particles. Therefore obtaining the phase shift for a given arbitrary potential is reduced to solving a first-order nonlinear differential equation according

to Eq. (5.7). Similarly, by eliminating the derivative of $\delta_l^\sigma(\rho)$ we can get the differential
equation for $A_l^\sigma(\rho)$

$$
\begin{aligned}
\frac{dA_l^\sigma(\rho)}{d\rho} = &-\frac{\pi}{2}\rho V(\rho)A_l^\sigma(\rho)\left[\cos\delta_l^\sigma(\rho)J_l(k\rho) - \sin\delta_l^\sigma(\rho)Y_l(k\rho)\right] \\
&\times \left[\sin\delta_l^\sigma(\rho)J_l(k\rho) + \cos\delta_l^\sigma(\rho)Y_l(k\rho)\right].
\end{aligned}
\tag{5.8}
$$

Integrating Eq. (5.8) yields

$$
\begin{aligned}
A_l^\sigma(\rho) = A_l^\sigma(\rho_0)\exp\Bigg\{ &-\frac{\pi}{2}\int_{\rho_0}^{\rho} d\rho V(\rho)\rho\left[\cos\delta_l^\sigma(\rho)J_l(k\rho) - \sin\delta_l^\sigma(\rho)Y_l(k\rho)\right] \\
&\times \left[\sin\delta_l^\sigma(\rho)J_l(k\rho) + \cos\delta_l^\sigma(\rho)Y_l(k\rho)\right]\Bigg\}
\end{aligned}
\tag{5.9}
$$

where $A_l^\sigma(\rho_0)$ is the amplitude at $\rho = \rho_0$. In contrary to the phase function, the amplitude
function is dependent on the phase.

In principal, while dealing with the phase shift we can integrate the second-order
Schrödinger equation. But the numerical calculation can be simplified by evaluating the
phase function which is governed by a differential equation of first-order Eq. (5.7), though
it is nonlinear.

Thus far we can check the consistency of properties between the exact and variable
phase method. One of them is the relation between the scattering phase shift and the
potential. Since the expression in Eq. (5.7)

$$
\left[\cos\delta_l^\sigma(\rho)J_l(k\rho) - \sin\delta_l^\sigma(\rho)Y_l(k\rho)\right]^2
$$

is always positive, the sign of the phase shift is uniquely determined by the sign of the
potential. Because of the boundary value $\delta_l^\sigma(0) = 0$, in the case of attractive potential,
the derivative of the phase function is positive and so is the phase shift, and vice versa.
The phase shift varies only within the range of the nonvanishing potential as shown in
Fig. 5.3, and has its value all negative with positive potential in the range of the ring as
described in Eq. (5.7).
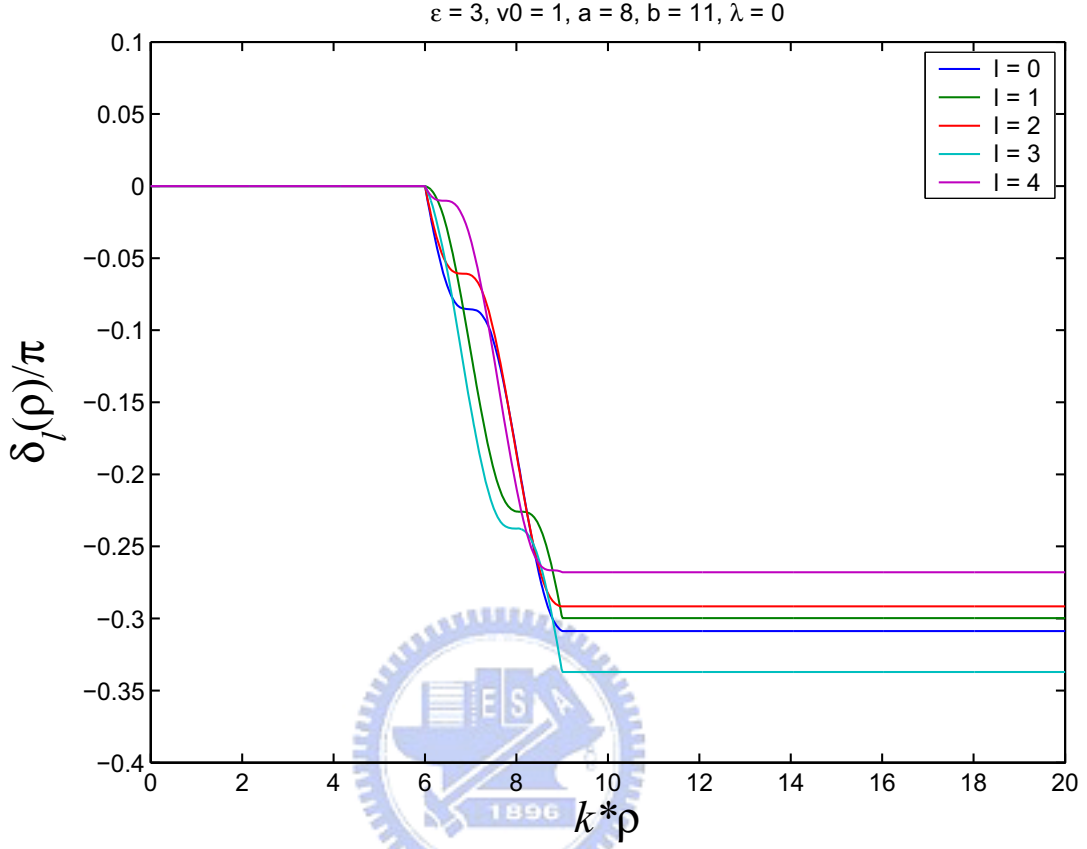
Figure 5.1: Variable phase function $\delta_l(\rho)$ vs. radial position without SOI for a step potential of a ring. Dimensionless parameters are $\varepsilon = 3$, $V_0 = 1$, $a = 6$, $b = 9$. We can see the variation of phase is only within the range of the ring potential between a and b.

5.2 Numerical results

A smooth profile of a gaussian variation of potential with its maximum value centered at ρ_0 and its measure in width h is considered in this numerical calculation. The potential form is written as

$$V(\rho) = V_0 \exp\left[-\frac{(\rho - \rho_0)^2}{h^2}\right].$$

Phase shifts for this smoother profile of potential also manifests resonant features at certain energies, as shown in Fig. 5.2. Phase shifts show an overall smooth negative trend of departure from zero as energy increasing and abruptly pulling back from below of $n\pi/2$

65
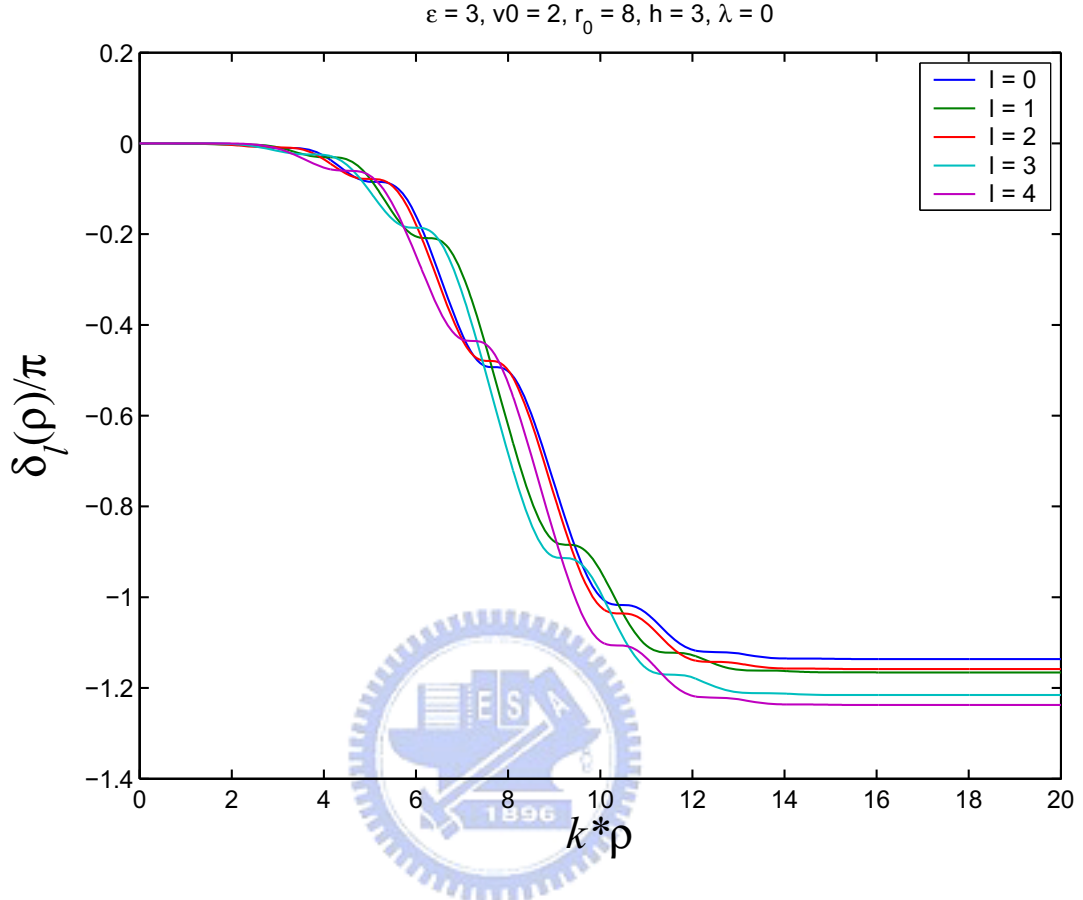
Figure 5.2: Variable phase function $\delta_l(\rho)$ vs. radial position without SOI for a gaussian radial potential profile. Dimensionless parameters are $\varepsilon = 3$, $V_0 = 1$, $\rho_0 = 8$, $h = 3$. We can see the variation of phase is only within the range of the ring potential between a and b.

(n is odd integer).

Next we demonstrate the charge and spin dipole strength against energy, as shown in Fig. 5.4 and Fig. 5.5. We can see from Fig. 5.4 and Fig. 5.5 that the characteristics of resonant behavior still remains intact.

5.3   Brief summary

The results of resonant features remains intact if we substitute the step radial profile by a smoother gaussian profile.
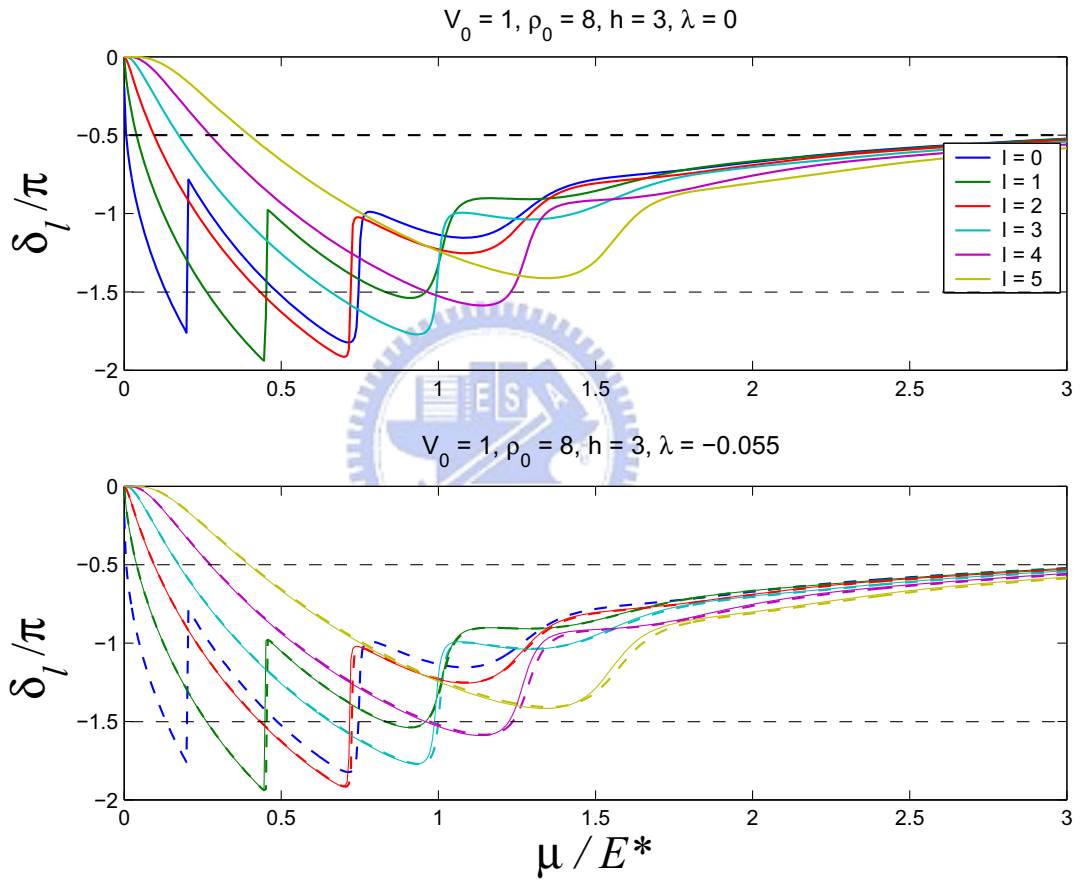
Figure 5.3: Phase shifts versus energy. We can see the splits of energies at which the phase crosses $n\pi/2$ (n is odd) from below. In the lower diagram, the solid curves are phase shifts for positive l, and the dashed curves are for negative $-l$, both with $\sigma = +1$. Parameters are: $\rho_0 = 8$, $h = 3$, $V_0 = 1$, and dimensionless spin-orbit coupling constant $\lambda = -0.055$.
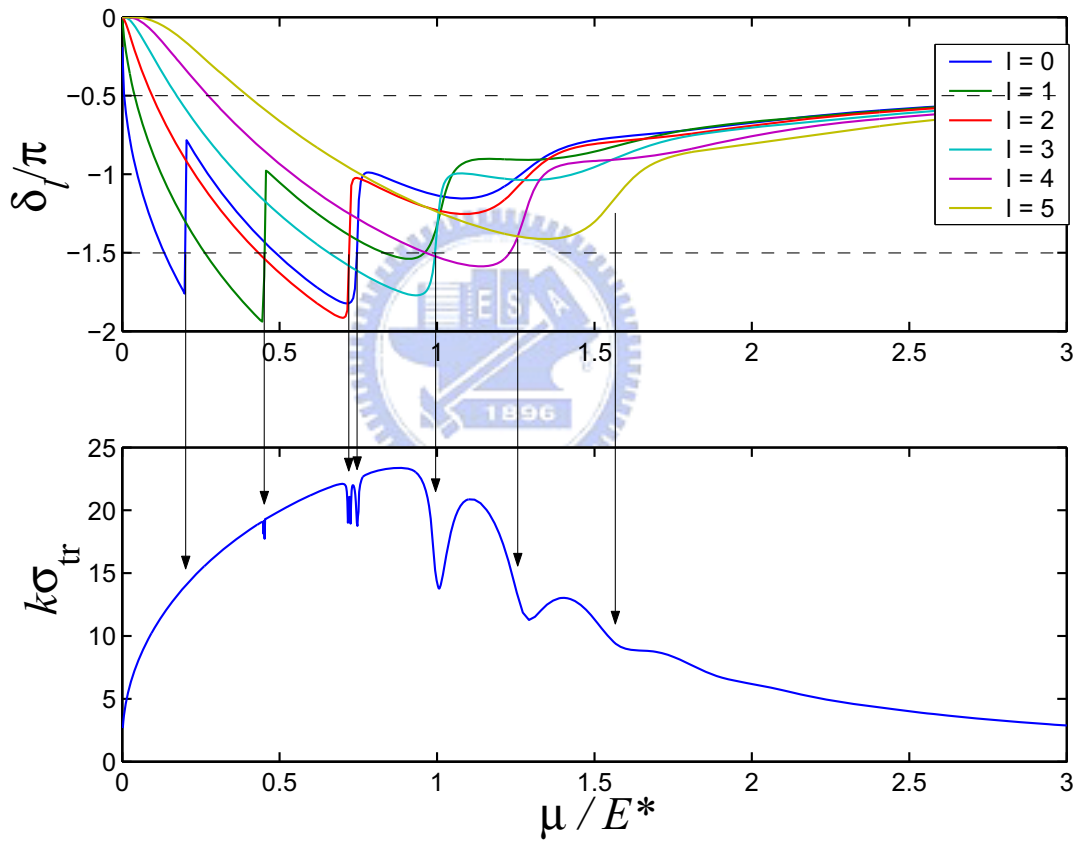
Figure 5.4: $k\sigma_{\mathrm{tr}}$ versus energy. Parameters are $\rho_0 = 8$, $h = 3$, $V_0 = 1$
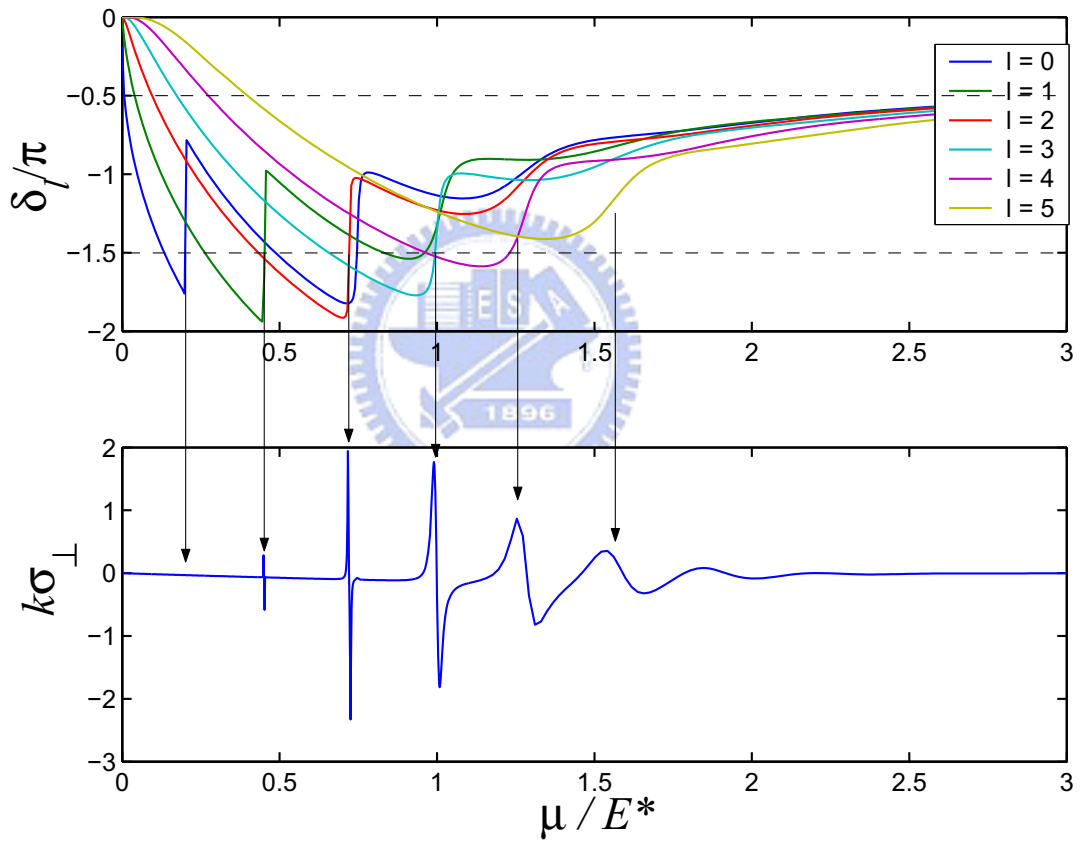
Figure 5.5: $k\sigma_\perp$ versus energy. Parameters are $\rho_0 = 8$, $h = 3$, $V_0 = 1$.

Chapter 6

Conclusion and future work

In conclusion, we have obtained the resonance structures in the Landauer RRD around a ring-shaped microstructure. The resonant structures exhibit as dip structures in the RRD strength, or a drop in the charge pile up. In the presence of in-plane potential gradient SOI, the resonant energies are spin-split. The dip structures in the RRD becomes double dip structures.

Concerning the spin accumulation, we obtain a spin dipole distribution. Resonant structures are in peak-dip pairs around each spin-split resonant energy pairs. Thus we have shown unambiguously that in-plane potential gradient SOI can be significant, especially when quantum resonances are involved. The peak-dip pairs in the spin dipole strength allow the possibility of switching spin accumulation direction by electrical gate-control method.

The spin dependent nonequilibrium solution to the kinetic equation with skew scattering in the collision term in 2D is solved. The residual spin dipole produced by the spin current arising from asymmetric scattering of impurities was shown to cause small correction to the spin dipole near the resonances but is relatively large away from resonant energies.

The robustness of the generation of spin dipole around the ring- shaped microstructure is obtained when the radial potential is replaced by a smooth profile.

In the future, the asymmetric scattering of an spin-polarized incoming beam of electrons could provide an alternative way for the detection of the spin current. Directly gauging the tilting angle of the charge RRD alignment could be used for the detection of the polarization in the incoming electron flux.

Appendix A

Derivation of charge accumulation

The charge dipole is produced by the nonequilibrium part of solution $g(\mathbf{k})$

$$\delta n(\boldsymbol{\rho}) = \frac{1}{2\pi^2} \int d\mathbf{k}\, g(\mathbf{k}) \left|\Psi_{\mathbf{k}}(\boldsymbol{\rho})\right|^2,$$

where $g(\mathbf{k}) = -\frac{e\tau\hbar}{m^*}\delta(\varepsilon_{\mathbf{k}} - \mu)\mathbf{E} \cdot \mathbf{k}$ and $\mathbf{E} = E_0\hat{\mathbf{x}}$. One can express the variable $\varepsilon_{\mathbf{k}} = \hbar^2 k^2/2m^*$ in the $\mathbf{k}$ space variables, that is,

$$
\begin{aligned}
g(k, \phi_k) &= -\frac{e\tau\hbar}{m^*} E_0 k \cos\phi_k\, \delta\!\left(\frac{\hbar^2}{2m^*}(k^2 - k_\mu^2)\right) \\
&= \frac{e\tau\hbar}{m^*} E_0 k \cos\phi_k \frac{2m^*}{\hbar^2} \frac{1}{2k_\mu} \left[\delta(k - k_\mu) + \delta(k + k_\mu)\right] \\
&= \frac{e\tau E_0}{\hbar k_\mu} k \cos\phi_k \left[\delta(k - k_\mu) + \delta(k + k_\mu)\right].
\end{aligned}
$$

Therefore,

$$
\begin{aligned}
\delta n(\boldsymbol{\rho}) &= -\frac{1}{2\pi^2}\frac{e\tau E_0}{\hbar k_\mu} \int_0^\infty dk\, k^2 \delta(k - k_\mu) \int_0^{2\pi} d\phi_k \cos\phi_k \left|\Psi_{\mathbf{k}}(\boldsymbol{\rho})\right|^2 \\
&= -\frac{e\tau E_0 k_\mu}{2\pi^2 \hbar} \int_0^{2\pi} d\phi_k \cos\phi_k \left|\Psi_{\mathbf{k}_\mu}(\boldsymbol{\rho})\right|^2.
\end{aligned}
\tag{A.1}
$$

APPENDIX A. DERIVATION OF CHARGE ACCUMULATION

The remaining integral in the above,

$$
\int d\phi_k \cos\phi_k \big|\Psi_{\mathbf{k}_\mu}(\boldsymbol{\rho})\big|^2
$$

$$
= \sum_{l,l'=-\infty}^{+\infty} i^l(-i)^{l'} R_l(\rho) R_{l'}^*(\rho) \int d\phi_k \cos\phi_k e^{i(l-l')(\phi_\rho-\phi_k)}
$$

$$
= \sum_{l,l'} e^{i(l-l')\pi/2} R_l R_{l'}^* \int d\phi_k \cos(\phi_k-\phi_\rho+\phi_\rho) e^{i(l'-l)(\phi_k-\phi_\rho)}
$$

$$
= \sum_{l,l'} e^{i(l-l')\pi/2} R_l R_{l'}^* \int_0^{2\pi} d\phi_k \left[\cos(\phi_k-\phi_r)\cos\phi_\rho - \sin(\phi_k-\phi_\rho)\sin\phi_\rho \right] e^{i(l'-l)(\phi_k-\phi_\rho)}
$$

$$
= \sum_{l,l'} e^{i(l-l')\pi/2} R_l R_{l'}^* \left[\cos\phi_\rho \int_0^{2\pi} d\phi \cos\phi e^{i(l'-l)\phi} - \sin\phi_r \int_0^{2\pi} d\phi \sin\phi e^{i(l'-l)\phi} \right].
$$

$$(A.2)$$

The two integrals in the above are

$$
\int_0^{2\pi} d\phi \cos\phi\, e^{i(l'-l)\phi} = \pi\left(\delta_{l',l+1} + \delta_{l,l'+1}\right)
\tag{A.3a}
$$

$$
\int_0^{2\pi} d\phi \sin\phi\, e^{i(l'-l)\phi} = i\pi\left(\delta_{l',l+1} - \delta_{l,l'+1}\right).
\tag{A.3b}
$$

Therefore, the integral (A.2) becomes

$$
\int d\phi_k \cos\phi_k \big|\Psi_{\mathbf{k}_\mu}(\boldsymbol{\rho})\big|^2
$$

$$
= \pi \sum_{l,l'} e^{i(l-l')\pi/2} R_l R_{l'}^* \left[\cos\phi_\rho\left(\delta_{l',l+1}+\delta_{l,l'+1}\right) - i\sin\phi_\rho\left(\delta_{l',l+1}-\delta_{l,l'+1}\right) \right]
$$

$$
= -i\pi \cos\phi_\rho \sum_l \left(R_l R_{l+1}^* - R_l^* R_{l+1} \right) - \pi \sin\phi_\rho \sum_l \left(R_l R_{l+1}^* + R_l^* R_{l+1} \right)
$$

$$
= 2\pi \left[\cos\phi_\rho \operatorname{Im} \sum_{l=-\infty}^{+\infty} R_l(\rho) R_{l+1}^*(\rho) - \sin\phi_\rho \operatorname{Re} \sum_{l=-\infty}^{+\infty} R_l(\rho) R_{l+1}^*(\rho) \right].
\tag{A.4}
$$

APPENDIX A. DERIVATION OF CHARGE ACCUMULATION

We can adjust the summation over l from zero to infinity by shifting the summation index, coupled with the relation $R_{-l} = (-1)^l R_l$, thus

$$\sum_{l=-\infty}^{+\infty} R_l(\rho) R_{l+1}^*(\rho) = R_0 R_1^* + \sum_{l=1}^{\infty} \left(R_l R_{l+1}^* + R_{-l} R_{-l+1}^* \right)$$

$$= R_0 R_1^* + \sum_{l=1}^{\infty} \left[R_l R_{l+1}^* + (-1)^{2l-1} R_l R_{l-1}^* \right]$$

$$= R_0 R_1^* + \sum_{l=1}^{\infty} R_l R_{l+1}^* - \sum_{l=0}^{\infty} R_{l+1} R_l^*$$

$$= 2i \, \text{Im} \sum_{l=0}^{\infty} R_l(\rho) R_{l+1}^*(\rho). \tag{A.5}$$

From Eq. (A.4) and Eq. (A.5), we obtain

$$\delta n(\boldsymbol{\rho}) = -\frac{2e\tau E_0 k_\mu}{\pi \hbar} \cos \phi_\rho \, \text{Im} \sum_{l=0}^{\infty} R_l(\rho) R_{l+1}^*(\rho).$$

In the presence of local SOI, the spin degeneracy is removed and charge accumulation is turned out to be

$$\delta n(\boldsymbol{\rho}) = -\frac{e\tau E_0 k_\mu}{\pi \hbar} \cos \phi_\rho \, \text{Im} \sum_{\sigma} \sum_{l=0}^{\infty} R_l^\sigma(\rho) R_{l+1}^{\sigma *}(\rho).$$

Appendix B

Derivation of spin accumulation

The nonequilibrium contribution to the spin accumulation is written as

$$
S_z(\boldsymbol{\rho}) = \frac{1}{4\pi^2} \int d\mathbf{k}\, f(\mathbf{k}) \sum_\sigma \sigma\, \Psi_{\mathbf{k}\sigma}^\dagger(\boldsymbol{\rho}) \Psi_{\mathbf{k}\sigma}(\boldsymbol{\rho})
$$
$$
= S_z^{\mathrm{eq}}(\boldsymbol{\rho}) + \delta S_z(\boldsymbol{\rho}),
$$

where $\Psi_{\mathbf{k}\sigma}(\boldsymbol{\rho}) = \psi_{\mathbf{k}}^\sigma(\boldsymbol{\rho})\chi_\sigma$ and

$$
S_z^{\mathrm{eq}}(\boldsymbol{\rho}) = \frac{1}{4\pi^2} \int d\mathbf{k}\, f_0(\mathbf{k}) \sum_\sigma \sigma\, |\psi_{\mathbf{k}}^\sigma(\boldsymbol{\rho})|^2;
$$
$$
\delta S_z(\boldsymbol{\rho}) = \frac{1}{4\pi^2} \int d\mathbf{k}\, g(\mathbf{k}) \sum_\sigma \sigma\, |\psi_{\mathbf{k}}^\sigma(\boldsymbol{\rho})|^2.
$$

For the temperature is low around $0\,\mathrm{K}$, the equilibrium function is a circular step function in $\mathbf{k}$ space, i.e. $f_0(k) = \theta(\mu - \varepsilon_{\mathbf{k}})$, the contribution due to nonequilibrium distribution is therefore

$$
S_z^{\mathrm{eq}}(\boldsymbol{\rho}) = \frac{1}{4\pi^2} \int dk k\theta(\mu - \varepsilon_{\mathbf{k}}) \sum_\sigma \sigma \sum_{l,l'=-\infty}^{+\infty} e^{i(l-l')\pi/2} R_l^\sigma R_{l'}^{\sigma*} \int d\phi_k e^{i(l-l')(\phi_k - \phi_\rho)}, \quad (\mathrm{B.1})
$$

where the angular integral is the Kronecker delta $\delta_{ll'}$, and therefore Eq. (B.1) is equal to

$$
\begin{aligned}
S_z^{\text{eq}} &= \frac{1}{4\pi^2} \int_0^{k_\mu} dk\, k \sum_\sigma \sigma \sum_{l=-\infty}^{+\infty} |R_l^\sigma|^2 \\
&= \frac{1}{4\pi^2} \int_0^{k_\mu} dk\, k \sum_\sigma \sigma \left[|R_0|^2 + \sum_{l=1}^{\infty} |R_l^\sigma|^2 + \left|R_{-l}^\sigma\right|^2 \right] \\
&= \frac{1}{4\pi^2} \int_0^{k_\mu} dk\, k \sum_{l=1}^{\infty} \left|R_l^+\right|^2 - \left|R_l^-\right|^2 + \left|R_l^-\right|^2 - \left|R_l^+\right|^2 \\
&= 0.
\end{aligned}
$$

In the above the terms associated with $R_0(\rho)$ are spin-independent and therefore can be eliminated. The remaining terms are exactly canceled as well. Therefore the total contribution to S_z is merely due to δS_z.

$$
S_z(\boldsymbol{\rho}) = \delta S_z(\boldsymbol{\rho}) = \frac{1}{4\pi^2} \int d\mathbf{k}\, g(\mathbf{k}) \sum_\sigma \sigma\, |\psi_{\mathbf{k}}^\sigma(\boldsymbol{\rho})|^2 .
$$

Similar to Eq. (A.1), Eq. (A.2), and Eq. (A.4)

$$
S_z = -\frac{e\tau E_0 k_\mu}{4\pi^2 \hbar} \int_0^{2\pi} d\phi_k \cos\phi_k \sum_\sigma \sigma\, |\psi_{\mathbf{k}}^\sigma(\boldsymbol{\rho})|^2 ,
\tag{B.2}
$$

and the integral is equal to

$$
\begin{aligned}
&\int d\phi_k \cos\phi_k \sum_\sigma \sigma \left|\psi_{\mathbf{k}_\mu}^\sigma(\boldsymbol{\rho})\right|^2 \\
&= 2\pi \left[\cos\phi_\rho \operatorname{Im} \sum_\sigma \sigma \sum_{l=-\infty}^{+\infty} R_l^\sigma(\rho) R_{l+1}^{\sigma*}(\rho) - \sin\phi_\rho \operatorname{Re} \sum_\sigma \sigma \sum_{l=-\infty}^{+\infty} R_l^\sigma(\rho) R_{l+1}^{\sigma*}(\rho) \right]
\end{aligned}
\tag{B.3}
$$

Then we can use the relation $R_{-l}^{\sigma} = (-1)^l R_l^{-\sigma}$ to reduce the summation

$$
\sum_{\sigma} \sigma \sum_{l=-\infty}^{+\infty} R_l^{\sigma}(\rho) R_{l+1}^{\sigma*}(\rho)
$$

$$
= \sum_{\sigma} \sigma R_0 R_1^{\sigma*} + \sum_{l=1}^{\infty} \left(R_l^+ R_{l+1}^{+*} - R_l^- R_{l+1}^{-*} + R_{-l}^+ R_{-l+1}^{+*} - R_{-l}^- R_{-l+1}^{-*} \right)
$$

$$
= \sum_{\sigma} \sigma R_0 R_1^{\sigma*} + \sum_{l=1}^{\infty} \left(R_l^+ R_{l+1}^{+*} - R_l^- R_{l+1}^{-*} - R_l^- R_{l-1}^{-*} + R_l^+ R_{l-1}^{+*} \right)
$$

$$
= \sum_{\sigma} \sigma R_0 R_1^{\sigma*} + \sum_{\sigma} \sigma \sum_{l=1}^{\infty} R_l^{\sigma} R_{l+1}^{\sigma*} + \sum_{\sigma} \sigma \sum_{l=0}^{\infty} R_{l+1}^{\sigma} R_l^{\sigma*}
$$

$$
= \sum_{\sigma} \sigma \sum_{l=0}^{\infty} \left(R_l^{\sigma} R_{l+1}^{\sigma*} + R_{l+1}^{\sigma} R_l^{\sigma*} \right)
$$

$$
= 2 \operatorname{Re} \sum_{l=0}^{\infty} R_l^{\sigma}(\rho) R_{l+1}^{\sigma*}(\rho). \tag{B.4}
$$

Therefore coupled with Eq. (B.3) and Eq. (B.4), the angular integral becomes

$$
\int d\phi_k \cos \phi_k \sum_{\sigma} \sigma \left| \psi_{\mathbf{k}_\mu}^{\sigma}(\boldsymbol{\rho}) \right|^2 = -4\pi \sin \phi_\rho \operatorname{Re} \sum_{l=0}^{\infty} R_l^{\sigma}(\rho) R_{l+1}^{\sigma*}(\rho),
$$

and then we can get the spin accumulation $S_z(\boldsymbol{\rho})$,

$$
S_z(\boldsymbol{\rho}) = \frac{e \tau E_0 k_\mu}{\pi \hbar} \sin \phi_\rho \operatorname{Re} \sum_{\sigma} \sigma \sum_{l=0}^{\infty} R_l^{\sigma}(\rho) R_{l+1}^{\sigma*}(\rho) \tag{B.5}
$$

Appendix C

Derivation of transport cross section

From Eq. (C.1), the scattering amplitude is

$$f_k(\phi) = \sqrt{\frac{2i}{\pi k}} \sum_{l=-\infty}^{+\infty} e^{i\delta_l} \sin \delta_l \, e^{il\phi}.$$

After decomposing $\sin \delta_l$ into exponentials, we get

$$f_k(\phi) = \sqrt{\frac{i}{2\pi k}} \sum_{l=-\infty}^{+\infty} \left(e^{2i\delta_l} - 1 \right) e^{il\phi}.$$

Therefore the scattering cross section is, by definition,

$$D(\phi) = |f_k(\phi)|^2 = \frac{1}{2\pi k} \sum_{l,l'} \left(e^{2i\delta_l} - 1 \right) \left(e^{-2i\delta_{l'}} - 1 \right) e^{i(l-l')\phi}. \tag{C.1}$$

The transport cross section is defined by an integral of $(1 - \cos \phi)$ times $D(\phi)$ with respect to ϕ,

$$\sigma_{\text{tr}} \equiv \int d\phi \, (1 - \cos \phi) \, D(\phi),$$

78

and then,

$$\sigma_{\text{tr}} = \sigma_{\text{tot}} - \frac{1}{2\pi k} \sum_{l,l'} \left(e^{2i\delta_l} - 1 \right) \left(e^{-2i\delta_{l'}} - 1 \right) \int d\phi \cos\phi \, e^{i(l-l')\phi}, \tag{C.2}$$

where σ_{tot} is the total cross section of scattered particles,

$$
\begin{aligned}
\sigma_{\text{tot}} &\equiv \int d\phi D(\phi) \\
&= \frac{1}{2\pi k} \sum_{l,l'} \left(e^{2i\delta_l} - 1 \right) \left(e^{-2i\delta_{l'}} - 1 \right) \int d\phi \, e^{i(l-l')\phi} \\
&= \frac{1}{k} \sum_{l,l'} \delta_{ll'} \left[e^{2i(\delta_l - \delta_{l'})} + 1 - \left(e^{2i\delta_l} + e^{-2i\delta_{l'}} \right) \right]
\end{aligned}
$$

Thus,

$$\sigma_{\text{tot}} = \frac{2}{k} \sum_{l=-\infty}^{+\infty} (1 - \cos 2\delta_l). \tag{C.3}$$

Since the integral in ϕ in Eq. (C.2), according to Eq. (??), is equal to

$$\int d\phi \cos\phi \, e^{i(l-l')\phi} = \pi \left(\delta_{l,l'+1} + \delta_{l',l+1} \right),$$

then,

$$
\begin{aligned}
\sigma_{\text{tr}} &= \sigma_{\text{tot}} - \frac{1}{2k} \sum_{l=-\infty}^{+\infty} \left[e^{2i(\delta_l - \delta_{l+1})} + 1 - \left(e^{2i\delta_l} + e^{-2i\delta_{l+1}} \right) \right] + \text{cc.} \\
&= \sigma_{\text{tot}} - \frac{1}{k} \operatorname{Re} \sum_{l=-\infty}^{+\infty} e^{2i(\delta_l - \delta_{l+1})} + 1 - \left(e^{2i\delta_l} + e^{-2i\delta_{l+1}} \right) \\
&= \sigma_{\text{tot}} - \frac{1}{k} \sum_{l=-\infty}^{+\infty} \cos\left[2(\delta_l - \delta_{l+1}) \right] + 1 - (\cos 2\delta_l + \cos 2\delta_{l+1}),
\end{aligned}
$$

where cc. stands for the complex conjugate. In the last line of the above equation, we use

Eq. (C.3) and shift the dummy index of summation in the last term, $\cos 2\delta_{l+1} \to \cos 2\delta_l$,

we have

$$
\begin{aligned}
\sigma_{\mathrm{tr}} &= \frac{2}{k} \sum_{l=-\infty}^{+\infty} (1 - \cos 2\delta_l) - \frac{1}{k} \sum_{l=-\infty}^{+\infty} \left[1 - 2\sin^2(\delta_l - \delta_{l+1}) + 1 - 2\cos 2\delta_l \right] \\
&= \frac{1}{k} \sum_{l=-\infty}^{\infty} (2 - 2\cos 2\delta_l) - \frac{1}{k} \sum_{l=-\infty}^{\infty} \left[2 - 2\sin^2(\delta_l - \delta_{l+1}) - 2\cos 2\delta_l \right] \\
&= \frac{2}{k} \sum_{l=-\infty}^{\infty} \sin^2(\delta_l - \delta_{l+1}).
\end{aligned}
$$

By the use of the relation $\delta_{-l} = \delta_l$, we can rearrange the summation,

$$
\begin{aligned}
\sigma_{\mathrm{tr}} &= \frac{2}{k} \left[\sin^2(\delta_0 - \delta_1) + \sum_{l=1}^{\infty} \sin^2(\delta_l - \delta_{l+1}) + \sin^2(\delta_{-l} - \delta_{-l+1}) \right] \\
&= \frac{2}{k} \left[\sin^2(\delta_0 - \delta_1) + \sum_{l=1}^{\infty} \sin^2(\delta_l - \delta_{l+1}) + \sin^2(\delta_l - \delta_{l-1}) \right].
\end{aligned}
$$

Shifting the index of summation again, we have

$$
\sigma_{\mathrm{tr}} = \frac{2}{k} \left[\sin^2(\delta_0 - \delta_1) + \sum_{l=1}^{\infty} \sin^2(\delta_l - \delta_{l+1}) + \sum_{l=0}^{\infty} \sin^2(\delta_{l+1} - \delta_l) \right].
$$

Therefore,

$$
\sigma_{\mathrm{tr}} = \frac{4}{k} \sum_{l=0}^{\infty} \sin^2(\delta_l - \delta_{l+1}). \tag{C.4}
$$

Appendix D

Derivation of transverse transport cross section

Similar to Eq. (C.1), the spin dependent scattering cross section, in terms of exponentials, reads

$$D_\sigma(\phi) = |f_k^\sigma(\phi)|^2 = \frac{1}{2\pi k} \sum_{l,l'=-\infty}^{+\infty} \left(e^{2i\delta_l^\sigma} - 1\right) \left(e^{-2i\delta_{l'}^\sigma} - 1\right) e^{i(l-l')\phi}. \tag{D.1}$$

The definition of transverse transport cross section is written as,

$$\sigma_\perp \equiv \int d\phi \sin\phi \sum_\sigma \sigma D_\sigma(\phi)$$

$$= \frac{1}{2\pi k} \sum_\sigma \sigma \sum_{l,l'=-\infty}^{+\infty} (e^{2i\delta_l^\sigma} - 1)(e^{-2i\delta_{l'}^\sigma} - 1) \int d\phi \sin\phi\, e^{i(l-l')\phi},$$

where the integral is equal to

$$\int d\phi \sin\phi\, e^{i(l-l')\phi} = -i\pi(\delta_{l',l+1} - \delta_{l,l'+1}),$$

therefore,

$$\sigma_\perp = \frac{-i}{2k} \sum_\sigma \sigma \sum_{l,l'=-\infty}^{+\infty} (e^{2i\delta_l^\sigma} - 1)(e^{-2i\delta_{l'}^\sigma} - 1)\left(\delta_{l',l+1} - \delta_{l,l'+1}\right)$$

$$= \frac{-i}{2k} \sum_\sigma \sigma \sum_{l=-\infty}^{+\infty} \left[e^{2i(\delta_l^\sigma - \delta_{l+1}^\sigma)} + 1 - (e^{2i\delta_l^\sigma} + e^{-2i\delta_{l+1}^\sigma})\right] - \text{cc.}$$

$$= \frac{1}{k} \operatorname{Im} \sum_\sigma \sigma \sum_{l=-\infty}^{+\infty} \left[e^{2i(\delta_l^\sigma - \delta_{l+1}^\sigma)} + 1 - (e^{2i\delta_l^\sigma} + e^{-2i\delta_{l+1}^\sigma})\right]$$

$$= \frac{1}{k} \sum_\sigma \sigma \sum_{l=-\infty}^{+\infty} \sin[2(\delta_l^\sigma - \delta_{l+1}^\sigma)] - (\sin 2\delta_l^\sigma - \sin 2\delta_{l+1}^\sigma).$$

We can cancel the last two terms by shifting the index of summation, and then we can get

$$\sigma_\perp = \frac{1}{k} \sum_{l=-\infty}^{+\infty} \left\{\sin[2(\delta_l^+ - \delta_{l+1}^+)] - \sin[2(\delta_l^- - \delta_{l+1}^-)]\right\}.$$

By expressing the summation over l from zero to infinity, we have

$$\sigma_\perp = \frac{1}{k} \left\{\sin[2(\delta_0 - \delta_1^+)] - \sin[2(\delta_0 - \delta_1^-)]\right\}$$

$$+ \frac{1}{k} \sum_{\substack{l=-\infty; \\ l\neq 0}}^{+\infty} \left\{\sin[2(\delta_l^+ - \delta_{l+1}^+)] - \sin[2(\delta_l^- - \delta_{l+1}^-)]\right\}$$

$$= \frac{1}{k} \left\{\sin[2(\delta_0 - \delta_1^+)] - \sin[2(\delta_0 - \delta_1^-)]\right\}$$

$$+ \frac{1}{k} \sum_{l=1}^{+\infty} \left\{\sin[2(\delta_l^+ - \delta_{l+1}^+)] + \sin[2(\delta_{-l}^+ - \delta_{-l+1}^+)]\right.$$

$$\left. - \sin[2(\delta_l^- - \delta_{l+1}^-)] - \sin[2(\delta_{-l}^- - \delta_{-l+1}^-)]\right\}.$$

By using the relation $\delta_{-l}^{\sigma} = \delta_l^{-\sigma}$, we have

$$
\begin{aligned}
\sigma_{\perp} &= \frac{1}{k}\left\{\sin[2(\delta_0 - \delta_1^{+})] - \sin[2(\delta_0 - \delta_1^{-})]\right\} \\
&\quad + \frac{1}{k}\sum_{l=1}^{\infty}\left\{\sin[2(\delta_l^{+} - \delta_{l+1}^{+})] - \sin[2(\delta_{l-1}^{-} - \delta_l^{-})]\right. \\
&\qquad\qquad \left. - \sin[2(\delta_l^{-} - \delta_{l+1}^{-})] + \sin[2(\delta_{l-1}^{+} - \delta_l^{+})]\right\} \\
&= \frac{1}{k}\sum_{\sigma}\sigma\left\{\sin[2(\delta_0 - \delta_1^{\sigma})] + \sum_{l=1}^{\infty}\left\{\sin[2(\delta_l^{\sigma} - \delta_{l+1}^{\sigma})] + \sin[2(\delta_{l-1}^{\sigma} - \delta_l^{\sigma})]\right\}\right\} \\
&= \frac{1}{k}\sum_{\sigma}\sigma\left\{\sin[2(\delta_0 - \delta_1^{\sigma})] + \sum_{l=1}^{\infty}\sin[2(\delta_l^{\sigma} - \delta_{l+1}^{\sigma})] + \sum_{l=0}^{\infty}\sin[2(\delta_l^{\sigma} - \delta_{l+1}^{\sigma})]\right\}.
\end{aligned}
$$

Combining the first two terms in the summation, then we can get

$$
\sigma_{\perp} = \frac{2}{k}\sum_{\sigma}\sigma\sum_{l=0}^{\infty}\sin[2(\delta_l^{\sigma} - \delta_{l+1}^{\sigma})]. \tag{D.2}
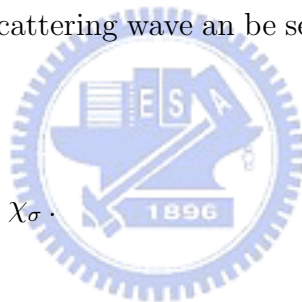$$
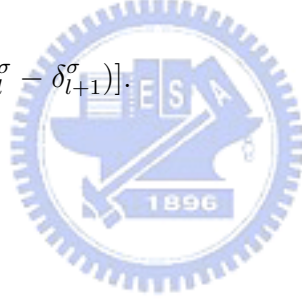
Appendix E

Asymmetric Mott skew scattering

The spatial part of the total scattering wave an be separated into the incident plane wave and a scattered wave,

$$\psi_{\mathbf{k}}^{\sigma}(\boldsymbol{\rho}) = \left[e^{i\mathbf{k}\cdot\boldsymbol{\rho}} + \psi_{\sigma}^{\mathrm{sc}}(\boldsymbol{\rho}) \right] \chi_{\sigma} .$$

We present here the asymmetric Mott skew scattering of an incident electron with its spin-polarization along $\hat{\mathbf{z}}$. In the following series of figures, we present the asymmetric scattering at resonant energies $E_{n,l}^{+}$ for ($n = 1$, $l = 0, \pm 1, \pm 2, \pm 3$), and an arbitrary incident energy.

In the following series of figures, the left-hand side shows the probability distribution of the total scattering wave function, while the right-hand side depicts that of the scattered wave, defined by $\left| \psi_{+}^{\mathrm{sc}}(\boldsymbol{\rho}) \right|^{2}$.

Figure E.1: Scattering of a plane wave with spin up polarization for both total wave and scattered wave: (a) off-resonance scattering. (b) scattering resonance contributed by partial waves labeled $l = 0$.

Figure E.2: Scattering of a plane wave with spin up polarization for both total wave and scattered wave: asymmetric scattering contributed by partial waves labeled (a) $l = 1$ and (b) $l = -1$.

Figure E.3: Scattering of a plane wave with spin up polarization for both total wave and scattered wave: asymmetric scattering contributed by partial waves labeled (a) $l = 2$ and (b) $l = -2$.
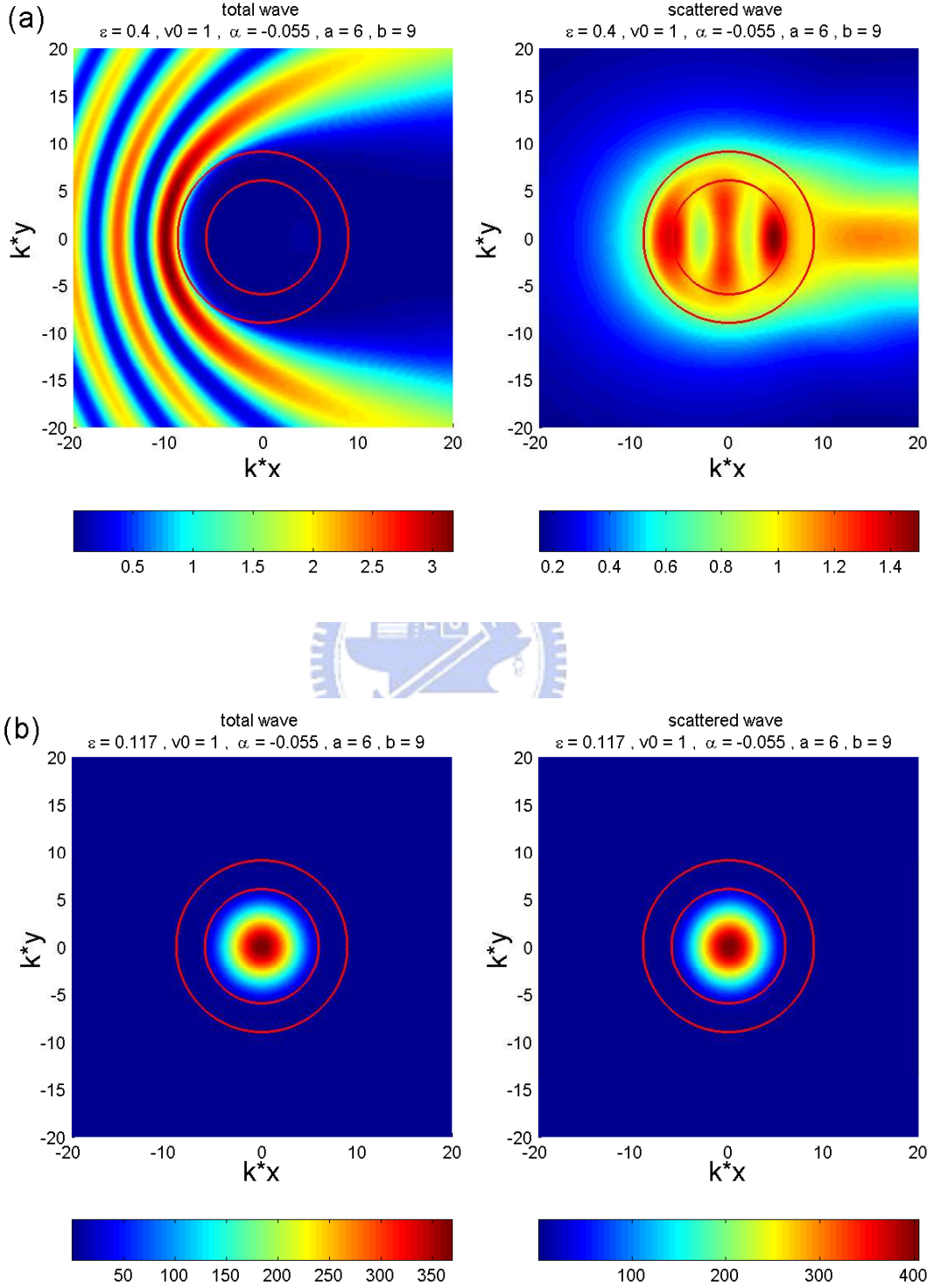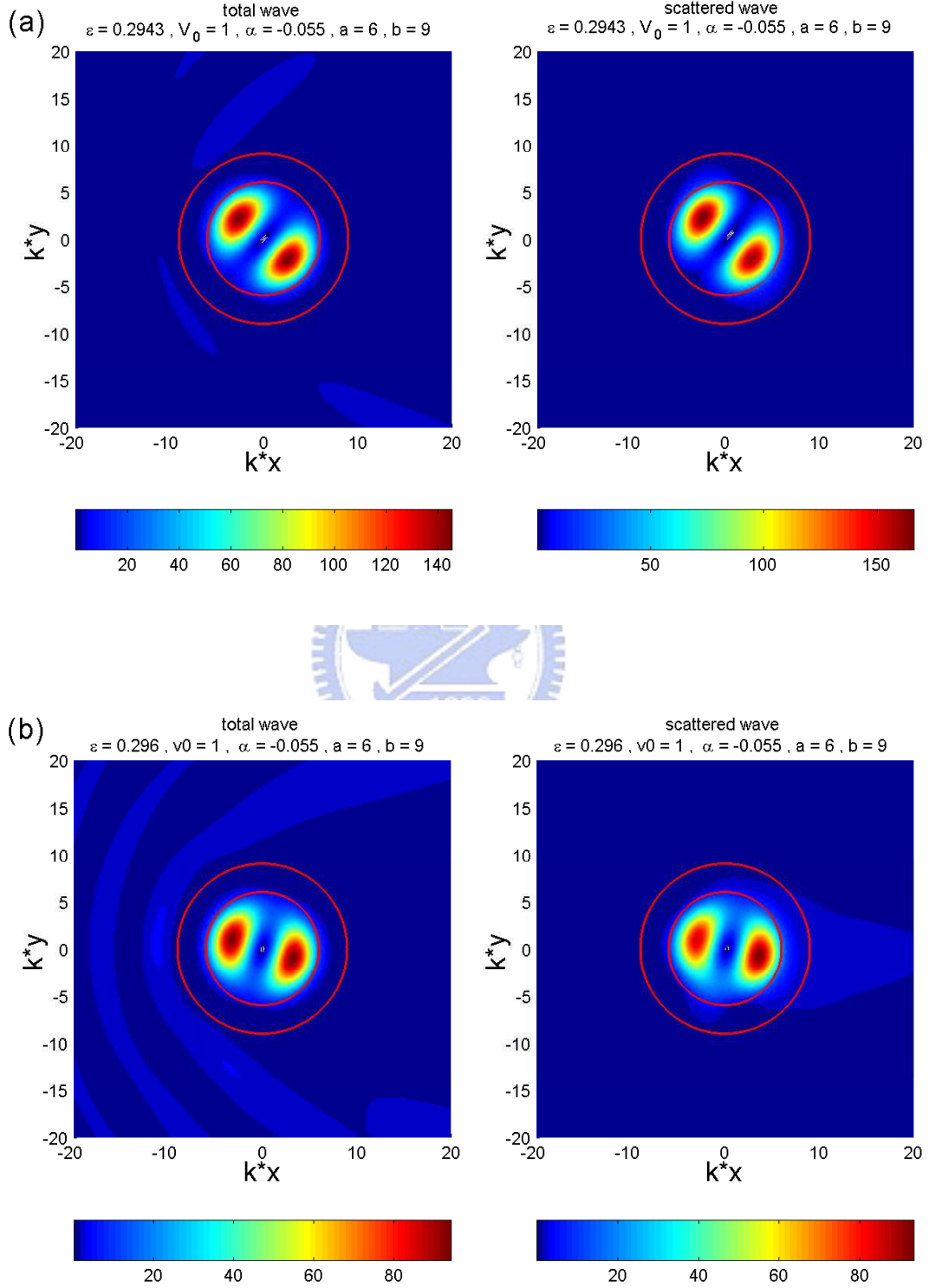
Figure E.4: Scattering of a plane wave with spin up polarization for both total wave and scattered wave: asymmetric scattering contributed by partial waves labeled (a) $l = 3$ and (b) $l = -3$.

Appendix F

Asymptotic expansion of residual resistivity dipole and charge dipole strength

The unscreened charge distribution is

$$\delta n(\boldsymbol{\rho}) = -\frac{2e\tau E_0 k_\mu}{\pi\hbar} \cos\phi_\rho \operatorname{Im} \sum_{l=0}^{\infty} R_l(\rho) R_{l+1}^*(\rho).$$

According to Eq. (2.6), the radial function is

$$\lim_{k\rho\to\infty} R_l(\rho) = \frac{1}{\sqrt{2\pi k\rho}} \left[e^{2i\delta_l} e^{i(k\rho - l\pi/2 - \pi/4)} + e^{-i(k\rho - l\pi/2 - \pi/4)} \right].$$

APPENDIX F. ASYMPTOTIC EXPANSION OF RESIDUAL RESISTIVITY DIPOLE AND CHARGE DIPOLE STRENGTH

Therefore, the asymptotic expansion of charge accumulation is

$$
\delta n(\boldsymbol{\rho}) \sim -\frac{2e\tau E_0 k_\mu}{\pi\hbar} \cos\phi_\rho \frac{1}{2\pi k_\mu \rho}
$$

$$
\times \operatorname{Im} \sum_{l=0}^{\infty} \left[\left(e^{2i\delta_l} e^{i(k\rho - l\pi/2 - \pi/4)} + e^{-i(k\rho - l\pi/2 - \pi/4)} \right) \right.
$$

$$
\left. \times \left(e^{-2i\delta_{l+1}} e^{-i(k\rho - (l+1)\pi/2 - \pi/4)} + e^{i(k\rho - (l+1)\pi/2 - \pi/4)} \right) \right]
$$

$$
= -\frac{e\tau E_0}{\pi^2\hbar} \frac{\cos\phi_\rho}{\rho} \operatorname{Im} \sum_{l=0}^{\infty} \left[e^{2i(\delta_l - \delta_{l+1})} e^{i\pi/2} + e^{i\pi/2} + e^{-2i\delta_{l+1}} e^{-i(2k\rho - l\pi - \pi)} \right.
$$

$$
\left. + e^{2i\delta_l} e^{i(2k\rho - l\pi - \pi)} \right]
$$

$$
= -\frac{e\tau E_0}{\pi^2\hbar} \frac{\cos\phi_\rho}{\rho} \operatorname{Im} \sum_l \left\{ i \left[e^{2i(\delta_l - \delta_{l+1})} - 1 \right] - \left[e^{-2i\delta_{l+1}} e^{-i(2kr - l\pi)} + e^{2i\delta_l} e^{i(2kr - l\pi)} \right] \right\}.
$$

The last two terms in the summation is referred to as the contribution to the well-known Friedel oscillation. The remaining terms becomes

$$
\delta n(\boldsymbol{\rho}) \sim -\frac{e\tau E_0}{\pi^2\hbar} \frac{\cos\phi_\rho}{\rho} \operatorname{Re} \sum_l \left[e^{2i(\delta_l^\sigma - \delta_{l+1}^\sigma)} - 1 \right]
$$

$$
= -\frac{e\tau E_0}{\pi^2\hbar} \frac{\cos\phi_\rho}{\rho} \operatorname{Re} \sum_l e^{i(\delta_l^\sigma - \delta_{l+1}^\sigma)} \left(e^{i(\delta_l^\sigma - \delta_{l+1}^\sigma)} - e^{-i(\delta_l^\sigma - \delta_{l+1}^\sigma)} \right)
$$

$$
= -\frac{2e\tau E_0}{\pi^2\hbar} \frac{\cos\phi_\rho}{\rho} \operatorname{Im} \sum_l e^{i(\delta_l^\sigma - \delta_{l+1}^\sigma)} \sin(\delta_l^\sigma - \delta_{l+1}^\sigma)
$$

$$
= \frac{2e\tau E_0}{\pi^2\hbar} \frac{\cos\phi_\rho}{\rho} \sum_l \sin^2(\delta_l^\sigma - \delta_{l+1}^\sigma)
$$

$$
= \frac{e\tau E_0}{2\pi^2\hbar} \frac{\cos\phi_\rho}{\rho} \left[4 \sum_l \sin^2(\delta_l^\sigma - \delta_{l+1}^\sigma) \right].
$$

Thus far the potential due to charge accumulation in the asymptotic region can obtained by multiplying the above a screening factor $-\pi\hbar^2/m^*e$,

$$
\delta\phi(\boldsymbol{\rho}) \sim p_{\mathrm{c}} \frac{\cos\phi_\rho}{\rho},
$$

where p_{c} is referred to as the RRD strength,

$$
p_{\mathrm{c}} = -\frac{E_0\hbar\tau}{2\pi m^*} k_\mu \sigma_{\mathrm{tr}}.
$$

90

APPENDIX F. ASYMPTOTIC EXPANSION OF RESIDUAL RESISTIVITY DIPOLE AND CHARGE DIPOLE STRENGTH

where σ_{tr} is defined as

$$\sigma_{\mathrm{tr}} \equiv \int_{-\pi}^{\pi} (1 - \cos\phi) D(\phi)$$

In the case the spin degeneracy is broken by SOI, the definition of charge dipole is the same

$$p_{\mathrm{c}} = -\frac{E_0 \hbar \tau}{2\pi m^*} k_\mu \sigma_{\mathrm{tr}},$$

where σ_{tr} is defined as

$$\sigma_{\mathrm{tr}} \equiv \frac{1}{2} \int_{-\pi}^{\pi} (1 - \cos\phi) \sum_\sigma \sigma D_\sigma(\phi)$$
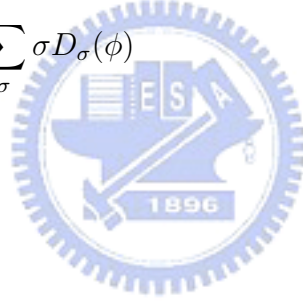
Appendix G

Asymptotic expansion of spin dipole and spin dipole strength

To define the spin dipole strength, we start from the expression of the spin-dipole, which is written as

$$S_z(\boldsymbol{\rho}) = \frac{e\tau E_0 k_\mu}{\pi\hbar} \sin\phi_\rho \operatorname{Re} \sum_\sigma \sigma \sum_{l=0}^\infty R_l^\sigma(\rho) R_{l+1}^{\sigma*}(\rho).$$

Again, using the radial function R_l^σ expanded in the first-order in ρ^{-1}, according to Eq. (2.6), is equal to

$$\lim_{k\rho\to\infty} R_l(\rho) = \frac{1}{\sqrt{2\pi k\rho}} \left[e^{2i\delta_l} e^{i(k\rho - l\pi/2 - \pi/4)} + e^{-i(k\rho - l\pi/2 - \pi/4)} \right]. \tag{G.1}$$

APPENDIX G. ASYMPTOTIC EXPANSION OF SPIN DIPOLE AND SPIN DIPOLE STRENGTH

Therefore, the spin accumulation in the asymptotic region is

$$
\begin{aligned}
S_z(\boldsymbol{\rho}) \sim\ & \frac{e\tau E_0 k_\mu}{\pi\hbar} \sin\phi_\rho \frac{1}{2\pi k_\mu \rho} \\
& \times \mathrm{Re} \sum_\sigma \sigma \sum_{l=0}^\infty \Big[\big(e^{2i\delta_l^\sigma} e^{i(k\rho - l\pi/2 - \pi/4)} + e^{-i(k\rho - l\pi/2 - \pi/4)} \big) \\
& \qquad\qquad\qquad \times \big(e^{-2i\delta_{l+1}^\sigma} e^{-i(k\rho - (l+1)\pi/2 - \pi/4)} + e^{i(k\rho - (l+1)\pi/2 - \pi/4)} \big) \Big] \\
=\ & \frac{e\tau E_0}{2\pi^2\hbar} \frac{\sin\phi_\rho}{\rho} \mathrm{Re} \sum_\sigma \sigma \sum_{l=0}^\infty \Big[e^{2i(\delta_l^\sigma - \delta_{l+1}^\sigma)} e^{i\pi/2} + e^{i\pi/2} + e^{-2i\delta_{l+1}^\sigma} e^{-i(2k\rho - l\pi - \pi)} \\
& \qquad\qquad\qquad\qquad\qquad + e^{2i\delta_l^\sigma} e^{i(2k\rho - l\pi - \pi)} \Big] \\
=\ & \frac{e\tau E_0}{2\pi^2\hbar} \frac{\sin\phi_\rho}{\rho} \mathrm{Re} \sum_\sigma \sigma \sum_l \Big\{ i \big[e^{2i(\delta_l^\sigma - \delta_{l+1}^\sigma)} - 1 \big] - \big[e^{-2i\delta_{l+1}^\sigma} e^{-i(2kr - l\pi)} + e^{2i\delta_l^\sigma} e^{i(2kr - l\pi)} \big] \Big\}.
\end{aligned}
$$

Here the last two terms can eliminate each other by a index-shifted summation:

$$
\begin{aligned}
& \sum_{l=0}^\infty \Big[e^{-2i\delta_{l+1}^\sigma} e^{-i(2kr - l\pi)} + e^{2i\delta_l^\sigma} e^{i(2kr - l\pi)} \Big] \\
=\ & e^{2i\delta_0} e^{2ikr} + \sum_{l=1}^\infty \Big[e^{2i\delta_l^\sigma} e^{i(2kr - l\pi)} - \mathrm{cc.} \Big] \\
=\ & e^{2i\delta_0} e^{2ikr} + 2i\,\mathrm{Im} \sum_{l=1}^\infty e^{2i\delta_l^\sigma} e^{i(2kr - l\pi)}
\end{aligned}
$$

The first term is spin-independent and thus can be eliminated while being summed over σ, and the remaining term does not contribute either after being taken the real part. It is interesting that the Friedel oscillation of spin does not appear in the first-order expansion in ρ^{-1}. Therefore,

$$
\begin{aligned}
S_z(\boldsymbol{\rho}) \sim\ & \frac{e\tau E_0}{2\pi^2\hbar} \frac{\sin\phi_\rho}{\rho} \mathrm{Re}\, i \sum_\sigma \sigma \sum_l e^{2i(\delta_l^\sigma - \delta_{l+1}^\sigma)} \\
=\ & -\frac{e\tau E_0}{2\pi^2\hbar} \frac{\sin\phi_\rho}{\rho} \mathrm{Im} \sum_\sigma \sigma \sum_l e^{2i(\delta_l^\sigma - \delta_{l+1}^\sigma)} \\
=\ & -\frac{e\tau E_0}{2\pi^2\hbar} \frac{\sin\phi_\rho}{\rho} \sum_\sigma \sigma \sum_l \sin[2(\delta_l^\sigma - \delta_{l+1}^\sigma)] \\
=\ & -\frac{e\tau E_0}{4\pi^2\hbar} \frac{\sin\phi_\rho}{\rho} \Big\{ 2 \sum_\sigma \sigma \sum_l \sin[2(\delta_l^\sigma - \delta_{l+1}^\sigma)] \Big\}.
\end{aligned}
$$

APPENDIX G. ASYMPTOTIC EXPANSION OF SPIN DIPOLE AND SPIN DIPOLE STRENGTH

Thus the asymptotics of $S_z(\boldsymbol{\rho})$ can be expressed in the form

$$S_z(\boldsymbol{\rho}) \sim p_{\mathrm{s}} \frac{\sin \phi_\rho}{\rho},$$

where

$$p_{\mathrm{s}} = -\frac{e\tau E_0}{4\pi^2 \hbar} \, k_\mu \sigma_\perp.$$

Appendix H

Collision integrals in detail

The projection of a vector $\mathbf{k}'$ to another one $\mathbf{k}$ is, in terms of $\phi \equiv \phi_{\mathbf{k}} - \phi_{\mathbf{k}'}$,

$$
\begin{aligned}
\mathbf{k}' &= \mathbf{k}'_{\parallel} + \mathbf{k}'_{\perp} \\
&= \hat{\mathbf{k}}(\mathbf{k}' \cdot \hat{\mathbf{k}}) + (\hat{\mathbf{k}} \times \mathbf{k}') \times \hat{\mathbf{k}} \\
&= k\hat{\mathbf{k}}(\hat{\mathbf{k}}' \cdot \hat{\mathbf{k}}) + k(\hat{\mathbf{k}} \times \hat{\mathbf{k}}') \times \hat{\mathbf{k}} \\
&= k\hat{\mathbf{k}} \cos \phi + k \sin \phi \, \hat{\mathbf{z}} \times \hat{\mathbf{k}} \\
&= \mathbf{k} \cos \phi + \hat{\mathbf{z}} \times \mathbf{k} \sin \phi
\end{aligned}
$$

The first collision term is

$$
\begin{aligned}
&\int d\phi_{\mathbf{k}'} I\left(\phi\right) [\delta \hat{f}\left(\mathbf{k}\right) - \delta \hat{f}\left(\mathbf{k}'\right)] \\
&= \int d\phi_{\mathbf{k}'} I\left(\phi\right) [\mathbf{a}\left(k\right) + \boldsymbol{\sigma} \times \mathbf{b}\left(k\right)] \cdot \left(\mathbf{k} - \mathbf{k}'\right) \\
&= [\mathbf{a}\left(k\right) + \boldsymbol{\sigma} \times \mathbf{b}\left(k\right)] \cdot \int d\phi_{\mathbf{k}'} I\left(\phi\right) \left(\mathbf{k} - \mathbf{k}'\right) \\
&= [\mathbf{a}\left(k\right) + \boldsymbol{\sigma} \times \mathbf{b}\left(k\right)] \cdot \int_{-\pi}^{\pi} d\phi_{\mathbf{k}'} I\left(\phi\right) \left(\mathbf{k} - \mathbf{k} \cos \phi - \hat{\mathbf{z}} \times \mathbf{k} \sin \phi\right) \\
&= [\mathbf{a}(k) \cdot \mathbf{k} + \sigma_z \hat{\mathbf{z}} \cdot \left(\mathbf{b}\left(k\right) \times \mathbf{k}\right)] \left[2 \int_0^{\pi} d\phi I\left(\phi\right) \left(1 - \cos \phi\right)\right].
\end{aligned}
$$

APPENDIX H. COLLISION INTEGRALS IN DETAIL

The second collision term is

$$
\int d\phi_{\mathbf{k}'} \sigma_z I\left(\phi\right) S\left(\phi\right) \left[g\left(\mathbf{k}\right) - g\left(\mathbf{k}'\right)\right]
$$

$$
= \sigma_z \int d\phi_{\mathbf{k}'} I\left(\phi\right) S(\phi) \left[\mathbf{k} \cdot \mathbf{a}(k) - \mathbf{k}' \cdot \mathbf{a}(k')\right]
$$

$$
= \sigma_z \int d\phi_{\mathbf{k}'} I\left(\phi\right) S(\phi)(\mathbf{k} - \mathbf{k}') \cdot \mathbf{a}(k)
$$

$$
= \sigma_z \int_{-\pi}^{\pi} d\phi_{\mathbf{k}'} I\left(\phi\right) S\left(\phi\right) \left(\mathbf{k} - \mathbf{k}\cos\phi - \hat{\mathbf{z}} \times \mathbf{k}\sin\phi\right) \cdot \mathbf{a}(k)
$$

$$
= -\sigma_z(\hat{\mathbf{z}} \times \mathbf{k}) \cdot \mathbf{a}(k) \left[2\int_0^{\pi} d\phi I\left(\phi\right) S\left(\phi\right) \sin\phi\right]
$$

$$
= \sigma_z \hat{\mathbf{z}} \cdot \left[\mathbf{a}(k) \times \mathbf{k}\right] \left[2\int_0^{\pi} d\phi I\left(\phi\right) S\left(\phi\right) \sin\phi\right].
$$

Bibliography

[1] M. Baibich et al., Phys. Rev. Lett. **61**, 1472 (1988).

[2] E. I. Rashba, Fiz. Tverd. Tela (Leningrad) **2**, 1224 (1960) [Sov. Phys. Solid State **2**, 1109 (1960)]; Y. A. Bychkov and E. I. Rashba, J. Phys. C **17**, 6039 (1984).

[3] G. Dresselhaus, Phys. Rev. **100**, 580 (1955).

[4] N. F. Mott and H. S. W. Massey, *The Theory of Atomic Collisions, 3rd ed.*, (Oxford University Press, 1965).

[5] M. I. Dyakonov and V. I. Perel, JETP Lett. **13**, 467 (1971); Phys. Lett. **35A**, 459 (1971).

[6] J. E. Hirsch, Phys. Rev. Lett. **83**, 1834 (1999).

[7] S. Murakami, N. Nagaosa, and S.-C. Zhang, Science **301**, 1348 (2003); J. Sinova *et al.*, Phys. Rev. Lett. **92**, 126603 (2004); D. Culcer *et al.*, Phys. Rev. Lett. **93**, 046602 (2004).

[8] H.-A. Engel, B. I. Halperin, and E. I. Rashba, Phys. Rev. Lett. **95**, 166605 (2005).

[9] J. Wunderlich *et al.*, Phys. Rev. Lett. **94**, 047204 (2005).

[10] Y. K. Kato, R. C. Myers, A. C. Gossard, and D. D. Awschalom, Science **306**, 1910 (2004).

[11] J. Shi, P. Zhang, D. Xiao, and Q. Niu, Phys. Rev. Lett. **96**, 076604 (2006).

BIBLIOGRAPHY

[12] P.-Q. Jin, Y.-Q. Li, and F.-C. Zhang, cond-mat/0502231.

[13] S. Murakami, N. Nagaosa, and S.-C. Zhang, Phys. Rev. B 69, 235206 (2004).

[14] A. G. Mal'shukov and C. S. Chu, Phys. Rev. Lett. **97**, 076601 (2006).

[15] A. O. Govorov, A. V. Kalameitsev, and J. P. Dulka, Phys. Rev. B **70**, 145310 (2004).

[16] H. Chen *et al.*, Appl. Phys. Lett. **86**, 32113 (2005).

[17] J. D. Walls *et al.*, Phys. Rev. B **73**, 35325 (2006).

[18] J. Y. Yeh, M. C. Chang, and C. Y. Mou, Phys. Rev. B **73**, 35313 (2006).

[19] A. Pályi, C. Péterfalvi, and J. Cserti, Phys. Rev. B **74**, 73305 (2006).

[20] R. Landauer, IBM J. Res. Dev. 1, 223 (1957); R. Landauer, Z. Phys.

[21] R. S. Sorbello and C. S. Chu, IBM J. Res. Dev. **32**, 58 (1988); C. S. Chu and R. S. Sorbello, Phys. Rev. B **38**, 7260 (1988).

[22] W. Zwerger, L. Bönig, and K. Schonhammer, Phys. Rev. B **43**, 6434 (1991).

[23] R. M. Feenstra, B. G. Briner, T. P. Chin, and J. M. Woodall, Phys. Rev. B **54**, R5283 (1996); R. M. Feenstra and B. G. Briner, Superlattices and Microstructures **23**, 699 (1998).

[24] *Topics in advanced quantum mechanics*, Barry R. Holstein (Addison Wesley).

[25] *Spin-Orbit Coupling in Two-Dimensional Electron and Hole systems*, Roland Winkler (Springer, 2003).

[26] E. I. Rashba, Physica E 34, 31 (2006).

[27] *Mathematical Methods for Physicists, 4th ed.*, G. B. Arfkan and H. J. Weber (Academic Press, 1995).

[28] S. K. Adhikari, Am. J. Phys. **54**, 362 (1986).

BIBLIOGRAPHY

[29] *Solid State Physics*, N. W. Ashcroft and N. D. Mermin (Saunders College, 1976).

[30] *Modern Quantum Mechanics, Revised ed.*, J. J. Sakurai (Addison-Wesley, 1994).

[31] V. Sih, W. H. Lau, R. C. Myers, V. R. Horowitz, A. C. Gossard, and D. D. Awschalom, Phys. Rev. Lett. **97**, 096605 (2006).

[32] T. Hada, T. Goto, J. Yanagisawa, F. Wakaya, Y. Yuba, and K. Gamo, J. Vac. Sci. Technol. B **18**, 3158 (2000).

[33] *Scattering Theory*, A. G. Sitenko (Springer-Verlag, 1991).

[34] *Variable phase approach to potential scattering*, F. Calogero (New York Academic, 1967).